Neuromorphic Models for Biological Photoreceptors

Eng-Leng Mah

THE UNIVERSITY OF ADELAIDE
AUSTRALIA

The University of Adelaide
Discipline of Physiology
School of Molecular and Biomedical Sciences

A thesis submitted for the degree of
Doctor of Philosophy

October 2007

To my family and friends

"Imagination is more important than knowledge"
-Albert Einstein-

Table of Contents

List of Figures

List of Tables

Abstract

Biological visual processing is extremely flexible and provides pixel-by-pixel adaptation. Millennia of evolution and natural selection have provided inspiration for robust, efficient and elegant solutions in artificial visual system designs. Physiological studies have shown that non-linear adaptation of biological visual processing is evident even at the first stage of the visual system pathway. Theory and modelling have shown that adaptation in the early visual processing is required to compress the high bandwidth visual environment into a sensible form prior to transmission via the limited bandwidth neuron channels. However, many current bio-inspired visual systems have neglected the importance of having a reliable early stage of visual processing. Having a robust and reliable early stage design not only provides a better mimic of the biology, but also allows better design and understanding of higher order neurons in the visual system pathway.

*(**Chapter 3:** A Non-linear Adaptive Artificial Photoreceptor Circuit - Design and Implementation)* The primary aim of this work was to design and implement an elaborated artificial photoreceptor circuit which faithfully mimics the actual biological photoreceptors, using standard analogue discrete electronic components. I have incorporated several key features of the biological photoreceptors in the implementation, such as non-linear adaptation to background luminance, adaptive frequency response and logarithmic encoding of luminance. Initial parameters for the key features of the model were based on existing literature and fine tuning of the circuit was done after analysis of actual recordings from biological photoreceptors.

*(**Chapter 2:** Dimmable Voltage-Controlled High Current LED Driver System for Vision Science Experiments)* The visual stimulus was a critical component in performing the vision experiments, and has historically been a limiting factor in performing experiments which ask critical questions about responses to complicated scenes, such as natural environments. The ability to reproduce the large dynamic range of the real-world luminance was important to correctly test the performance of the model. I evaluated the performance of several existing light emitting diode (LED) drivers and commercial products and found that none of them provided adequate dynamic range and freedom from noise. I therefore designed and implemented a stable multi-channel, high-current LED driver that allowed creation of light stimuli with inexpensive analogue discrete electronic components, and was used for the experiments described in this thesis. This LED driver, which was properly calibrated to the real-world luminance, was used in conjunction with a standard commercial data acquisition card.

*(An Elaborated Electronic Prototype of a Biological Photoreceptor - Steady-state Analysis (**Chapter 4**) & Dynamic Analysis (**Chapter 5**))* I performed electrophysiological experiments measuring the responses of the intact hoverfly photoreceptor cells (R1-6) using both characterised and dynamic (naturalistic) stimuli. The analysed data were used to fine tune the circuit parameters in order to realise a faithful mimic of the actual biological photoreceptors. Similar experiments were performed on the artificial photoreceptor circuit to thoroughly evaluate the robustness and performance of the circuit against actual biological photoreceptors. Correlation and coherence analyses were used to measure the performance of the circuit with respect to its biological counterpart in both time and frequency domains respectively.

Chapter 6: *Early Visual Processing Maximises Information for Higher Order Neurons)* The artificial photoreceptor circuit was then further evaluated against a complex natural movie scene in which the full dynamic range of the original scenario was maintained. Again, I performed experiments on both the circuit and actual biological photoreceptors. Correlation and coherence analyses of the circuit against the biological photoreceptors showed that the circuit was robust and reliable even under complex naturalistic conditions. I managed to design and implement an add-on electronic circuit to the elaborated photoreceptor circuit that crudely mimicked the temporal high-pass nature of the second order Large Monopolar Cell (LMC) in order to observe how the non-linear features in the early stage of visual processing assists higher order neurons in efficiently coding visual information.

Based on this research, I found that the first stage of visual processing consists of numerous non-linearities, which have been proven to provide optimal coding of visual information. The variable frequency response curve of the hoverfly, *Eristalis tenax* was mapped out against large range of background luminance. Previous studies have suggested that such variability in frequency response was to improve signal transmission quality in the insect visual pathway, even though I have not made any quantitative measurements of the improvements. I also found that high dynamic range images (32-bit floating point numbers) are better representations of the real-world luminance for naturalistic visual experiments compared to the conventional 8-bit images. I have successfully implemented a circuit that faithfully mimicked the biological photoreceptors and it has been evaluated against characterised and dynamic stimuli. I found that my circuit design was far better than using just a normal linear

phototransducer as the front-end of a vision system as it is more capable of compressing visual information in a way which maximises the information content before transmission to higher order neurons.

Acknowledgements

First of all, I would like to thank my **parents** for being very supportive during my Ph.D. years, not only showering me with encouragement but also providing me with a great sense of financial security. I would also like to thank my sister, **Siau-Siah Mah**, who was always there to listen to me during my ups and downs and my little sister, **Fanny Mah** who is always very proud of me.

I would also like to express my thanks to the following friends and colleagues:
Stella Moh for accompanying me with great moral support - I bet the Lord has received plenty of her requests to ensure that I complete my Ph.D. on time. **Chong-Zhi Liaw**, for spending many restless nights on proofreading and grammar. **June Lim**, for cooking me nice dinners when I was extremely busy with my thesis writing. **Tien-Peng Ho**, **Angelynn Lim**, **Dancy Chan** and **Sean Goh**, who showed great concern about my research progress. **Russell Brinkworth**, for being very helpful especially when it came to data analysis involving complicated statistics. **Matthew Sorell**, for providing a solution to an image statistics problem. **Tamath Rainsford** and other members in my lab, for offering some advice on data analysis.

Last but not least, **David O'Carroll** for providing me with such a great research opportunity (an excellent stepping stone to my future career) in his insect vision lab. I have learnt a lot from him.

Declarations

This work contains no material which has been accepted for the award of any other degree or diploma in an university or other tertiary institution and, to the best of my knowledge and belief, contains no material previously published or written by another person, except where due reference has been made in the text.

I give consent to this copy of my thesis, when deposited in the University Library, being made available in all forms of media, now or hereafter known.

Statement of Contributions

As the chapters in this thesis are presented in manuscript format, two individuals, namely Dr. David O'Carroll and Dr. Russell Brinkworth, may be listed as co-authors. In these cases, their contributions were primarily in the form of suggestions and assistance in the application of data analysis; however the majority of the research was conducted by the primary author, Eng-Leng Mah.

.....

Eng-Leng Mah

.....

Dr. David O'Carroll

Dr. Russell SA Brinkworth

1

Chapter 1: Introduction

1.1 Why Insect Visual Systems?

A great deal can be learned from insect visual systems, as they are the product of millennia of evolution and natural selection. The fact that insects have survived and flourished points to the success of these natural systems and this is one of the reasons why researchers are drawing inspiration from nature to find robust, efficient and elegant designs. Although the biological details of insect visual systems have been studied for decades, it is only relatively recently that research has focused on applying this knowledge to real-world tasks. Research has shown that insect visual systems already have several characteristics which are desirable for certain real-world applications (Franceschini et al. 1992; Srinivasan et al. 1997; Srinivasan et al. 1999; Srinivasan et al. 2004; Ruffier et al. 2005), such as insect-inspired navigation for autonomous vehicles or motion detection in surveillance systems.

One very useful aspect of insect visual systems is that they employ various strategies to achieve good performance despite the biological constraints. If you have ever wondered why flying insects are able to manoeuvre at high speed through cluttered, complex environments while easily avoiding obstacles in spite of their relatively tiny brains, have no doubt that such magnificent manoeuvring aptitudes are not

capricious accidents - physiological evidence suggests that flight control in the flying insects is primarily guided by a simple but clever visual system of neurons tuned to very specific types of complex motion (Collett et al. 1975; Hausen 1982; Egelhaaf et al. 1988; Egelhaaf et al. 2002). For instance, small-target neurons found in the optic ganglia of a fly are specifically responsible for visually tracking small moving targets (mating and predation), even across cluttered backgrounds (Nordström et al. 2006; Nordström et al. 2006). Two types of specialised wide-field detection neurons also exist which respond exclusively to either horizontal or vertical motion respectively and which are thought to play a major role in optomotor course stabilisation and figure-ground discrimination (Gronenberg et al. 1990; Ibbotson et al. 1991). The remarkable navigational skills of insects are thus closely matched by evolution to the environments and lifestyles in which those flight controls must work.

An artificial visual system which emulates the features found in insect visual pathways would theoretically be able to achieve comparable performance in a real-world application, for example making use of the robust motion detection capabilities of insects in a collision avoidance system. Such an artificial visual system could also provide more experimental flexibility in the study of other aspects of insect vision, for example allowing very long recordings from a "virtual neuron", under conditions which would not be possible with actual insects. This could be a quick way of gathering data to facilitate the investigation of models for certain higher order neurons in the insect visual system.

1.1.1 Evolutionary Convergence in Visual Processing

Apart from the potential benefit to improving the knowledge of insect visual systems, there are also some ways in which this research may benefit studies in other animals, including humans. Despite the differences between the phototransduction processes of the primate and fly photoreceptors, their visual systems have evolved to deal with visual environments according to the same underlying computational principle of maximising visual information (van Hateren 1992) and thus employ similar strategies such as the compression and conversion of naturally occurring intensity variations into contrast variations in order to increase the dynamic range of encoded information (van Hateren et al. 2006).

The primate cerebral cortex contains multiple representations of visual space, of which MT or V5 is considered to be one of the most important visual areas involved in processing information about movement. Studies suggest that the primate visual cortex (MT or V5 area) has neurons that behave similarly to the motion sensitive neurons in insects (Duffy et al. 1981; Duffy et al. 1991). A similar set of cells has been identified in the visual areas of human brains at Brodmann's area 19/37, 39 and 7 (Vaina et al. 2001). In the case of insects, motion sensitive neurons are largely found in the lobula plate in the optic lobe of the visual system pathway (Hausen 1982; Douglass et al. 1996). Several types of neurons have been well identified, such as the HS (horizontal system) and the VS (vertical system) neurons, which are only activated whenever there is horizontal motion and vertical motion, respectively (Ibbotson et al. 1991; Douglass et al. 1995). The overall similarity between functional properties in the two animal groups makes it likely that principles learned from studying one can be applied to the other.

Visual Illusions

One feature of visual systems which mammals, birds and insects share in common is that of visual illusions. For example, the 'waterfall illusion', which is one of the more famous illusions used extensively to understand motion processing, is evident in both the human (Anstis et al. 1998) and blowfly visual systems (Srinivasan et al. 1979). A person that subsequently turns away from staring at objects in motion, especially those which move very rapidly (e.g. waterfalls or rivers), will experience an opposite visual direction in motion even though the person is looking at a stationary object. The phenomenon, also called the "motion after-effect", can be explained by adaptation in visual neurons that respond selectively to moving contours in the scenes (Anstis et al. 1998; Harris et al. 2000). Other illusions such as illusory contours are also evident across several types of animal (Nieder 2002). Illusory contours as shown in Figure 1-1 are contours which appear to make up meaningful shapes perceived in fragmented visual stimuli. The ability to perceive illusory contours which help distinguish an object from its environment could be an important feature in the visual systems of organisms.

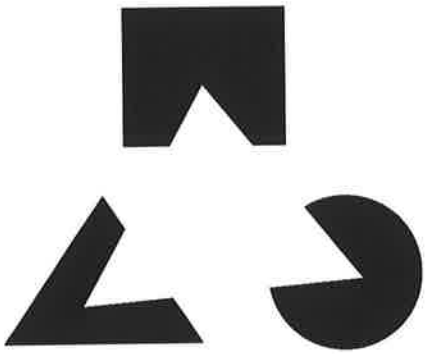

Figure 1-1: Example of illusory contours. The outlines of the solid shapes imply the presence of an opaque white triangle superimposed on the solid shapes.

Adaptation

It is common for people to experience a sudden temporary "blindness" after turning off the light in your room at night. Similarly, right after turning the light on, several seconds may pass before vision returns. These phenomena, called the light and dark adaptations respectively, have evolved in our eyes to automatically adjust their light sensitivity. This allows our eyes to accommodate not only the dynamic range within a scene but also the luminance difference between day and night of greater than six orders of magnitude (Järemo Jonson et al. 1998). Again, insects such as flies also experience similar phenomena, where the photoreceptor cells will respond with a plateau level when the retina is suddenly exposed to an extremely bright light source. Subsequent processes take place, both anatomically, as investigated by Wallcott (1975), where the rhabdomeres move further away from the facet lens to accept less light and photochemically, where the sensitivity of the photoreceptor cells is adjusted in order to accommodate the bright light level.

Insects as a Viable Model

Research into an artificial insect visual system could not only aid the development of low-cost artificial seeing systems, especially in applications such as collision avoidance devices, target tracking systems and possibly "bionic eyes" for the visually impaired, there is also the potential for gaining further insight in the areas of insect vision. In addition, the functional and physiological parallels between insect and human vision may allow the study of certain features in humans to benefit from this research. The usual method of gathering results on primates includes conducting psychophysical and *in-vivo* experiments. However, safely obtaining direct recording

of neuronal activity is a delicate procedure. With insects, direct recording is much more accessible despite their small size. As an additional advantage study insects raises fewer ethical issues.

1.2 Information Theory

Organisms in nature have evolved in such a way that their visual systems are properly tuned towards the organism's ecological purposes. This was investigated by Snyder et al. in studies on the fly *Musca* where theoretical parameters of compound eye geometry were manually optimised for the best compromise between spatial resolving power and contrast sensitivity and were found to agree closely with the geometry found in actual insect eyes (Snyder et al. 1977; Snyder et al. 1977), suggesting that biological insect eyes are optimised for these characteristics.

One important challenge faced by the visual systems of insects in their ecological environment is that of efficiently encoding the visual information present in the high dynamic range environment, within the limited neuronal bandwidth available to such biological systems. An example of an evolutionary adaptation to meet this challenge can be found in the hoverfly *Eristalis tenax*, which in addition to being excellent at hovering flight is capable of manoeuvring at an average speed of approximately $10ms^{-1}$ (Golding et al. 2001). In order to fly at such speed without colliding into any obstacles, the hoverflies need to have photoreceptors that are able to decode the high temporal frequency visual contents. Physiological studies have shown that *Eristalis tenax* has high bandwidth photoreceptors with a -3dB corner frequency at approximately 10-90 Hz (Mah et al. 2006). In comparison, a slow moving insect such as Tipulid has low

bandwidth photoreceptors with a corner frequency of approximately 7-20Hz (Laughlin et al. 1993).

1.2.1 Efficiency and Redundancy in Early Visual Processing

What are the underlying principles or algorithms that govern such robust visual systems? Attneave (1954) and Barlow (1961) suggest that highly efficient encoding of visual information is carried out in the first stage of sensory processing before transmission to higher order visual neurons by eliminating redundancy in natural visual information. Natural scenes contain a large amount of redundancies due to the non-random variation of intensity values from point to point, i.e. correlation (Simoncelli et al. 2001).

Several models have also been proposed to explain the underlying mechanisms by which biological systems efficiently compress visual information and these are largely based on maximising information theory, which assumes that the early sensory processing is aimed at maximising the information rate into the limited dynamic range of the visual channels (van Hateren 1992). This theory allows a quantitative prediction of how the sensory data are to be processed by the early sensory system. The model developed by van Hateren describes a neuronal compression algorithm that compresses visual signals into an effective functional range for the following stages. The theoretical output calculated by this model for naturalistic images was found to closely resemble results from second order neural recordings (van Hateren 1992; van Hateren 1992).

A second well-known model for second order neurons supposes that predictive coding is also used to reduce the redundancy of the scenes. Signals from the surrounding receptors can be linearly

summed and compared with the signal from the central receptor to remove strongly correlated (and hence redundant) information. Theoretical results for the receptive fields of second order neurons (in particular, the large monopolar cells of *Lucilia cuprina*) based on this model assuming predictive coding have been found to agree with experimentally measured results (Srinivasan et al. 1982).

1.3 Light Adaptation

An obvious example of redundancy reduction is light adaptation. In studying the basic characteristics of the fly photoreceptor, we must examine its response to different intensities of light, i.e. luminance. The response of biological photoreceptors to both steady-state as well as dynamic characterised stimuli such as impulse, step and white noise analysis has been well studied (Baumann 1975; Laughlin et al. 1993) and shown to exhibit several non-linear adaptive characteristics.

To characterise light adaptation in animal eyes, V Log I functions have been widely used: A V Log I function represents the response of a photoreceptor to impulse stimuli of varying intensities. In insects, the effect of the photoreceptor's light adaptation response on its V Log I function has previously been demonstrated with *Calliphora Stygia* (Matic et al. 1981). Impulse responses against several adapting backgrounds of the fly photoreceptors have been used to plot the V Log I curves of the dark and light adapted responses. For each adapting state, the V Log I curve has a sigmoidal shape and can be simply equated to a self-shunting formula (The Lipetz equation) shown in Equation 1-1.

$$\frac{V}{V_{max}} = \frac{(RI)^n}{(RI)^n + 1} \qquad \textbf{(Eq 1-1)}$$

Where I is the stimulus intensity, V is the amplitude of the photoreceptor response, V_{max} is the saturated response amplitude and R is the reciprocal of the intensity yielding a response of 50% V_{max}. The sigmoidal shape has been shown for several different insect (Eguchi et al. 1894) and vertebrate photoreceptors (Burkhardt 1994).

The adaptation to different levels of background luminance has several effects. As the adapting background luminance increases, the V Log I curve shifts towards the right. This means that for a particular stimulus, the magnitude of the response will be smaller at higher background intensities, and this represents a form of automatic gain control. As a result, the photoreceptor does not code luminance in absolute term, but rather *contrast* between the stimulus and recently experienced stimuli. Contrast coding is also highly dependent on the adapting background luminance as well as the duration of contrast stimulus. At low background intensities, photoreceptor responses are linear regardless of the contrast step durations (Juusola 1992). Upon close examination of the impulse responses of biological photoreceptors, it can be observed that with a dark-adapting background, the impulse responses are generally monophasic. For the same contrast input stimuli, if the background intensity is increased, the impulses tend to become bi-phasic. Bi-phasic impulse responses are more characteristic of a system which rejects static stimuli (i.e. are high pass filters).

Increase in the background intensity has also been shown to cause the phototransduction cascade and photoreceptor membrane to

produce smaller but, faster and increasingly accurate voltage responses to a given contrast (Juusola et al. 2001). Biological photoreceptors share the same characteristics as second order low pass filters and studies have shown that as the background intensity increases, the -3 dB corner frequency and thus frequency bandwidth increases non-linearly, eventually saturating at a particular frequency which varies between species (Juusola et al. 1995).

Different species have a different range of bandwidth capabilities in perceiving visual information (Howard et al. 1984). For instance, fast-flying diptera have fast photoreceptors with higher corner frequencies of between 50 and 107 Hz, in comparison with dark-adapted photoreceptors and those of slow flying species with corner frequencies of 10-12Hz (Laughlin et al. 1993). As a result of their high speed in coding luminance, these photoreceptors are usually over compensated with K+, which causes their impulse responses to become bi-phasic (Laughlin et al. 1993; Weckström et al. 1995).

Higher surrounding temperatures have also been found to broaden the signalling bandwidth, i.e. high body temperature offers significant advantages in visual performance of an insect (Tatler et al. 2000; Juusola et al. 2001; Franz et al. 2002). The extreme temperature-sensitivity of biological photoreceptors makes it important to maintain a constant temperature during experiments and to consider the appropriate temperature given "normal operating conditions".

At lower background intensities, even low levels of light/noise such as quantum bumps become increasingly apparent (Laughlin 1995). Thus, one hypothesis is that the variable corner frequency of the photoreceptor is beneficial in that it allows the insect to reduce the

corner frequency and thereby attenuate high frequency noise, rather than be flooded by it and unable to see anything.

As has been shown in previous studies (tested on H1 neurons of the blowfly), adaptive mechanisms in the early visual pathway are responsible in maximising information transmission to higher order neurons, e.g. motion sensitive and small target cells (Laughlin 1989; Brenner et al. 2000). Similarly, this study will show through intracellular recordings from the fly photoreceptors that the adaptations in the early visual pathway maximise information transmission, specifically for target detection neurons, with the effect of enhancing the contrast of small targets against cluttered backgrounds.

1.4 Modelling Approaches

1.4.1 Computer Vision Modelling

In most engineered systems, the higher visual functions are typically implemented through designed algorithms. Computer vision, which is a subfield of artificial intelligence, describes the programming of a computer to "understand" features in a scene or image and usually does not involve any biological inspiration in the process. Unlike photoreceptors, artificial intelligent systems typically use modern digital imaging, and sensors/amplifiers that have inherent linear properties. In this area of research, visual problems are tackled by programs or algorithms which make use of the digital processors of computers. The performance of these often computationally expensive solutions is dependent on the computing power of the hardware and the efficiency of the programming algorithms and so may not be ideal or practical for certain tasks. For example, a previous work in controlling the vision system of a robot (Breazeal

2003) involved huge amounts of computing power. Similarly, a car with "smart vision" required several desktop computers in the back of the car (Dankers et al. 2005).

Digital computer vision per se is a very wide and challenging field but will not be further discussed in this thesis, being presented here simply as an alternative to the "bio-inspired" approach to implementing higher order visual functions such as visual recognition and target tracking through biological modelling of neuronal characteristics. Unfortunately, the present understanding of such higher functions in biological systems is incomplete and thus they have not as yet been fully reproduced in an engineered system.

1.4.2 Bio-inspired Modelling

As an alternative to "traditional" computer vision, the bio-inspired approach aims to develop novel systems by taking inspiration from nature. It generally does not aim to accurately reproduce the complete behaviour of the biological system, focusing instead on certain useful features of interest to a real-world application. The implementation of these features also does not need to be perfectly faithful to the biological system but may be customised or supplemented in order to improve the application performance. One possible drawback to this approach is that although it may be well suited for a specific application, it may not be as robust as the biological system and may malfunction under certain conditions.

A well-known example of a bio-inspired application involves an autonomous robot that uses a motion detection algorithm similar to that of insects in order to solve a challenging navigational task such

as obstacle avoidance (Franceschini et al. 1992). Other examples include automated systems which make use of optical flow encoding to perform hover stabilisation and landing (Barrows et al. 2004), in a similar manner to insects.

Many silicon chips based on analogue Very Large Scale Integration (aVLSI) circuits have also been designed over the past decade in order to emulate specific features of biological neurons such as motion detection and small target detection (Tanner et al. 1988; Etienne-Cummings et al. 1993; Sarpeshkar et al. 1993; Kramer et al. 1995; Liu 1996; Sarpeshkar et al. 1996; Kramer et al. 1997; Yakovleff et al. 1998; Liu 1999; Delbrück et al. 2004). One of the earliest motion detector chips was by Tanner and Mead (1984), employing latches to store digitised samples of images for later comparison with analogue images and performing multiplication using switched current mirror design. A later sensor by Delbrück (1993) used a unidirectional delay line as a tuned filter which needs to be adjusted for particular velocities, thus requiring multiple detectors to measure over a range of velocities. Studies have shown, however, that the need for velocity tuning can be eliminated by a front-end which provides automatic gain adjustment in a similar manner to insect photoreceptors, thus improving the velocity estimation of the detector (O'Carroll et al. 2006). Pant and Higgins (2004) constructed a chip using a modified version of Delbrück's (1996) adaptive photoreceptor as a front-end to an elaborated Reichardt Correlator to perform target-tracking in cluttered scenes. Several other designs based on a Reichardt Correlator have also been developed by Harrison and Koch (1999; 2000), incorporating biologically-inspired circuit non-linearities which allow for improved performance in noisy environments. Although there have been various VLSI chips such as these designed for potential use in real-

world applications, few have actually been applied. One of the main issues has been their limited ability to perform reliably in a wide range of natural environments rather than under specific conditions.

1.4.3 Biomimetic Modelling

Since the main aims of this study include both developing a simple yet functional photoreceptor model and improving the understanding of the visual systems of insects, a biomimetic approach has been taken. A biomimetic approach is one that mimics all the characteristics of a biological system as faithfully as possible, without taking into consideration possible redundancies. This starts from a detailed physiological understanding of the biological system and its characteristics, typically expressed through mathematical models. By faithfully emulating the biological system with a detailed understanding of its function, one may develop a system that provides a simple solution to many problems.

Modelling Early Processing

Several mathematical models exist to mimic the neurons of the fly eyes. Payne and Howard (1981) developed a simple log-normal model to emulate photoreceptor responses. However this model mimics only one important feature of the biological photoreceptors, i.e. linear temporal response. Juusola (1995) developed a model widely used in higher order neural modelling that makes use of complex mathematical equations (Volterra series, cascades of linear and non-linear stages) to model the dynamic non-linearity of the insect photoreceptor as measured by randomly modulated light stimuli. Again, the emphasis is only on the non-linear compression feature of the biological photoreceptors, neglecting the importance of non-linear adaptation.

Delbrück and Mead (1996) have recently designed and implemented an analog VLSI chip of a photoreceptor model incorporating several non-linear properties of biological photoreceptors such as light-adaptation and logarithmic encoding. However, this design lacks other useful non-linear features such as a variable frequency response (changing the corner frequencies of the system for better signal-to-noise ratio). Furthermore, the circuit has not been thoroughly tested under dynamic conditions and thus may or may not perform properly in a complex real-world environment.

By using the same photoreceptor model described above as the front-end visual processing, our own laboratory has implemented a bio-inspired silicon chip to mimic higher order neuron (insect motion detection) in the insect visual pathway (Shoemaker et al. 2001). The adaptive photoreceptor circuit outputs were fed to the cascaded higher order neuron stages (motion sensitive neurons) that integrated with contrast adaptation feature. This feature is important in regulating the contrast output of the chip, i.e. to avoid possible hard saturation. However, due to the limitations of the technology, there are issues with device mismatches in implementing such a multi-pixel system.

Perhaps the best model to date for non-linear dynamics of the fly photoreceptor is that of van Hateren and Snippe (van Hateren et al. 2001). This parametric model uses a cascade of two dynamic divisive feedback stages and one static non-linear stage. The output of this model was shown to be highly correlated to that of the actual photoreceptors in response to natural image scenes. In addition, frequency domain analysis (coherence) also showed that the model is a great mimic of the biological photoreceptors. However, this model

takes no account of the change in temporal coding between day/night, and hence is not "optimal" in terms of information theory.

Biomimetic Models for Higher Order Neurons

One of the first parametric models widely used in many neuromorphic motion detector chip designs is the Classic Reichardt Correlator model (Reichardt 1961). This design uses a linear photodetector as the front-end processing, with a delay (low pass filter) and a correlator (multiplier) to mimic the motion sensitive neurons of insects. This model performs very well with standard characterised stimuli input such as sinusoidal gratings, pulses and steps.

An area of particular interest is modelling higher order neurons such as the group of neurons (small target neurons) in the lobula plate of an insect's eye which only activate whenever there is a small target which falls in the region of interest of the insect's eyes. For instance, Higgins and Pant (2004) have recently developed an elaborated version of the small-target system model of Reichardt et al. (1989) that may be used to allow a simulated fly to track a small moving target in a cluttered background. This could have various potential applications in visual target-tracking.

1.5 Natural Scenes

With current technology, it is impossible to study the fly's visual system intracellularly while having the subject manoeuvre freely in their natural habitat and environments. Why should we use natural environments and not just characterised stimuli such as pulses, steps and white noise? Dynamic naturalistic stimuli are very

important in characterising and evaluating the robustness of a non-linear system (Niven et al. 2004). If we were to take a snap shot of a natural scene and statistically analyse it, we would find that the scene possesses substantial spatiotemporal correlations, which means that there is a lot of redundancy in the image. This has been shown to have a significant effect, as the earliest mathematical model of a biological motion detector, i.e. the classic Reichardt Correlator (Reichardt 1961) fails to perform as a velocity estimator when natural scenes are used as input stimuli, despite showing good correlation to the biological systems using standard characterised stimuli (Dror et al. 2001). Interestingly recent work on fly HS neurons shows that they behave very differently when stimulated with natural scenes and are excellent velocity coders (Shoemaker et al. 2005).

While recent work highlights the importance of appropriate natural scenes, there are numerous technical difficulties in working with such stimuli. Instead of trying to develop a technology that would allow scientists to perform experiments in the real-world, alternative approaches have been used to work around this limitation while at the same time producing similar results. For example, by creating a flight arena in which the fly sits (stationary) and natural scenes are artificially generated using computer displays or Light Emitting Diodes (LED) (Horstmann et al. 2000; Schuster et al. 2002). To generate computer displays, software packages have previously been developed, such as *Vision Egg* (www.visionegg.org), which is a stable and reliable open source program that harnesses the power of current consumer graphic cards to produce visual stimuli of research quality using no specialised hardware beyond a relatively recent computer and graphic card. To reconstruct naturalistic stimuli using LEDs, a single-pixel photodetector has been used to

record the dynamic natural luminance along outdoor flight paths to evaluate the motion-sensitive neurons in blowflies (van Hateren 1997).

References

Anstis, S., F. A. J. Verstraten and G. Mather (1998). "The motion aftereffect." Trends in Cognitive Sciences **2**(3): 111-117.

Attneave, F. (1954). "Some informational aspects of visual perception." Psychol Rev **61**: 183-193.

Barlow, H. B. (1961). "Possible principles underlying the transformations of sensory messages." Sensory communication: 217–234.

Barrows, G. L., J. S. Chahl and M. V. Srinivasan (2004). Biomimetic visual sensing and flight control. TTVI Vanguard, Georgia Tech Conference Center and Hotel Atlanta, Georgia.

Baumann, F. (1975). Electrophysiological properties of the honey bee retina. The Compound Eye and Vision of Insects. London, Oxford University Press: 53-74.

Breazeal, C. (2003). "Emotion and sociable humanoid robots." Int. J. Human-Computer Studies **59**: 119-155.

Brenner, N., W. Bialek and R. R. de Ruyter van Steveninck (2000). "Adaptive rescaling maximizes information transmission." Neuron **26**: 695-702.

Burkhardt, D. A. (1994). "Light adaptation and photopigment bleaching in cone photoreceptors *in situ* in the retina of the turtle." Journal of Neuroscience **14**(3): 1091-1105.

Collett, T. S. and M. F. Land (1975). "Visual control of flight behaviour in the hoverflySyritta pipiens L." Journal of Comparative Physiology A **99**(1): 1-66.

Dankers, A., N. Barnes and A. Zelinsky (2005). Active vision for road scene awareness. Intelligent Vehicles Symposium, Proceedings IEEE, IEEE.

Delbrück, T. (1993). "Silicon retina with correlation-based velocity-tuned pixels." IEEE Trans. Neural Network **4**: 529-541.

Delbrück, T. and S. C. Liu (2004). "A silicon early visual system as a model animal." Vision Research **44**: 2083-2089.

Delbrück, T. and C. A. Mead (1996). Analog VLSI phototransduction by continuous time, adaptive, logarithmic photoreceptor circuits. Pasadena, California, California Institute of Technology Computation and Neural Systems Program: 30.

Douglass, J. K. and N. J. Strausfeld (1995). "Visual motion detection circuits in flies: peripheral motion computation by identified small-field retinotopic neurons." Journal of Neuroscience **15**: 5596-5611.

Douglass, J. K. and N. J. Strausfeld (1996). "Visual motion-detection circuits in flies: Parallel direction- and non-direction- sensitive pathways between medulla and lobula plate." Journal of Neuroscience **16**(15): 4551-4562.

Dror, R. O., D. C. O'Carroll and S. B. Laughlin (2001). "Accuracy of velocity estimation by Reichardt correlators." J. Opt. Soc. Am A **18**(2): 241-251.

Duffy, C. J. and R. H. Wurtz (1981). "Sensitivity of MST neurons to optic flow stimuli. II. Mechanisms of response selectivity revealed by small-field stimuli." J Neurophysiol **65**(6): 1346-1359.

Duffy, C. J. and R. H. Wurtz (1991). "Sensitivity of MST neurons to optic flow stimuli. I. A continuum of response selectivity to large-field stimuli." J Neurophysiol **65**: 1329-1345.

Egelhaaf, M., K. Hausen, W. Reichardt and C. Wehrhahn (1988). "Visual course control in flies relies on neuronal computation of object and background motion." Trends Neurosci **11**: 351-358.

Egelhaaf, M., R. Kern, H. G. Krapp, J. Kretzberg, R. Kurtz and A. K. Warzecha (2002). "Neural encoding of behaviourally relevant visual-motion information in the fly." Trends in Neurosciences **25**(2): 96-102.

Eguchi, E. and T. Horikoshi (1894). "Comparison of stimulus-response (V-log I) functions in five types of lepidopteran compound eyes (46 species)." Journal of Comparative Physiology A **154**(1): 3-12.

Etienne-Cummings, R., S. Fernando, N. Takahashi, V. Shtonov, J. V. d. Spiegel and P. Mueller (1993). A new temporal domain optical flow measurement technique for focalplane VLSI implementation. Computer Architectures for Machine Perception.

Franceschini, N., J. M. Pichon and C. Blances (1992). "From insect vision to robot vision." Philos. Trans. R. Soc. London,Ser **B337**: 283-294.

Franceschini, N., J. M. Pichon and C. Blances (1992). "From insect vision to robot vision." Phil. Trans. R. Soc. Lond. B **337**: 283-294.

Franz, A. and B. Ronacher (2002). "Temperature dependence of temporal resolution in an insect nervous system." Journal of Comparative Physiology A **188**: 261-271.

Golding, Y. C., A. R. Ennos and M. Edmunds (2001). "Similarity in flight behaviour between the honeybee Apis mellifera (Hymenoptera: apidae) and its presumed mimic, the dronefly Eristalis tenax (Diptera: syrphidae)." Journal of Experimental Biology **204**(1): 139-145.

Gronenberg, W. and N. J. Strausfeld (1990). "Descending neurons supplying the neck and flight motor of Diptera: physiological and anatomical characteristics." J. Comp. Neurol **302**(4): 973-991.

Harris, R. A., D. C. O'Carroll and S. B. Laughlin (2000). "Contrast gain reduction in fly motion adaptation." Neuron **28**: 595-606.

Harrison, R. R. and C. Koch (1999). "A robust analog VLSI motion sensor based on the visual system of the fly." Auton. Robots **7**: 221-224.

Harrison, R. R. and C. Koch (2000). "A robust analog VLSI Reichardt motion sensor." Analog Integrated Circuits and Signal Processing **24**: 213-229.

Hausen, K. (1982). "Motion sensitive interneurons in the optomotor system of the fly." Biol. Cybern. **45**(2): 143-156.

Higgins, C. M. and V. Pant (2004). "An elaborated model of fly small-target tracking." Biol. Cybern. **91**: 417-428.

Horstmann, W., M. Egelhaaf and A. K. Warzecha (2000). "Synaptic interactions increase optic flow specificity." European Journal of Neuroscience **12**: 2157-2165.

Howard, J., A. Dubs and R. Payne (1984). "The dynamics of phototransduction in insects." Journal of Comparative Physiology A **154**: 707-718.

Ibbotson, M. R., T. Maddess and R. DuBois (1991). "A system of insect neurons sensitive to horizontal and vertical image motion connects the medulla and midbrain." Journal of Comparative Physiology A **169**(3): 355-367.

Järemo Jonson, A. C., M. F. Land, D. C. Osorio and D.-E. Nilsson (1998). "Relationships between pupil working range and habitat luminance in flies and butterflies." J. comp. Physiol. A **182**: 1-9.

Juusola, M. (1992). "Linear and non-linear contrast coding in light-adapted blowfly photoreceptors." Journal of Comparative Physiology A **172**: 511-521.

Juusola, M. (1995). "Nonlinear models of the first synapse in the light-adapted fly retina." Journal of Neurophysiology **74**(6): 2538-2547.

Juusola, M. and R. C. Hardie (2001). "Light Adaptation in *Drosophila* Photoreceptors: I. Response Dynamics and Signalling Efficiency at 25°C." J. Gen. Physiol. **117**: 3-25.

Juusola, M. and R. C. Hardie (2001). "Light Adaptation in *Drosophila* Photoreceptors: II Rising Temperature Increases the Bandwith of Reliable Signalling." J. Gen. Physiol. **117**: 27-41.

Juusola, M., R. O. Uusitalo and M. Weckström (1995). "Transfer of graded potentials at the photoreceptors-interneuron synapse." J. Gen. Physiol. **105**: 117-148.

Kramer, J., R. Sarpeshkar and C. Koch (1995). An analog VLSI velocity sensor. IEEE International Symposium on Circuits and Systems.

Kramer, J., R. Sarpeshkar and C. Koch (1997). "Pulse-based analog VLSI velocity sensors." IEEE Trans. Circuits and Systems II **44**: 86-101.

Laughlin, S. B. (1989). "A role of sensory adaptation in the retina." J. exp. Biol. **146**: 39-62.

Laughlin, S. B. (1995). "Matched flitering by a photoreceptor membrane." Vision Research **36**(11): 1529-1541.

Laughlin, S. B. and M. Weckström (1993). "Fast and slow photoreceptors - a comparative study of the functional diversity of coding and conductances in the diptera." Journal of Comparative Physiology A **172**: 593-609.

Liu, S.-C. (1996). Silicon Model of Motion Adaptation in the Fly Visual System. Proceedings of the 3rd UCSD-Caltech Symposium on Neural Computation.

Liu, S.-C. (1999). "Silicon Retina with Adaptive Filtering Properties." Analog Integrated Circuits and Signal Processing **18**: 1-12.

Mah, E. L., R. S. A. Brinkworth and D. C. O'Carroll (2006). "Implementation of an elaborated neuromorphic model of a biological photoreceptor." Biological Cybernetics **submitted on Dec 2006**.

Matic, T. and S. B. Laughlin (1981). "Changes in the intensity-response function of an insect's photoreceptors due to light adaptation." Journal of Comparative Physiology A **145**: 169-177.

Nieder, A. (2002). "Seeing more than meets the eye:processing of illusory contours in animals." Journal of Comparative Physiology A **188**(4): 249-260.

Niven, J. E., M. Vähäsöyrinki, M. Juusola and A. S. French. (2004). "Interactions between light-induced currents, voltage-gated currents, and input signal properties in Drosophila photoreceptors." J Neurophysiol **91**: 2696-2706.

Nordström, K., P. D. Barnett and D. C. O'Carroll (2006). "Insect detection of small targets moving in visual clutter." PLoS Biol. **4**(3): e54.

Nordström, K. and D. C. O'Carroll (2006). "Small object detection neurons in female hoverflies." Proceedings of the Royal Society B **273**(1591): 1211 - 1216.

O'Carroll, D. C., P. D. Barnett, E. L. Mah, K. Nordström and R. S. A. Brinkworth (2006). A Neuromorphic Model For A Robust, Adaptive Photoreceptor Reduces Variability In Correlation Based Motion Detectors. Brain Inspired Cognitive Systems, Lesbos, Spain.

Pant, V. and C. M. Higgins (2004). "A biomimetic VLSI architecture for small target tracking." IEEE Transactions on Circuits and Systems I **12**: 2384-2394.

Payne, R. and J. Howard (1981). "Response of an insect photoreceptor: a simple log-normal model." Nature **290**(5805): 415-416.

Reichardt, W. (1961). Autocorrelation, a principle for the evaluation of sensory information by the central nervous system, in principles of sensory communications. New York, John Wiley.

Reichardt, W., M. Egelhaaf and A. K. Guo (1989). "Processing of figure and background motion in the visual-system of the fly." Biol. Cybern. **61**: 327-345.

Ruffier, F. and N. Franceschini (2005). "Optic flow regulation:the key to aircraft automatic guidance." Robotics and Autonomous Systems **50**(4): 177-194.

Sarpeshkar, R., W. Bair and C. Koch (1993). "Visual motion computation in analog VLSI using pulses." Advances in Neural Information Processing Systems **5**: 781-788.

Sarpeshkar, R., J. Kramer, G. Indiveri and C. Koch (1996). Analog VLSI architectures for motion processing: from fundamental limits to system applications, Proceedings of the IEEE.

Schuster, S., R. Strauss and K. G. Götz (2002). "Virtual-reality techniques resolve the visual cues used by fruit flies to evaluate object distances." Current Biology **12**: 1591-1594.

Shoemaker, P. A., D. C. O'Carroll and A. D. Straw (2005). "Velocity constancy and models for wide-field visual motion detection in insects." Biol. Cybern. **93**(4): 275-287.

Shoemaker, P. A., D. D. O'Carroll and A. D. Straw (2001). Implementation of Visual Motion Detection with Contrast Adaptation. Electronics and Structures for MEMS II, Adelaide, Australia, Proceedings of SPIE.

Simoncelli, E. P. and B. A. Olshausen (2001). "Natural image statistics and neural representation." Annual Review of Neuroscience **24**: 1193-1216.

Snyder, A. W., S. D.G. and S. B. Laughlin (1977). "Spatial information capacity of compound eyes." Journal of Comparative Physiology A **116**: 183-207.

Snyder, A. W., S. B. Laughlin and D. G. Stavenga (1977). "Information capacity of eyes." Vision Research **17**: 1163-1175.

Srinivasan, M. V., J. S. Chahl, K. Weber, S. Venkatesh, M. G. Nagle and S. W. Zhang (1999). "Robot navigation inspired by principles of insect vision." Robotics and Autonomous Systems **26:**: 203–216.

Srinivasan, M. V., J. S. Chahl and S. W. Zhang (1997). "Robot navigation by visual dead-reckoning: Inspiration from insects." International Journal of Pattern Recognition and Artificial Intelligence (IJPRAI) **11**(1): 35-47.

Srinivasan, M. V. and D. R. Dvorak (1979). "The waterfall illusion in an insect visual system." Vision Research **19**(12): 1435-1437.

Srinivasan, M. V., S. B. Laughlin and A. Dubs (1982). "Predictive coding: A fresh view of inhibition in the retina." Proceedings of the Royal Society of London **216**(1205): 427-459.

Srinivasan, M. V., S. W. Zhang, J. S. Chahl, G. Stange and M. Garratt (2004). "An overview of insect-inspired guidance for application in ground and airborne platforms." Journal of Aerospace Engineering **218**(6): 375-388.

Tanner, J. and C. Mead (1984). "A correlating optical motion detector." MIT Advanced Research in VLSI: 57-64.

Tanner, J. and C. Mead (1988). "An integrated analog optical motion sensor." IEEE Press: 59-87.

Tatler, B., D. C. O'Carroll and S. B. Laughlin (2000). "Temperature and the temporal resolving power of fly photoreceptors." Journal of Comparative Physiology A **186**: 399-407.

Vaina, L. M., J. Solomon, S. Chowdhury, P. Sinha and J. W. Belliveau (2001). "Functional neuroanatomy of biological motion perception in humans." Neurobiology **90**(28): 11656-11661.

van Hateren, J. H. (1992). "Real and optimal neural images in early vision." Nature **360**: 68-69.

van Hateren, J. H. (1992). "Theoretical predictions of spatiotemporal receptive fields of fly LMCs, and experimental validation." Journal of Comparative Physiology A **171**: 157-170.

van Hateren, J. H. (1992). "A theory of maximizing sensory information." Biol. Cybern. **68**: 23-29.

van Hateren, J. H. (1997). "Processing of natural time series of intensities by the visual system of the blowfly." Vision Research **37**: 3407-3416.

van Hateren, J. H. and H. P. Snippe (2001). "Information theoretical evaluation of parametric models of gain control in blowfly photoreceptor cells." Vision Research **41**: 1851-1865.

van Hateren, J. H. and H. P. Snippe (2006). "Phototransduction in primate cones and blowfly photoreceptors: different mechanisms, different algorithms, similar response." Journal of Comparative Physiology A **192**: 187-197.

Wallcott, B. (1975). Anatomical changes during light-adaptation in insect compound eyes. The Compound Eye and Vision of Insects. London, Oxford University Press: 20-33.

Weckström, M. and S. B. Laughlin (1995). "Visual ecology and voltage-gated ion channels in insect photoreceptors." Trends in Neurosciences **18**: 17-21.

Yakovleff, A. J. S. and A. Moini (1998). "Motion perception using analog VLSI." Analog Integrated Circuits and Signal Processing **15**: 183-200.

2

Chapter 2: Dimmable Voltage-Controlled High Current LED Driver System for Visual Science Experiments

ENG-LENG MAH, RUSSELL SA BRINKWORTH AND DAVID C. O'CARROLL
Discipline of Physiology, School of Molecular and Biomedical Science and the Centre for Biomedical Engineering, The University of Adelaide SA 5005, Australia.

Abstract

Recent advances in light emitting diode (LED) technology make it possible to produce visual stimuli that are bright enough to represent real-world luminance levels. However, such technology requires a stable high current driver to constantly supply the necessary currents to the LED. We have designed and implemented a fully dimmable multi-channel voltage-controlled high current LED driver system that is capable of running multiple ultra-bright LEDs simultaneously during experiments. The performance of the system was found to be highly robust and reliable for the purpose of visual physiological experiments. When coupled with appropriate LEDs and driven by a 16-bit control signal, the usable dynamic range exceeds 120dB with a maximum luminance of approximately 70 000cd/m^2, an accuracy in excess of 0.1cd/m^2 at the low end of the luminance range and a response time less than 0.25ms.

Key words: High Current Amplifier, LED Driver, Voltage-Controlled Current Source.

Correspondence to: Eng-Leng Mah (email: eng.mah@adelaide.edu.au)

2.1. Introduction

Insect photoreceptor cells are capable of coding visual information under various lighting conditions (Wuff et al. 1975; Laughlin et al. 1978; Weckström et al. 1995). The response of these cells is highly non-linear, displaying luminance adaptation to background intensity for optimising the light information perceived from high dynamic range real-world environments before transmission to higher order neurons via limited bandwidth channels (Snyder et al. 1977; Snyder et al. 1977; van Hateren 1992). Physiological studies suggest that the non-linear adaptive feature of a photoreceptor cell improves the visual coding power of the photoreceptor by approximately 2-3 times (giving a total signalling range of 8 log units), depending on species (Matic et al. 1981; Laughlin 1989). Thus, in order to thoroughly investigate the capability and operation of photoreceptors there is a need to devise a system that is capable of artificially generating natural scenes with a large luminance dynamic range. Such a system must be laboratory based since it is not feasible to conduct intracellular electrophysiological experiments outdoor with subjects freely manoeuvring in the natural environments.

Recently, the usage of light-emitting diodes (LED) has become ubiquitous in the field of vision science research, due to their high performance and reliability. Unlike the previously commonly-used Xenon Arc Lamps (Grum 1968), which require complicated and expensive systems to run, LEDs have a relatively long lifespan and consume only a fraction of the power. They are also cheap and commercially available, which makes them an ideal low-cost light

source for experiments in vision laboratories. The typical conventional white bright LED (5mm) has a current rating of approximately 100mA and has the capability to emit a maximum of 10cd (Nichia Corporation).

For a greater than 10 times increase in maximum light level and only a small trade off in power consumption, Luxeon™ has introduced an ultra-bright LED called the Luxeon™ Star LED. This LED is estimated to have a very long operating life (up to 100k hours) and is packaged with a heat sink mounted at its back for maximum heat dissipation (better performance). It has a maximum current rating at 350mA and a maximum light-producing capability of 120cd, making this LED the best candidate for many vision experiment applications.

Since the LED consumes an appreciable amount of current (350mA maximum) to generate maximum brightness, a stable high current LED driver is required. There are many companies that manufacture high current LED drivers specifically for the Luxeon™ Star LEDs. Most of them are capable of producing a constant high-current source but none are sufficiently stable to act as a current source when operated at low levels, i.e. they are not 100% dimmable. Such instability in dimming is a particularly undesirable imperfection in vision experiments. Table 2-1 shows a list of the standard commercial LED drivers that were tested and proven to not meet our requirements.

Driver	Model	Size	Lowest Limit*	Accuracy	Cost
Integrated Illumination Systems	Smart Dimming Driver	Small	1-2%	High	mid
LUXDRIVE™	BUCKPUCK3021	Small	1-2%	High	mid
OPTOTRONIC®	OTDIM	Medium	0.5-1%	High	mid
Linear Technology	LT1932	Very small (SMD)	0.5-1%	High	low
Agilent Programmable DC Power Supplies	363xA-Series	Large	0.5-1%	Very High	very high

*Lowest limit – A stability point where anything dimmed below this limit starts to display unwanted flickers.

Table 2-1: A list of standard commercial LED drivers that failed to meet the requirements of our LED driver system due to poor signal stability at low light levels (<1%).

Most of these LED drivers claimed to be fully dimmable but in actual fact were not. At low light levels, the output current started to oscillate and caused a flicker in the LED (the frequency of the flicker was directly proportional to the output current of the driver). Such flickers in the light source are highly undesirable in photoreceptor experiments since the photoreceptors can potentially pick up frequencies below 200Hz, depending on species (Howard 1981).

In this paper, we will discuss the design and implementation of a customised high current LED driver that is capable of running multiple Luxeon™ Star LEDs simultaneously. The brightness of each of the driven LEDs was carefully calibrated with a light detector from a digital camera (Nikon D-70) and a low noise, high precision current amplifier (PDA750, Terahertz Technology Inc™).

2.2 Methods

The aforementioned problems with commercially available LED drivers led us to the decision to custom build our own LED driver. A multi-channel voltage-controlled dimmable LED Driver was implemented using standard discrete electronic components. The driver circuit was initially built on a breadboard for testing and prototyping purposes. The final working circuit was then implemented on vero boards and housed in a plastic box.

2.2.1 Specifications

The prototype LED driver was capable of supplying current to three LEDs (Luxeon™ Star) simultaneously. The driver was powered from a ±15V power supply and had a maximum current rating of 1.5A. Each channel had its own port for controlling the output current of each driver to its corresponding LED. Heat sinks were attached to some discrete components (OPA 547T) in order to reduce any thermal hysteresis at the output of the driver.

The completed circuit was enclosed in a plastic box and a +12V fan was mounted to ensure that all the discrete components in the box were operating at sufficiently low temperature. At the rear of the plastic box, three tactile switches were available for turning individual channels on or off. Figure 2-1 shows the customised LED driver in a plastic box.

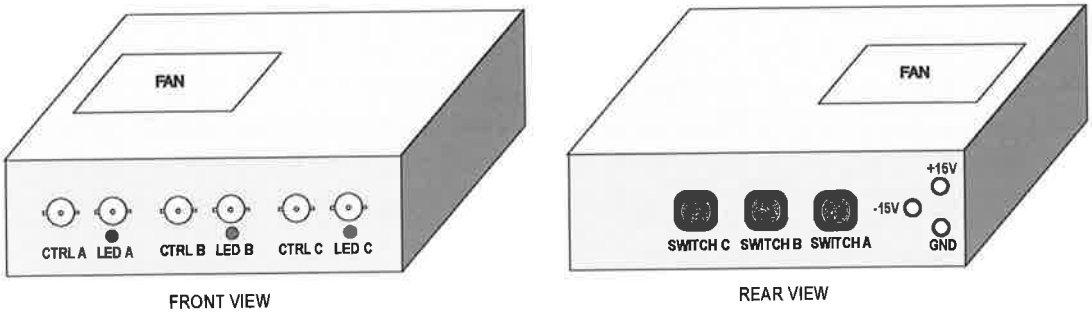

Figure 2-1: Customised LED driver. Front *(left)* and rear view *(right)* of the customised three-channel LED driver. CTRL A, B and C were the input ports for the control signals of the Luxeon™ Star LEDs connected to output ports A, B and C respectively. Each channel had a dedicated switch at the rear of the box and was powered with ±15VDC.

2.2.2 Circuit Implementation

This driver was implemented based on a voltage controlled voltage source (VCVS) configuration using standard electronic discrete components. Figure 2-2 shows the circuit diagram of the three-channel LED driver. The LED (green) was initially tested with a standard voltage power supply to observe the luminance output against voltage input. The LED started to display a dimly noticeable (measured using light detector) amount of light at an input voltage of about 1.6V. The LED then reached its maximum brightness with an input voltage of approximately 3.3V.

A custom-written LabVIEW® software module was used to communicate with a 16-bit data acquisition card (NI PCI6221, National Instruments™) to send control signals ranging from -10V – +10V to drive the LED. Since the LED only works in the range of 1.6V – 3.3V, a simple linear conversion circuit was designed based on equation 2-1 to fully utilise the dynamic range of the data acquisition card to maximise signal resolution.

$$Output = \frac{CS}{11.76} + 2.54V \qquad \textbf{(Eq 2-1)}$$

CS is a control signal from the data acquisition card which ranges from -10V to 10V. These signals were de-gained using an inverting amplifier and constantly summed with a constant voltage of 2.54V. The de-gained signals were then inverted in sign before being fed to a subsequent unity gain amplifier. This simple unity gain voltage amplifier (standard non-inverting amplifier configuration) was designed and implemented using a high current operational amplifier (OPA 547T) and a couple of resistors in order to drive the LED.

2.2.3 Calibration

The LED driver system was carefully calibrated using a photodiode amplifier (PDA750, Terahertz Technology Inc™). The calibrated system was then mapped to a real world luminance values, cd/m^2 by use of a camera spot meter (Nikon D70).

Linearisation of the LED Driver System

LEDs are semiconductors that produce light with luminance linearly proportional to the input current source. Since our LED driver was designed to be a voltage-controlled voltage source, the output luminance of the system varied non-linearly with respect to the control signal and hence the system had to be linearised. This involved measuring the output current using the photodiode amplifier and recording the relationship between the output current and input control signals, to be used in a look-up table for the purpose of producing a linear output. The new linearised system had its control signal defined in terms of percentage and output luminance defined in terms of current.

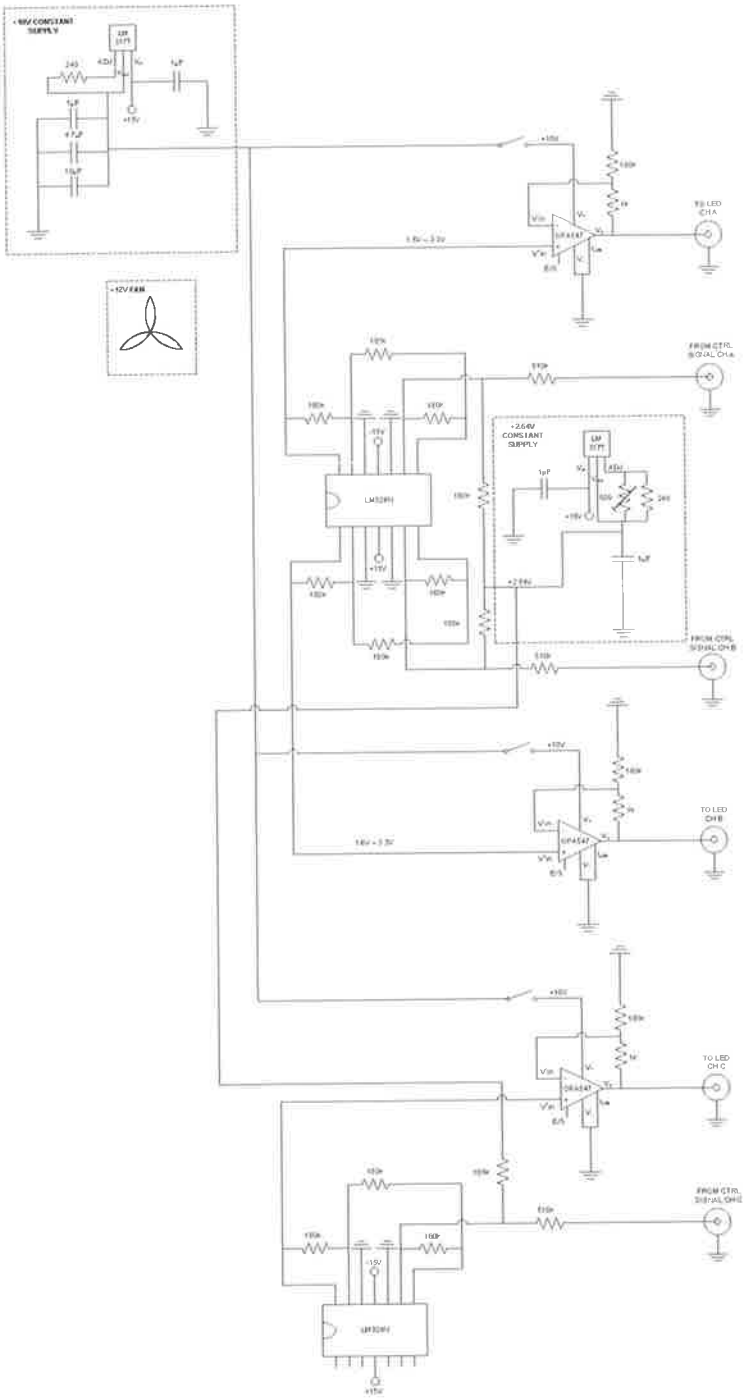

Figure 2-2: An electronic schematic diagram of a three-channel LED driver. The control signal from the data acquisition system was connected to the input port "From Ctrl Signal Ch A". A low noise operational amplifier was used in order to perform the operation shown in Eq 2-1 to provide the rescaled version (higher dynamic range) of the control signal prior to transmission to the high current amplifier (OPA 547T). An output port at "To LED Ch A was

connected to the LED to produce light output. The remaining two channels (Ch B and Ch C were duplicates of Ch A.

Brightness Measurement

There were several methods of measuring the real-world luminance (cd/m^2) of the LED driver system and the cheapest way was to use the light meter in a conventional digital camera (Nikon D-70). The camera was preset with an ISO of 200, spot-metering mode and infinite focus. It was then mounted on a tripod and by holding the capture button of the camera half-way, the light meter of the camera measured the luminance level of the object that was in the middle of the viewfinder of the camera. The light meter had to be fixed at 0EV level to indicate that it is measuring the right exposure value and this could be done by adjusting the combinations of aperture size and shutter speed of the camera. From the values obtained, the corresponding brightness of the LED could then be converted to unit of luminance, cd/m^2 based on the following equations (The photometric system)

$$Ev = Av + Tv = Sv + Bv \qquad \textbf{(Eq 2-2)}$$

Where:

$$Ev = ExposureValue$$

$$Av = ApertureValue = \frac{\ln N^2}{\ln 2}$$

$$Tv = TimeValue = \frac{\ln(t^{-1})}{\ln 2}$$

$$Sv = SpeedValue = \frac{\ln(0.3S)}{\ln 2}$$

$$Bv = BrightnessValue = \frac{\ln Bfl}{\ln 2}$$

N is the f-stop number of the camera lens, t is the time in seconds of the shutter speed, Bfl is the object luminance in foot-Lamberts, Bv is the object brightness in cd/m^2 and S is the ISO speed of the camera film.

Figure 2-3 shows the non-linear relationship between the input control signal and the output intensity of the LED driver system. At low input control signal levels (between -8.37V and -2.52V), increasing the control signal voltage only caused minor increments in output intensity, i.e. more accurate control of the luminance was available in this area. As soon as the control signals increased from -2.52V to 1.47V, the output intensities increased drastically in a non-linear fashion. From 1.47V to 8.43V, the output looked very close to a linear response.

2.3 Results

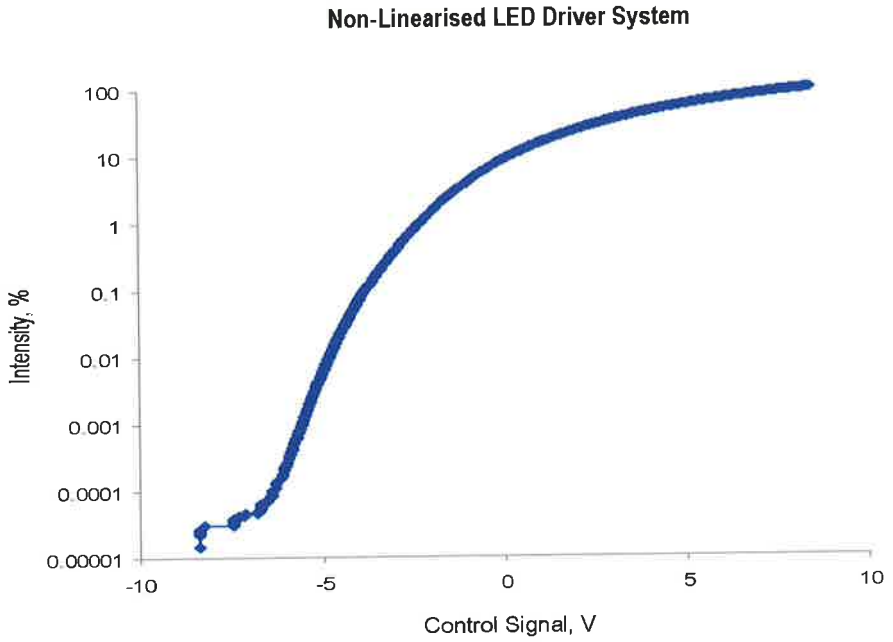

Figure 2-3: Output of the non-linearised LED driver system. The system produced no output when the control signal was at -8.37V and maximum output when the control signal was at 8.43V.

Figure 2-4 *(Right Axis)* illustrates the linearised output of the LED driver system where the current measured had a linear relationship with the input control signal. The lowest current measured was at 0nA while the highest current was measured at approximately 26μA. On the left axis of the same figure the relationship between the brightness of the LED (cd/m²) against the linearised control signal (%) is shown. The calculated values based on equation 2-2 suggest a linear relationship between the brightness values and the control signal input. A simple linear fitted curve algorithm was used to fit a curve to the calculated raw data. By having this fitted curve equation, The real world brightness values of any type of stimuli can be easily retrieved. The lowest displayable brightness value was calculated to be approximately 0.07cd/m² while the highest (based on extrapolation of the fitted curve) was more than 70 000cd/m².

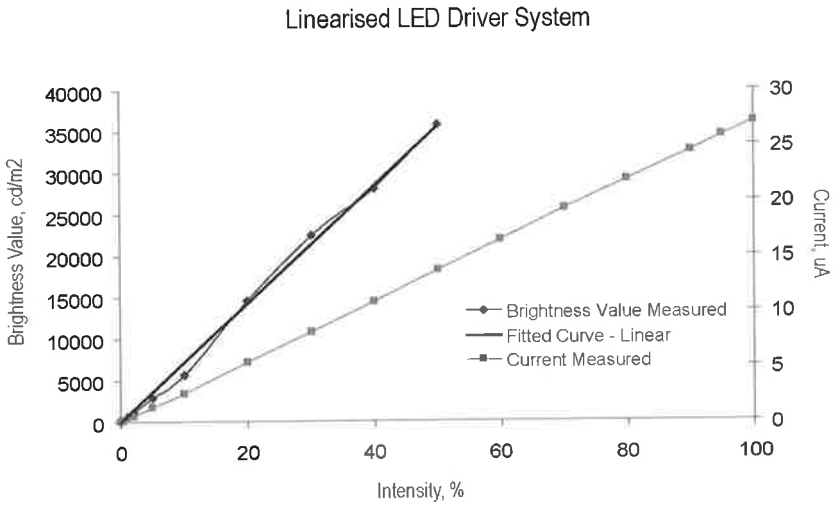

Figure 2-4: *(Right Axis)* Output of a linearised LED driver system. The output current measured was directly proportional to the percentage of the input intensity (control signals). Measurements were taken on a logarithmic scale starting from 0% to 100% of the control signal input. *(Left Axis)* Linear mapping of the equivalent real world brightness value based on the percentage of the input intensity. A simple linear equation was fitted to the raw data with an equation Bv (cd/m²) = 713.43*(control signal). The fitted curve had a high correlation value of $r^2>0.99$

2.4 Discussions

The LED driver system was implemented using standard discrete electronic components and the Luxeon™ Star LED was used as the front-end of the system to emit light. Calibrations of the system had confirmed that the system was capable of producing light ranges from 0.07 – 70 000cd/m². By linearising the system (see Figure 2-3), a simple equation was found for converting the control signal in percentage to actual brightness values in cd/m² (Bv =713.43*control signal).

Such a reliable system provides a cheap solution to many visual experiments, particularly for those that require high intensity playback whilst having full control over the system. Additionally, the low current input (<20mA) of the control signal ports for the driver also allow it to be controlled by any standard type of data acquisition system.

Several electrophysiological experiments have been successfully performed using the LED driver system as a means of displaying light stimuli. The system is able to display characterised (pulse, step and white noise) and dynamic (naturalistic) stimuli for the purpose of our experiments (Mah et al. 2005).

2.4.1 Light Emitting Diode (LED)

The Luxeon™ Star LED has the capability to reproduce a sufficiently stable bright light from a 350mA constant current source with junction temperature maintained at or below 90°C. The LED was specifically chosen to be green since insect photoreceptors are green-sensitive (Horridge et al. 1975). There were several reasons why we used LEDs instead of other light sources (bulb or lights from a

monitor). Firstly, the LED light source was reasonably cheap and durable. Secondly, the LED produced a constant luminance (not flickering) since a constant voltage or current source was used to power the LED. Lastly, the colour temperature of the LED was invariant within its optimum operating range. Furthermore, it was commercially available in electronic stores.

2.4.2 Brightness Value - Extrapolation

The light meter of the conventional digital camera (Nikon D70) that was used for calibrations had an exposure value (EV) dial precision of ±0.3EV. For small EV, the camera had a good accuracy (< 1cd/m^2) in measuring luminance. As the EV increased, the accuracy of the camera decreased (> 30 000 cd/m^2) dramatically due to the limitation of the precision of the EV dial, i.e. the light meter of the digital camera became less reliable in determining brightness values as the exposure value increased. Therefore, we only used the calculation points from 0-50% of the control signal input for linear curve fitting. A linear algorithm was used during curve fitting because the luminance output of the LED driver system had a linear relationship with the current measured from the photodiode amplifier and the current was linearly proportional to the control signal input (see Figure 2-3).

References

Grum, F. (1968). "Artificial light sources for simulating natural daylight and skylight." Appl. Opt. **7**: 183.

Horridge, G. A., K. Mimura and Y. Tsukahara (1975). "Fly photoreceptors II. Spectral and polarized light sensitivity in the drone fly *Eristalis*." Proc. R. Soc. Lond. B **190**: 225-237.

Howard, J. (1981). "Temporal resolving power of the photoreceptors of *Locusta migratoria*." J. Comp. Physiol. A **144**(1): 61-66.

Laughlin, S. B. (1989). "A role of sensory adaptation in the retina." J. exp. Biol. **146**: 39-62.

Laughlin, S. B. and R. C. Hardie (1978). "Common strategies for light adaptation in the peripheral visual systems of fly and dragonfly." J. Comp. Physiol. **128**: 319-340.

Mah, E. L., R. S. A. Brinkworth and D. C. O'Carroll (2005). Bio-inspired analog circuit model of insect photoreceptor cells. Proceedings SPIE, Sydney.

Matic, T. and S. B. Laughlin (1981). "Changes in the intensity-response function of an insect's photoreceptors due to light adaptation." J. comp. Physiol. A **145**: 169-177.

Nichia Corporation "http://www.rpelectronics.com/Data/NSPL500S.pdf."

Snyder, A. W., S. D.G. and S. B. Laughlin (1977). "Spatial information capacity of compound eyes." J. Comp. Physiol. A **116**: 183-207.

Snyder, A. W., S. B. Laughlin and S. D.G. (1977). "Information capacity of eyes." Vision Research **17**: 1163-1175.

The photometric system "http://www.ibiblio.org/pub/multimedia/3d/3d-photo/photometry."

van Hateren, J. H. (1992). "A theory of maximizing sensory information." Biol. Cybern. **68**: 23-29.

Weckström, M. and S. B. Laughlin (1995). "Visual ecology and voltage-gated ion channels in insect photoreceptors." Trends in Neurosciences **18**: 17-21.

Wuff, V. J. and W. J. Mueller (1975). The origin of the receptor potential of the lateral eye of Limulus. The Compound Eye and Vision of Insects. London, Oxford University Press: 37-52.

3

Chapter 3: A Non-linear Adaptive Artificial Photoreceptor Circuit – Design and Implementation

ENG-LENG MAH AND DAVID O'CARROLL

Discipline of Physiology, School of Molecular and Biomedical Science and the Centre for Biomedical Engineering, The University of Adelaide SA 5005, Australia.

Abstract

We present here an analogue circuit implementation of a bio-inspired non-linear adaptive artificial photoreceptor using discrete electronic components. This analogue neuromorphic circuit is designed and built based on the understanding and detailed studies of the biological photoreceptors of the hoverflies, *Eristalis tenax*. An amplified photodiode (TSL251) is used as the front-end of the analogue circuit to convert photon energy into electrical energy for the circuit to process. The circuit consists of two non-linear divisive feedback stages and one static non-linear stage. We have tested and evaluated the analogue circuit using artificial light stimuli and confirmed that this circuit is capable of performing robustly in any lighting conditions and could be beneficial as a pre-processor for higher order neuron designs.

Keywords: Artificial Photoreceptor, Neuromorphic Circuit, Adaptive Photoreceptor.

Correspondence to: Eng-Leng Mah (email: eng.mah@adelaide.edu.au)

3.1. Introduction

Insects, especially flies, have remarkably fewer neurons in their visual pathway as compared to humans. Despite their simple visual systems, insects are able to manoeuvre through complex environment with remarkable ease and accuracy. Such great evolutionarily aptitudes have inspired many engineers to design and implement robust, reliable bio-inspired vision systems such as motion detection, target tracking and collision avoidance systems, simply because nature has the solution to these problems.

There are several methods of implementing a bio-inspired circuit. If cost is not an issue, fabricating a circuit using the state-of-the-art analogue VLSI (Very Large Scale Integrated Circuit) technology is probably the way to go. Millions of transistors can be packed into a single small-sized silicon chip, depending on the complexity of the circuit design. Analogue VLSI silicon chips usually consume only a small amount of power, which is a key requirement of many applications.

The next best option is to use FPGA (Field Programmable Gate Array) technology. Logic gates can be pre-programmed into an FPGA chip (e.g. SPARTAN) in order to execute an algorithm which performs the same function as the circuit. Unlike the VLSI technology, the same chip can be reprogrammed anytime to function differently since the chip is mainly controlled by a software program. No doubt, this feature is beneficial if the circuit implementation requires tuning for better performance.

However, the most commonly used method in circuit implementation is board- prototyping, where discrete analogue circuit components are put together on breadboards/veroboards to realise a design. This

method is very economical for evaluating circuit designs since the components are commercially available and relatively cheap compared to the other methods mentioned earlier.

In this paper, we discuss the design and implementation of an elaborated bio-inspired artificial photoreceptor circuit. This circuit was built using discrete electronic components (analogue) on breadboards based on a mathematical model previously proposed by van Hateren and Snippe (van Hateren et al. 2001), together with some additional elaborations to better mimic the actual biological photoreceptors.

This analogue neuromorphic circuit mimicked most of the important characteristics of a biological photoreceptor. It was capable of automatically adapting to any background intensities in order to increase its input dynamic range, similar to the biological photoreceptors (Laughlin et al. 1978; Matic et al. 1981; Laughlin 1989). Not only that, the circuit also incorporated a static non-linear Naka-Rushton stage in order to mimic the sigmoidal soft saturation of the biological photoreceptor response against input pulse intensity. Automatic variable corner frequency control was also integrated in the analogue circuit for realising an adaptive frequency response feature of the biological photoreceptors (Laughlin et al. 1993).

This faithful photoreceptor circuit could potentially serve as a reliable front-end for many higher order neurons designs such as motion detection and target tracking neurons. Not only that, this circuit also provides a solution to experiments that were previously considered to be impossible such as experiments that require many hours of recording in a single session. It is also impossible to perform intracellular experiments on an insect while having the

insect manoeuvring freely in natural environments. However, with this analogue circuit real-time recordings in this complicated naturalistic scenario can now be done.

3.2 Methods

3.2.1 Specifications

The artificial adaptive photoreceptor circuit was built using standard analogue discrete electronic components. It consists of one input from an amplified photodiode (TSL251) and one photoreceptor-like output. The circuit is tuned to take in a minimum voltage of 0V and a maximum voltage of 4V from the amplified photodiode. Anything above that will cause some unwanted clippings at the output. The output of the artificial adaptive photoreceptor circuit ranges from 0 to 1V. Table 3-1 summarises all the electrical properties of the analogue circuit.

	Min	Typical	Max
Number of Inputs		1	
Number of Outputs		1	
Input voltage		±15	
Input rated current	100mA		500mA

Table 3-1: Electrical properties of the artificial photoreceptor circuit.

3.2.2 Computer Modelling – Matlab and Simulink

We started off by modelling the non-linear photoreceptor model mathematically using Matlab and Simulink software. This model was implemented based on a mathematical model proposed by van Hateren and Snippe (2001), with some additional modifications to

better mimic the biological photoreceptors. Figure 3-1 shows the Simulink block diagram of our mathematical model design. Since it was not feasible to design a circuit with an infinite output response, an additional block called the saturation block was integrated in our mathematical model to limit the signal of the model. In this case, we limited the signal magnitude such that the minimum is -15 and the maximum is +15. As for the static non-linear stage, we modified the Naka-Rushton equation that was proposed by van Hateren and Snippe. Instead of using input/(1+input), we changed it to input/(0.05+input). This was to shift the input dynamic range of the model so that it was feasible for implementation.

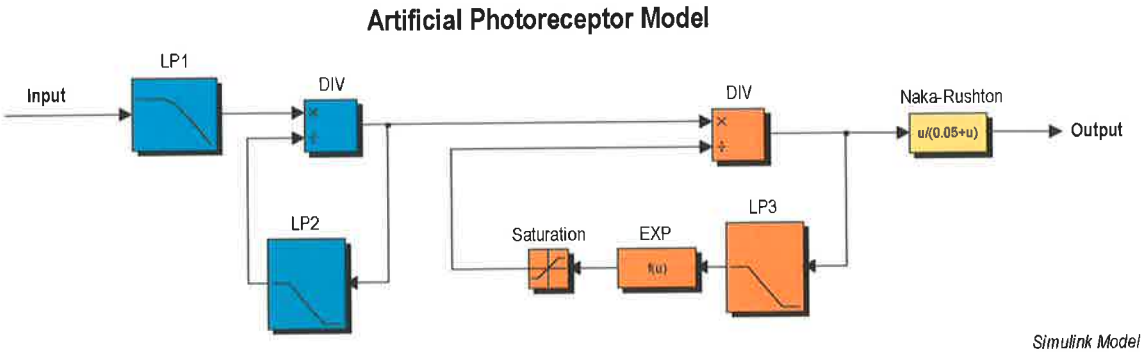

Figure 3-1: Simulink mathematical block diagram of the adaptive non-linear photoreceptor model. LP1, LP2 and LP3 are low pass filters with a time constant of 1.764 ms, 397.84 ms and 3.978 s respectively. EXP is a simple exponential function k1 (exp (k2*input)) where k1 = 2.57 and k2 = 10.

LP1 and LP2 were both second and first order filters respectively. Time constants for these low pass filters were also modified to fine tune the output responses of the mathematical model design in order to approximately match those in physiological recordings (Mah et al. 2005). The steady-state equation of the model was described as below:

$$\text{output} = \left(\frac{A}{0.05 + A} \right) \qquad \textbf{(Eq 3-1)}$$

where $A = \sqrt{\frac{\sqrt{\text{input}} . \exp(-k2\sqrt{\text{input}})}{k1}}$.

Output from the first divisive feedback stage was passed through the second divisive feedback stage. At this stage, the signal was automatically adjusted (adaptive) based on the input background value and the time course of the adaptation was fully controlled by the time constant set in the first order filter, LP3. The output signal from the second divisive feedback stage was then compressed non-linearly in the final static non-linear Naka-Rushton stage. The Simulink model was then tested and evaluated with a range of intensity steps and impulses by using custom programs written in Matlab.

3.2.3 Electronic Circuit Modelling – SPICE Simulation

The finalised mathematical model of the artificial photoreceptor was used as a basis to design a prototype SPICE model. This SPICE model was used as a guide prior to implementing a prototype circuit. Standard electronic discrete component blocks in the simulation software were used to build the SPICE model. This was to ensure the SPICE model was feasible for actual circuit prototyping. Steady-state tests such as impulse and step response tests were done on the SPICE model to evaluate and test its response. Parameter values of some stages of the model were changed to better mimic the biological photoreceptor. Figure 3-2 shows the schematic diagram of the SPICE model.

This SPICE model consisted of several additional elaborations that were not modelled in our mathematical model discussed previously. The reason for not having them in the mathematical model was simply because of the limitations in the Matlab and Simulink software which are unable to incorporate certain complex functional blocks during simulation.

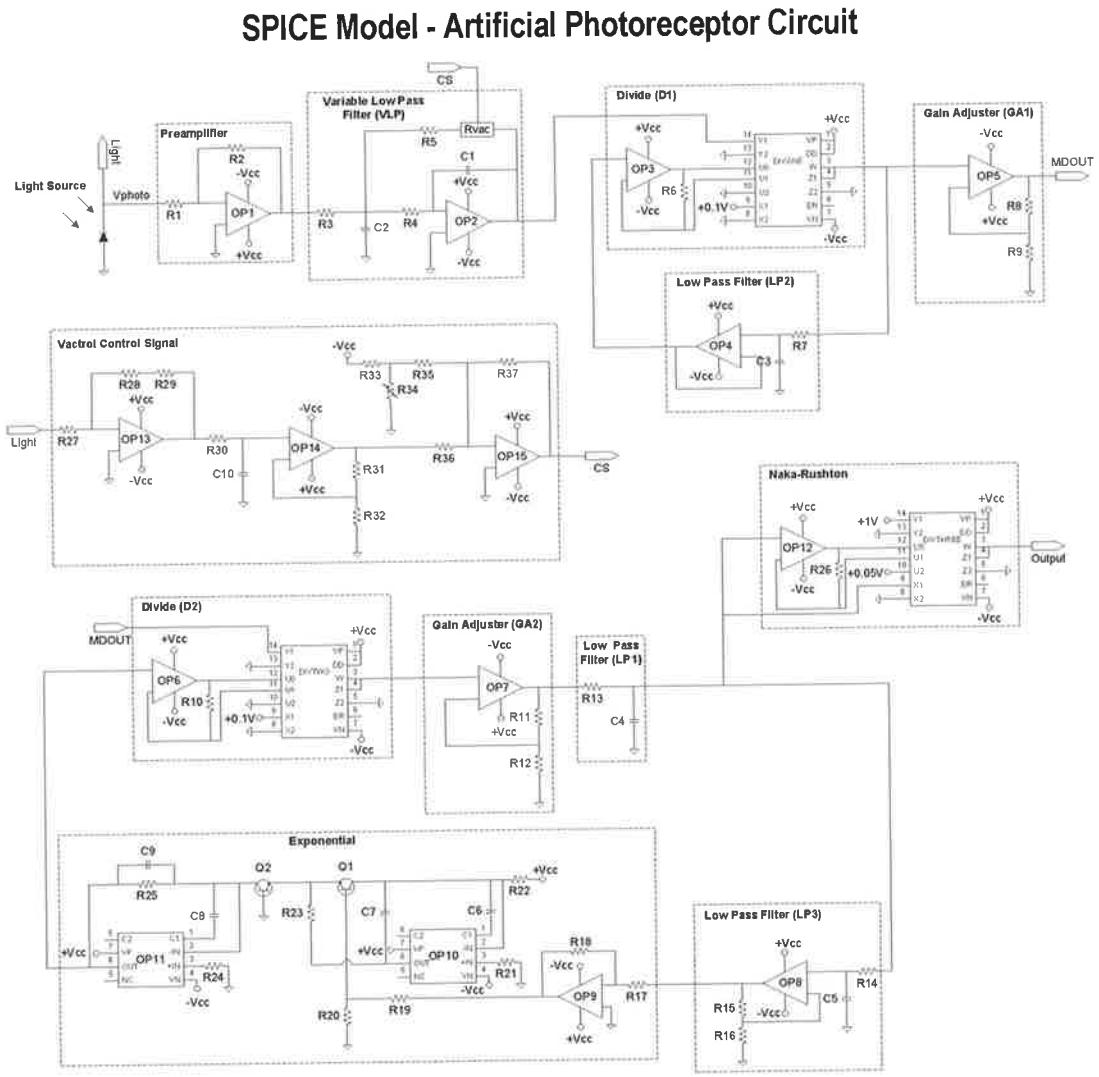

Figure 3-2: A schematic diagrams of the artificial photoreceptor circuit SPICE model.

An amplified photodiode with an output (V_{photo}) ranging from 0-4V was used to convert photon energy into its corresponding electrical energy (current) before transmitting it into the circuit. This voltage is linearly proportional to the input intensity (Bv in cd/m²) at the photodiode, according to equation 3-6. The signal from the amplified photodiode was initially passed through a linear preamplifier stage prior to any non-linear processes. The amplified signal was then transmitted to the Variable Low Pass filter, VLP the gain, K_{VLP} and frequency response, F_{VLP} of which were dependent on the average luminance measured by the Vactrol Control Signal stage, VCS.

$$K_{VLP} = \frac{-(33x10^3 + R_{vac})}{36x10^3} \qquad \textbf{(Eq 3-2)}$$

$$F_{VLP} = \frac{1}{29.77x10^{-6}\sqrt{33x10^3 + R_{vac}}} \qquad \textbf{(Eq 3-3)}$$

Where $R_{vac} = 3.09x10^{29}\exp(-38.12CS) - 5.66x10^{22}\exp(-27.56CS)$ **(Eq 3-4)**

$$CS = 1.481 + 0.237V_{photo} \qquad \textbf{(Eq 3-5)}$$

$$V_{photo} = \frac{Bv}{1750} \qquad \textbf{(Eq 3-6)}$$

The output signal from the VLP stage was used as a numerator for the first divider stage, D1 and the output signal from the first order low pass filter, LP2 was used as the denominator. Notice that the circuit configuration of the divider, D1 was set according to the following equation:

$$W_{D1} = \frac{(X_1 - X_2)(Y_1 - Y_2)}{(U_1 - U_2)} + Z_2 \qquad \textbf{(Eq 3-7)}$$

where W_{D1} was the output of D_1, and X_2, Y_2, U_2 and Z_2 were connected to electric ground (0V). Y1 was the input of the VLP and because X1 was connected to a constant voltage 0.1V, hence the equation becomes:

$$W_{D1} = \frac{(0.1)(InputfromVLP)}{InputfromLP2} \qquad \textbf{(Eq 3-8)}$$

The output of D1 was deliberately degained by 10 times in order to overcome one of the instability constraints of the divider chip, which was that the input magnitude X has to be less than 1.25U. Thus, a gain adjuster stage, GA1 was cascaded straight after the D1 stage for compensating the gain loss in the divider stage, D1.

The output of GA1 was then transmitted as a numerator to a second divider stage, D2. Again, this divider was designed to have a gain loss of 10 times in order to overcome the same chip limitation as previously noted. The output signal from GA2 was then filtered with a low pass filter to remove any unwanted high frequency noise. The filtered signal was passed through both the low pass filter, LP3 and the final compressive non-linear stage, Naka-Rushton. The low pass filtered signal from LP3 was exponentially amplified in the exponential stage according to the equation:

$$ExpOut = k1 * \exp(k2 * input) \qquad \textbf{(Eq 3-9)}$$

where k1 = 13.3 and k2 = -4.3. The output signal from the exponential stage was used as the denominator for the second divider stage, D2.

The Naka-Rushton stage was designed using a simple divider configuration, similar to D1 and D2. The input magnitude X for the divider, D3 was fed with a signal coming from the second divider, D2 and the input magnitude Y was powered with a constant voltage, 1V. Below is the equation that describes the final Naka-Rushton stage:

$$W_{D3} = \frac{W_{D2}}{W_{D2} + 0.05} \qquad \textbf{(Eq 3-10)}$$

3.2.4 Circuit Prototyping

Once we had the finalised SPICE model, the artificial adaptive photoreceptor circuit was implemented using discrete electronic components. All the components were connected according to the SPICE model on breadboards. Variable resistors were used at some parts of the circuit to allow for the possibility of fine tuning its output. Standard 5mm single core wires were used for interconnecting the discrete components to realise a working circuit.

3.3 Results

3.3.1 Matlab and Simulink Model

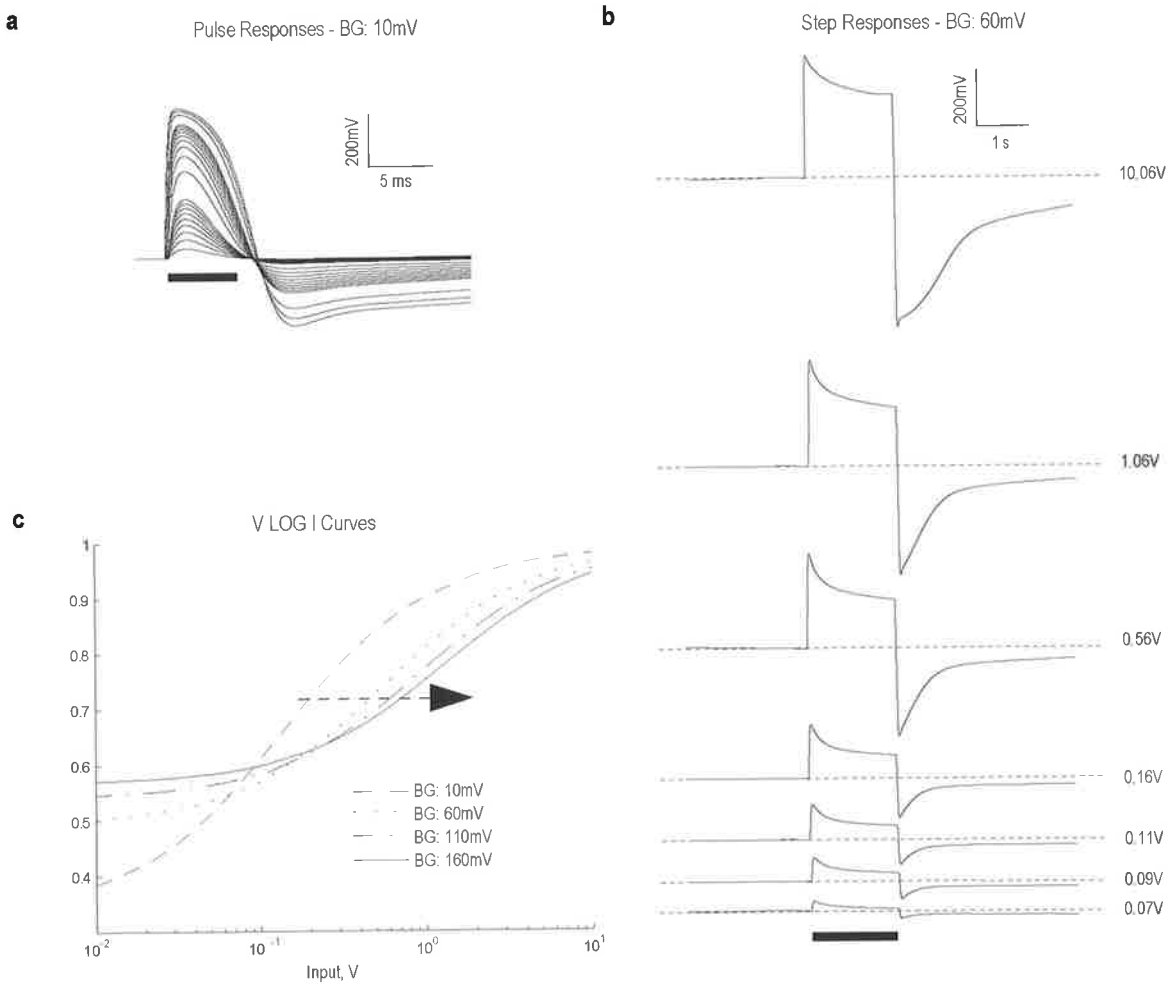

Figure 3-3: Matlab and Simulink output of the neuromorphic photoreceptor model. a. Pulse response curves with pulses of 5ms at relative background luminance of 10mV. b. Step response curves with steps of 1.5s at relative background luminance of 60mV – step sizes: 0.07V, 0.09V, 0.11V, 0.16V, 0.56V, 1.06V and 10.06V. c. V LOG I curves with different relative background luminance (10mV, 60mV, 110mV and 160mV).

Figure 3-3a shows the pulse responses of the Matlab and Simulink model with several pulse intensities at relative background

luminance of 10mV. The model responded non-linearly to the pulse intensities, with obvious hyperpolarisation effects during offset of input stimuli. Notice that the time taken for the hyperpolarisation effects to recover to its initial resting potential state increased as the pulse intensity increased. The stimuli durations were increased from 5ms to 1.5s and the corresponding step responses are as shown in Figure 3-3b. During a bright step (in relative to its background luminance) simulation, the model depolarised at stimuli onset, following a long exponential decaying adaptation to its background luminance. From the pulse responses of various pulse intensities and background luminance, the non-linearity of the model can be further illustrated as shown in Figure 3-3c. These V LOG I curves have a sigmoid-like function and they were shifted to the right as the background luminance increased. The magnitude of the right shift was not proportional to the input pulse intensity.

3.3.2 SPICE Model

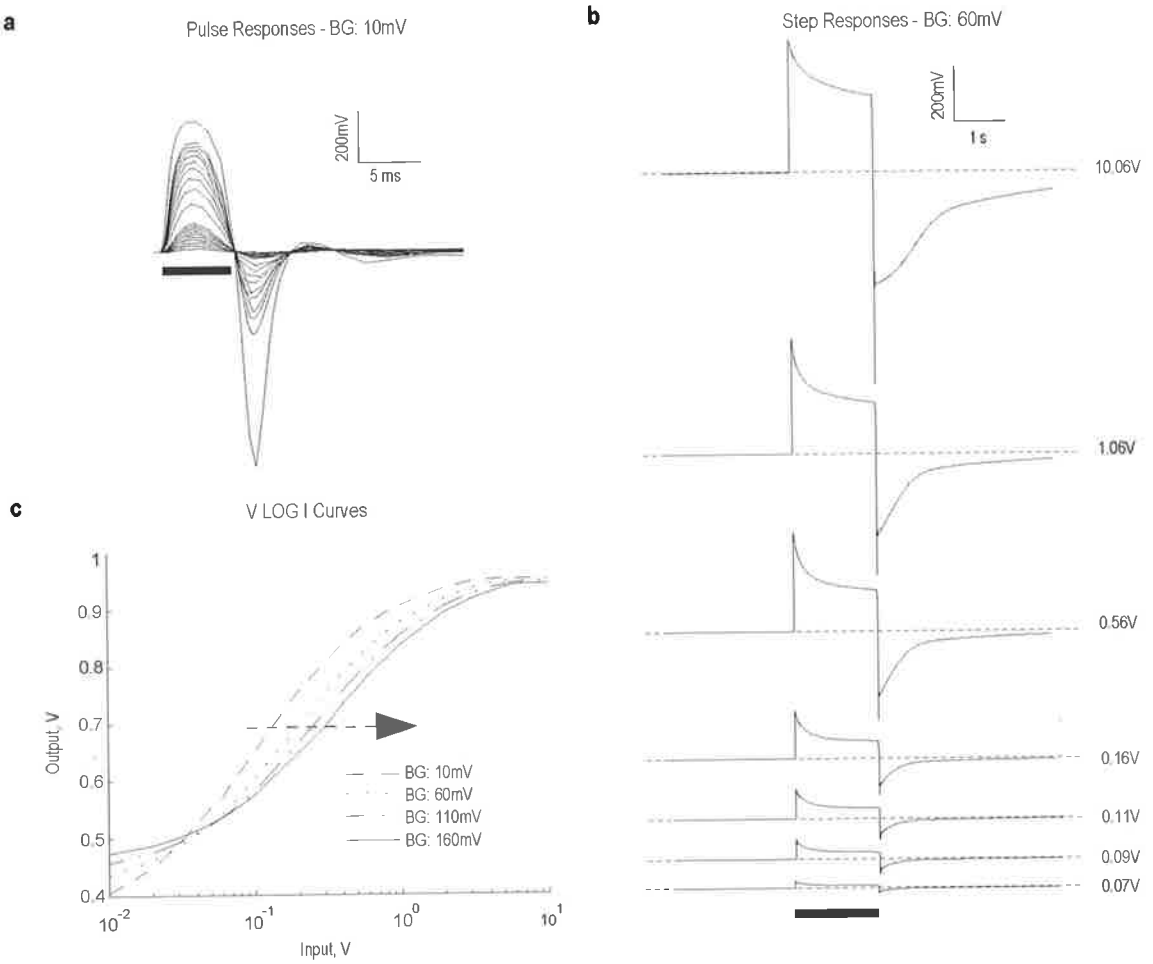

Figure 3-4: SPICE output of the neuromorphic photoreceptor model. a. Pulse response curves with pulses of 5 ms at relative background luminance of 10mV. b. Step response curves with steps of 1.5s at relative background luminance of 60mV– step sizes: 0.07V, 0.09V, 0.11V, 0.16V, 0.56V, 1.06V and 10.06V. c. V LOG I curves with different relative background luminance (10mV, 60mV, 110mV, 160mV).

Figure 3-4a shows the pulse responses of the SPICE model with various pulse intensities. Again, the SPICE model responded non-linearly to the input pulse stimuli, together with clear hyperpolarisation effects on the offset stimuli, which increased in

magnitude as the pulse intensity increased. This model was also tested with various step intensities for several background luminances. Figure 3-4b shows the step responses of the model with background luminance at 60mV. Similar to the Matlab and Simulink model, this model showed clear luminance adaptation, typically during the onset of the input step stimuli. Not only that, the model also showed great hyperpolarisation effect during the offset of the stimuli, where the magnitude of the hyperpolarisation increased as the step intensity increased. Again, by further analysing the pulse responses under several background luminances, the corresponding V LOG I characteristic curves were plotted (Figure 3-4d). Notice that the V LOG I curves shifted to the right as the background luminances increased and all the curves showed a sigmoid-like function.

3.3.3 Actual Circuit

Figure 3-5 shows the final circuit that was implemented on breadboards. The circuit performed very close to the actual biological photoreceptors such as adaptive logarithmic encoding of luminance. Detailed evaluations of the circuit are discussed in the following chapters.

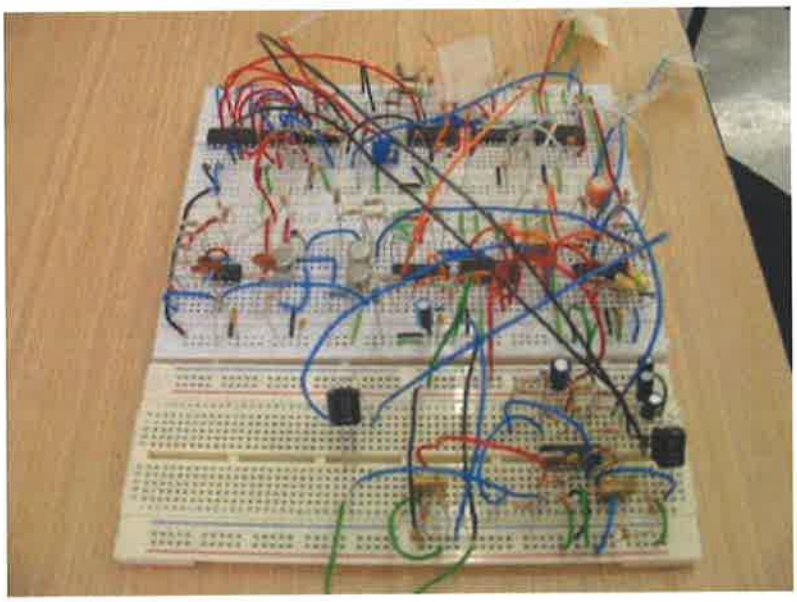

Figure 3-5: Prototype circuit implemented on breadboards.

The circuit could be minimized in the future by using small surface mount components (SMT) on a printed circuit board (PCB). Not only would this reduce the overall size of the circuit, it would also reduce the circuit noise, i.e. increase the signal to noise ratio. Figure 3-6 shows the three- dimensional rendered PCB design of the circuit.

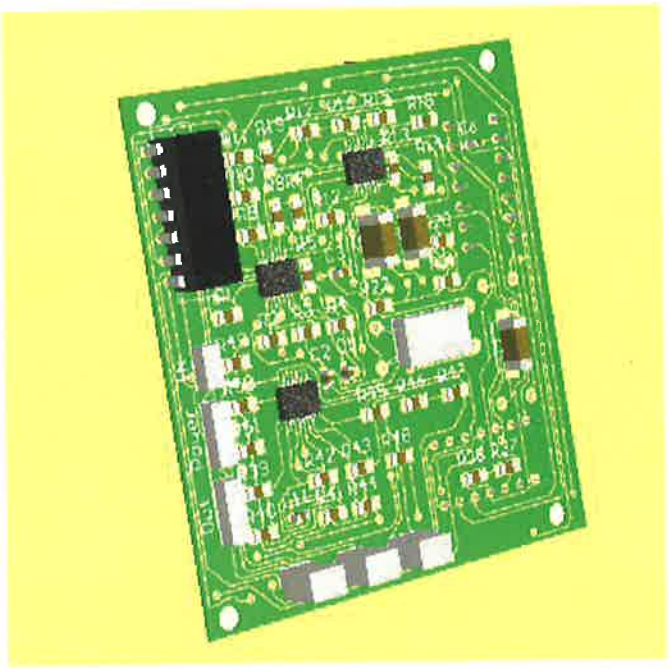

Figure 3-6: Printed Circuit Board design of the artificial insect photoreceptor circuit. It uses both front and back layers with an actual size of approximately 60mm x 60mm.

3.4 Discussions

Insect photoreceptors are highly non-linear, displaying adaptation to both luminance and contrast under natural conditions (Baumann 1975; Matic et al. 1981). From an engineering perspective, it is not easy to model a non-linear system. However, a reliable mathematical model that was proposed by van Hateren and Snippe (2001) has allowed us to use it as a basic model to our elaborated prototype circuit design. Additional enhancements to the basic model, which were based on the physiological understanding of the actual photoreceptors, have allowed us to implement a much more faithful circuit model of the actual biological photoreceptors. This robust, reliable circuit has proven to be beneficial in higher order neuron designs (O'Carroll et al. 2006), where data recorded from the output

of the circuit can be used to feed in to the higher order neuron designs for detailed evaluation.

This faithful circuit not only provides a solution to better higher order neuron designs but it also allows one to further develop one's understanding of the biological photoreceptor cells. Experiments that require exhaustive duration, which are not feasible for a single cell recording (intracellularly), are no longer a problem with this photoreceptor circuit. Not only that, the circuit can be mounted on a robotic platform and record real-time responses in naturalistic environments, which again is not feasible to be performed on an actual biological photoreceptor.

References

Baumann, F. (1975). Electrophysiological properties of the honey bee retina. The Compound Eye and Vision of Insects. London, Oxford University Press: 53-74.

Laughlin, S. B. (1989). "A role of sensory adaptation in the retina." J. exp. Biol. **146**: 39-62.

Laughlin, S. B. and R. C. Hardie (1978). "Common strategies for light adaptation in the peripheral visual systems of fly and dragonfly." J. Comp. Physiol. **128**: 319-340.

Laughlin, S. B. and M. Weckström (1993). "Fast and slow photoreceptors - a comparative study of the functional diversity of coding and conductances in the diptera." J. comp. Physiol. A **172**: 593-609.

Mah, E. L., R. S. A. Brinkworth and D. C. O'Carroll (2005). Bio-inspired analog circuitry model of insect photoreceptor cells. SPIE, Brisbane.

Matic, T. and S. B. Laughlin (1981). "Changes in the intensity-response function of an insect's photoreceptors due to light adaptation." J. comp. Physiol. A **145**: 169-177.

O'Carroll, D. C., P. D. Barnett, E. L. Mah, K. Nordström and R. S. A. Brinkworth (2006). A Neuromorphic Model For A Robust, Adaptive Photoreceptor Reduces Variability In Correlation Based Motion Detectors. Brain Inspired Cognitive Systems, Lesbos, Spain.

van Hateren, J. H. and H. P. Snippe (2001). "Information theoretical evaluation of parametric models of gain control in blowfly photoreceptor cells." Vision Research **41**: 1851-1865.

4

Chapter 4: Implementation of an Elaborated Neuromorphic Model of a Biological Photoreceptor

ENG-LENG MAH, RUSSELL SA BRINKWORTH and DAVID C. O'CARROLL

Discipline of Physiology, School of Molecular and Biomedical Science and the Centre for Biomedical Engineering, The University of Adelaide SA 5005, Australia.

Abstract

We describe here an elaborated neuromorphic model based on the photoreceptors of flies and realised in both software and using discrete circuit components. The design of the model is based on optimisations and further elaborations to the mathematical model initially developed by van Hateren and Snippe that has been shown to work in computer simulations of both steady-state and limited dynamic (natural) conditions. The model includes an adaptive time constant, non-linear adaptive gain control, logarithmic saturation and a non-linear adaptive frequency response mechanism. It consists of a linear phototransduction stage, a dynamic filter stage, two divisive feedback loops and a static non-linearity. In order to test the biological accuracy of the model impulses and step responses were used to test and evaluate the steady-state characteristics of both the biological (fly) and artificial (new neuromorphic model) photoreceptors. These tests showed that the model responded in an

almost identical way to the actual insect photoreceptor cells. The model showed a decreasing response to impulsive stimuli when the background intensity was increased, indicating that the circuit adapted to background luminance in order to improve the overall operating range and better encode the contrast of the stimulus rather than luminance. The model also showed the same change in its frequency response characteristics as the biological photoreceptors, with the corner frequency of the circuit ranging from 10Hz – 90Hz depending on the current state of adaptation. Our model provides an excellent platform for future experiments that could be carried out in scenarios where *in-vivo* intracellular recording from biological photoreceptors would be impractical or impossible.

Key words: Insect Vision, Visual System, Adaptive Photoreceptor, Neuromorphic, Bio-inspired, Artificial Vision

Correspondence to: Eng-Leng Mah (email: eng.mah@adelaide.edu.au)

4.1. Introduction

The biological visual system is capable of adapting to light in order to enhance the encoded information from the earliest stages of visual processing (Wuff et al. 1975; Laughlin et al. 1978; Weckström et al. 1995; van Hateren et al. 2005). In any one state of adaptation, depending on species, biological eyes can only effectively detect changes in light intensity of approximately 2-3 log units (Wallcott 1975). Since the luminance transition from day to night is approximately 8 log units, adaptation mechanisms are required to alter the effective range in which the visual system operates. Such mechanisms are mainly due to anatomical changes and biochemical

processes in the photoreceptor cells, which take place during light-adaptation (Baumann 1975; Baumann 2000).

All artificial imaging systems require a means of transducing light into a usable electrical signal, however most vision use a linear detector stage (Francheschini et al. 1992; Moini et al. 1997; Netter et al. 2002). Both theory and modelling have shown that non-linearities, such as those seen in biological photoreceptors, improve the coding of visual information (Laughlin 1989). van Hateren and Snippe (2001) recently developed a mathematical model for non-linear luminance coding by fly photoreceptors. They incorporated several elements directly inspired by studying key stages of the blowfly visual system. Their model, when implemented in software provided an excellent fit to biological photoreceptor data under both steady-state and limited dynamic conditions; while several other models (such as direct logarithmic encoding, which does not incorporate adaptation) have been shown to be inferior in either steady-state behaviour or once more complex optical flow is introduced (Dror et al. 2001).

The van Hateren and Snippe model was proposed primarily to explain dynamic behavior under photopic conditions. An additional feature of the physiology of the fly photoreceptor not accounted for by this model is that (and unlike mammalian cones) it is also adapted to low light levels by virtue of a large change in time constant (nearly 10 fold change in corner frequency) (Weckström et al. 1995). Coupled to additional changes in the underlying transduction cascade, this allows fly photoreceptors to operate over an extended luminance range.

Several different analogue vision chips have been built to mimic the response of biological systems to a variety of visual stimuli (Tanner et al. 1988; Delbrück 1993; Etienne-Cummings et al. 1993; Sarpeshkar et al. 1993; Kramer et al. 1995; Delbrück et al. 1996; Liu 1996; Moini et al. 1996; Sarpeshkar et al. 1996; Kramer et al. 1997; Yakovleff et al. 1998; Liu 1999; Delbrück et al. 2004) and some of these have taken advantage of the 'neuromorphic' approach, incorporating some principles akin to those in biological visual processing, with varying degrees of success . Perhaps the most successful of these neuromorphic designs is that of Delbrück et al (1996), who have implemented an artificial photoreceptor chip by using neuromorphic analogue Very Large Scale Integrated (aVLSI) technology (Delbrück 1993; Delbrück et al. 1996; Delbrück et al. 2004). These chips provided rudimentary approximations to several key aspects of biological photoreceptors, including non-linear luminance adaptation and logarithmic coding. While these designs may provide an improvement over simple linear detectors under many conditions, to date they have not been tested against their biological counterpart under dynamic conditions that would be experienced during normal behaviour. Also steady state testing of these devices reveals no evidence of the 'soft' saturation which is found at high luminance in biological photoreceptors and which was incorporated into the parametric model of van Hateren et al (2001). And which was reported by Dror et al (2001) to be advantageous for post-detector visual processing. Despite these limitations, the Delbrück model is currently one of the best developed neuromorphic hardware models for biological photodetection, and has been incorporated by other groups into similar neuromorphic chip designs as a front-end for higher-level processing tasks (Shoemaker et al. 2001; Shoemaker et al. 2005).

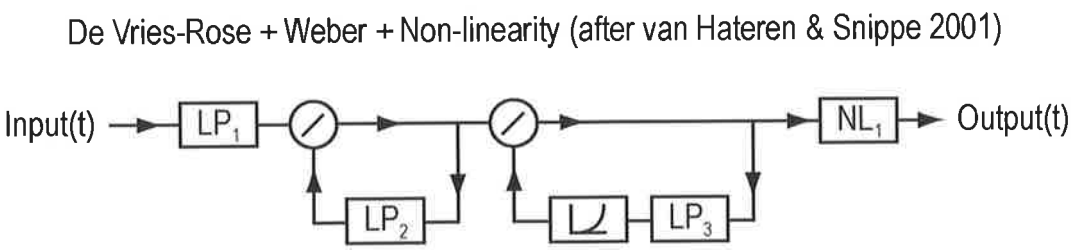

Figure 4-1: A mathematical model proposed by van Hateren and Snippe to mimic the insect photoreceptor cell. LP1, LP2 and LP3 are low pass filters. To the left of the LP3 is an exponential stage with a function of k_1*exp (k_2*x) +c. NL1 is the static non-linear stage (Equation 4-1).

Figure 4-1 shows a simplified block diagram of the previously proposed mathematical model (van Hateren et al. 2001). It consisted of a cascade of two dynamic non-linear stages and a static non-linear stage. The first dynamic non-linear divisive feedback loop compresses fast and large transients and causes a semi-logarithmic response in the steady-state. The second non-linear divisive feedback loop is responsible for slow adaptation (4-5s) to large steps in intensity, and also acts as an automatic gain control for the system. Any remaining peaks that would drive the photoreceptor out of its dynamic range are handled by the final compressive non-linearity.

The purpose of this paper was to implement and evaluate a robust, adaptive non-linear artificial insect photoreceptor model in analogue circuitry, complete with details (such as real-world limitations and optimised values for each stage) omitted from the van Hateren and Snippe model. Our model also incorporates further elaborations such as an adaptive time-constant that even more closely mimic the response of biological photoreceptors. The implementation of this neuromorphic model, which faithfully mimics biological photoreceptors, could be beneficial when studying how the

photoreceptors perceive complex scenes in natural environments, since it is practically impossible to perform *in-vivo* intracellular experiments with an animal that is moving freely. The analogue nature of the implementation also acts as a powerful tool in sampling data of any scenarios and thus provides reliable, data for the design of higher order neurons - discrete time animation such as computer screen displays, which are widely used in visually stimulating higher order neurons in an insect visual pathway, may introduce non-linear artefacts during recordings. In addition, any physiological experiments that were previously considered non-feasible due to their extreme duration can now be realised by having this implementation, thus improving the consistency in data collection and testing experimental designs. We chose a discrete component approach to designing this model because it allows us more flexibility in implementation of key stages that are missing from earlier VLSI devices. Although impractical for implementation in multi-pixel applications, our model provides an excellent basis for future experiments in real-world scenarios where direct intracellular recording of fly photoreceptors would be impractical.

4.2 Methods

4.2.1. Stimuli Generation

Pre-programmed visual stimuli were presented to the fly photoreceptors and the prototype photoreceptor circuit using an ultra bright green Light Emitting Diode (LED; Luxeon Star, Luxeon™). The LED was electrically isolated using an optical fibre core light guide to eliminate electrical artefacts. The optical fibre core also diffused light source from the LED to provide an extended luminance 'patch' source at 45° across the eyes of the fly. The LED

was driven by a custom designed calibrated high current amplifier (350mA maximum current output) and the luminance level was fully controlled via a 16-bit data acquisition card (NI PCI6221, National Instruments^{TM}). The non-linear response of the LED with input voltage was calibrated using a high precision photodiode (265, UDT Instruments^{TM}) and photodiode amplifier (PDA750, Terahertz Technology Inc^{TM}) to derive a transfer function that was used to produce a linearised response curve for the system. The maximum playback luminance of the LED was recorded to be approximately 70,000cd/m^2 (100%), similar to the luminescence of the sky close to the sun on bright day. Due to the non-linear action of the LED close to threshold it was possible to accurately modulate extremely dim stimuli (0.0001%) at the lower end while still being able to deliver very bright stimuli. The usable dynamic range was 6 log units (120dB), which is greater than that permitted by a 16-bit linear system which would have a range of 4.8 log units (96dB) or a standard 8-bit display system (2.4 log units; 48dB). A high precision 5-axes Cadan-Arm system was used to move the light source during experiments so that the stimulus patch was centred on the receptive field.

Two sets of stimuli were generated to investigate the non-linearities of the fly photoreceptors and the prototype circuit. Impulse responses were obtained from the photoreceptor or prototype circuit using brief flashes of light on top of predefined constant background intensity. The intensity of the brief flashes, typically of 1ms (for frequency analysis) and 5ms (for time domain analysis) durations, ranged from 0% (near dark) to 100%. The responses were then used to produce stimulus (V LOG I) curves (Matic et al. 1981; Laughlin et al. 1993) and to study the frequency responses of the photoreceptors

and the prototype circuit against different background intensities (steady-state adaptation).

By increasing the duration of the flashes to 3s, step responses were obtained. Such long stimulus durations allowed the photoreceptor to (partially) adapt to the stimulus level. The step response stimuli set was used to investigate the adaptation rate of the photoreceptors, and the prototype circuit, under different background illumination conditions.

4.2.2 Electrophysiological Recordings

A number of electrophysiological experiments were conducted to evaluate the responses of biological photoreceptors to the stimuli. All experiments were performed intracellularly on the photoreceptors of intact hoverflies (*Eristalis tenax*) at a temperature range of 22-24°C. Individual R1-6 photoreceptor cells were penetrated with a manipulated micropipette filled with 2.0M KCl, with a resistance of 100-200MΩ. The microelectrode was connected to a pre-amplifier (npi, BA1S) and the amplified output was passed through a high precision 50Hz adaptive noise removal filter (Quest Scientific, Hum Bug) to eliminate unwanted power line interference. The output of the Hum Bug was monitored using a digital oscilloscope (TDS210, Tektronix™) and recorded using a 16-bit data acquisition card system (NI PCI6221, National Instruments™) and custom software written in LabVIEW® at a sampling rate of 5kHz. All the experiments on either biological receptor or the circuit were done in a darkened room.

4.2.3 Circuit Modelling and Recordings

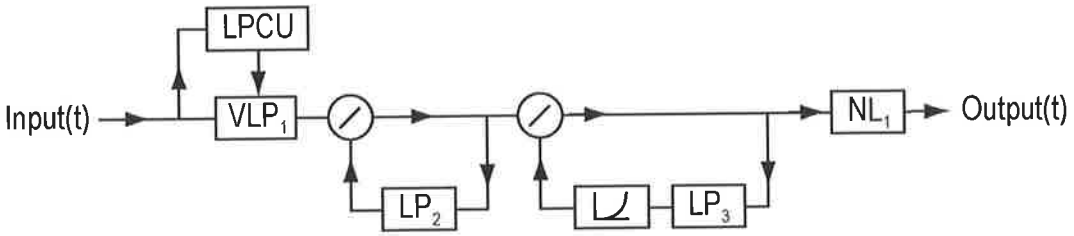

Figure 4-2: A simplified block diagram of a single pixel adaptive photoreceptor model. LPCU was the low pass control unit that functioned to provide a control voltage signal to the variable low pass filter, VLP1, based on the average luminance measured. Since this circuit design is a continuous system, the control voltage signals from the LPCU continuously changed according to the luminance history of that point. VLP1 used the control voltage signal to automatically determine the parameter settings in order to provide an appropriate output signal and frequency range for the remaining stages. Signal output from the first divisive feedback was then sent to the second divisive feedback stage and at the same time to the low pass filter, LP2 as a feedback signal for the first divisive feedback stage. The long (4-5s) term adaptation of the system was automatically controlled via a cascade of LP3 (low pass filter) and the exponential stage. The final stage, NL1 was responsible for compressing the output signal and producing a sigmoidal transfer-function.

The prototype circuit was initially designed using Matlab and Simulink software. The parameter values of the model were then re-designed and re-evaluated to make sure that it was feasible to be implemented using discrete electronic components. This new mathematical model, shown in Figure 4-2, was then used as a base for the next design level, a SPICE circuit model, which was designed using the DXP Circuit Simulation Software. All the components used to build the SPICE model were real components available for purchase. Impulse and step response tests were simulated to evaluate the output response of the SPICE model. The finalised SPICE model was then used as a reference model for the hardware

prototype implementation using discrete electronic components. The same test stimuli described above were used to evaluate and study the implemented prototype circuit.

The circuit consisted of a variable gain and corner frequency filter (VCFF) stage, two divisive feedback stages and one static non-linear stage. The low pass control unit (LPCU), shown in Figure 4-2, automatically adjusted both the gain and corner frequency of the variable low pass filter (VLP). The adjustment was based on a heavily low-pass filtered version of the input stimulus. If the average background luminance was low the LPCU sent a voltage signal to VLP in order to reduce the corner frequency and increase the gain of the circuit and vice versa for high inputs. Since different biological species have different performance requirements, and thus have different speed photoreceptors, the LPCU, as with other sections of the circuit, was designed to be fully adjustable.

Low pass filter, LP2, was used as part of the first divisive feedback stage to realise a logarithmic steady-state response with dynamics similar to biological photoreceptors. The long time constant of the circuit was controlled via the parameters settings of the low pass filter, LP3, and the cascaded exponential stage. The longer the time constant of LP3 the longer it took the circuit to adapt from its original steady-state level and vice versa.

The final stage, NL1, logarithmically saturated the circuit output in a similar way to biological photoreceptors. Equation 4-1 shows the mathematical formula used to realise such saturation:

$$NL1 = \frac{Input}{Input + c} \qquad \textbf{(Eq 4-1)}$$

Where 'NL1' is the non-linear output of the system and 'c' a constant. The output of the system was always less than 1 and produced a smooth saturation curve when the input was large with respect to c.

4.2.4 Circuit Design

The prototype circuit was designed and implemented in stages based on the block diagram shown in Figure 4-2. Discrete analogue components were used to build each stage on breadboards and all the stages were evaluated prior to combining them as one complete circuit.

A linear amplified photodetector (TSL251) was used as the front end of the circuit to transform light signals into electrical signals. To avoid any hard saturation at the output of the photodetector, a neutral density filter (1/8) was used to cover the field of view of the photodetector. The filtered photodetector, which had an output ranged from 0-4V, was thus capable of performing linearly (unsaturated) even though it was seeing a 70,000 cd/m^2 light source.

Signals from the photodetector were averaged in the LPCU using a standard active low pass filter. The averaged signal, which was an approximation to the mean background luminance, was used as a measuring point to trigger the variable resistor in VLP1. The design made VLP1 a variable gain and frequency low pass filter that was dependant on recent luminance history.

LP2 and LP3 were both first order low pass filters. They were constructed as active filters using standard low noise JFET

operational amplifiers, resistors and capacitors. Because the circuit was powered with ±15V, the signal output from both the filters was designed in such a way that they would not hit the power supply rails, i.e. no hard saturation.

Standard analogue divider chips (AD734) were used to realise the mathematical division stages in the circuit. Because it is mathematically impossible to have a zero denominator in division, dark current leakage from the photodetector was deliberately not calibrated to zero in order to create non-zero initial conditions for these stages.

4.2.5 Data Analyses

Relative Gain

By using the impulse responses at a various background luminance levels, the relative gains were calculated based on equation 4-2.

$$RelativeGain = \frac{Output(V)}{InputPulseIntensity(\%)} \qquad \textbf{(Eq 4-2)}$$

where *Output* is the peak of the impulse response relative to the background potential and *Input Pulse Intensity* is the percentage brightness of the impulse stimulus.

Frequency Response

In order to analyse the linear component of the frequency response of the photoreceptor cells, 1ms impulse stimuli were used during experiments. Small impulses were used to ensure that they were low

enough not to elicit significant non-linear behaviour, i.e. the impulse responses had to be monophasic (Matic et al. 1981). From the impulse responses, the frequency responses were determined by fitting a simple log-normal curve, shown in equation 4-3 (Payne et al. 1981), and then calculating the Fourier Transforms of the curve fitted responses.

$$V(t) = a.\exp[-(\log(t/\mu))^2/2\sigma^2] \qquad \textbf{(Eq 4-3)}$$

where V(t) is the output voltage at time t, a is the amplitude scaling factor, σ is the standard deviation and μ is the mean of the log transformed Gaussian curve.

4.3 Results

4.3.1 Pulse Response

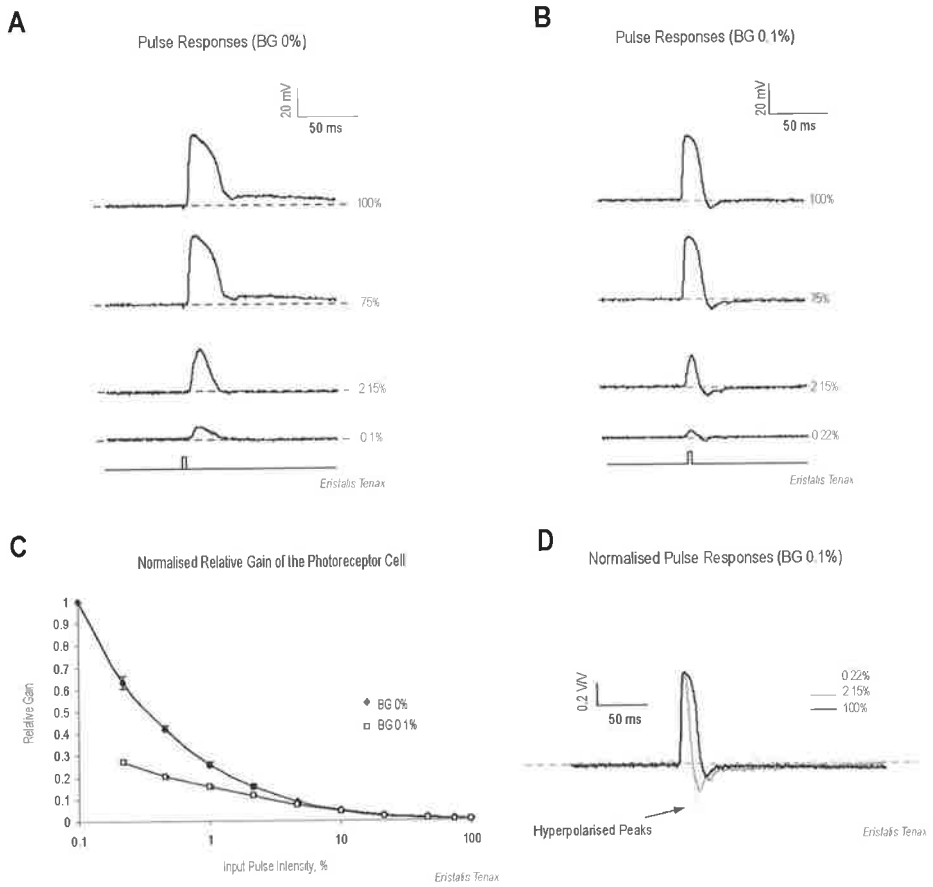

Figure 4-3: Pulse responses of the actual insect photoreceptor cell. A. Pulse responses of the actual insect photoreceptor cell with a background luminance of 0% *(average of 5 trials for each intensity step, 1 cell)*. B. Pulse responses of the insect photoreceptor with a background luminance of 0.1% *(average of 3 trials for each intensity step, 1 cell)*. C. Relative gain of the photoreceptor cells for both backgrounds 0% and 0.1% *(average of 3 cells)*. Error bars are one standard error of the mean. The system displayed a much greater relative gain to low intensity stimuli at BG 0%, i.e. the gain of the system reduced as the background light increased. D. Normalised pulses responses of the cell when the background luminance was at 0.1% *(average of 3 trials for each intensity steps, 1 cell)*. These pulses were highly non-linear, had no general trend to each other when normalised and show hyperpolarisation effects, the result of adaptation to the level of light. Time of stimuli, shown below data traces, was 5ms.

The first stage of investigating the biological photoreceptor cells was to conduct a series of pulse responses, where brief flashes of light were used to stimulate the photoreceptors from varying background illuminations. Figure 4-3a shows typical responses of the fly photoreceptor cells to 5ms pulses of light when the light was off between pulses, i.e. pulses were delivered from near darkness. The recording of each flash was set to be 59s apart in order to ensure that the photoreceptor was properly adapted to its original adaptation state before recording consecutive responses. Notice that the peak of the pulse response (Figure 4-3a) increased non-linearly as the pulse intensity increased and saturated (plateaued) as the pulse intensity approached 100%. The time taken for the response to return to the pre-stimulus level increased as the size of the stimulus increased.

In order to study the response of the photoreceptors under different background lighting conditions, the pulse response test was repeated with changes to the pre- and post-stimulus intensity levels. Instead of using 0% between stimuli, the LED was offset to a constant background intensity. Figure 4-3b shows an example of the pulse responses of the fly photoreceptor with a constant background intensity of 0.1%. Notice that there is not much of a difference with the general shapes of the pulse responses compared to the responses when the LED was off between stimuli (Figure 4-3a). The peak of the response increased as the pulse intensity increased and it also tended to saturate at large stimulus levels. However, there were some significant differences with the duration of the pulse responses. The width of the response was longer when the LED was 0% between trials compared to when it was set to 0.1%, i.e. the cell took longer to depolarise from resting potential to peak potential and back to the original resting potential when the background was

lower. Another observation, shown in Figure 4-3c, which is probably not as obvious from Figures 4-3a and b is that the relative gain (shown in equation 4-2) of the responses against the impulse intensity was higher when the background illumination was lower; i.e. at low input pulse intensities the relative gain of the system was higher at lower illumination levels. However, both of the curves start to meet at a stimulus level of approximately 10%, which is the point where the cell reached its saturation threshold.

Figure 4-3d shows the normalised figure of the pulse responses of the light-adapted cell. Notice that the responses were all biphasic, i.e. they contained hyperpolarised peaks. The pulse width only underwent a relatively small amount of change throughout the whole range of input pulse intensities as the frequency range of the system was set by the slowly adapting LPCU.

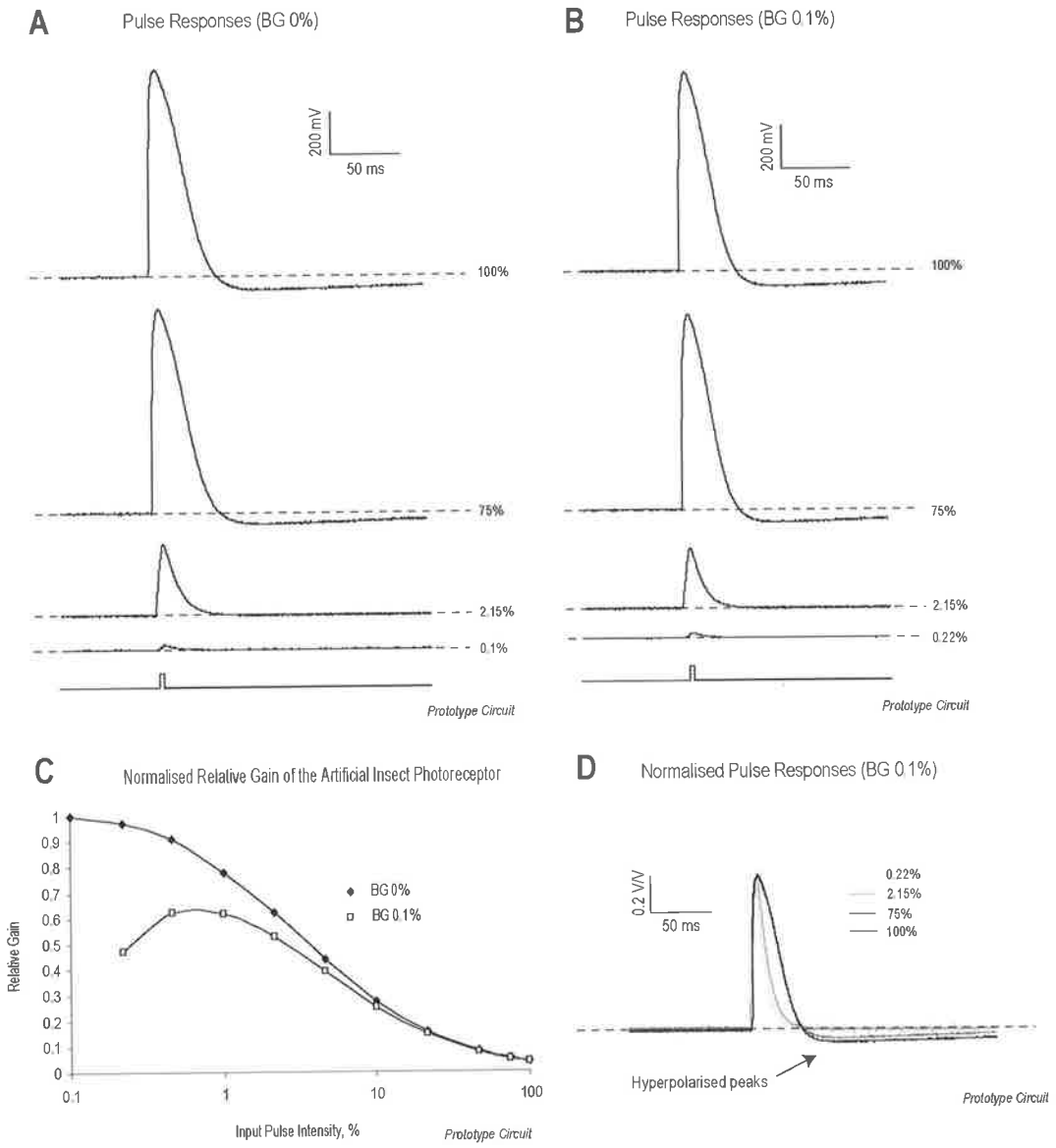

Figure 4-4: Pulse responses of the prototype circuit. A. Pulse responses of the prototype circuit with a background luminance of 0% *(average of 5 trials for each intensity step)*. B. Pulse responses of the circuit with a background luminance of 0.1% *(average of 3 trials for each intensity step)*. C. Relative gain of the circuit output for both backgrounds 0% and 0.1%. This graph shows significant pulse gain differences at the different background levels (similar to the biological data in Figure 4-3c). D. Normalised pulses responses of the circuit when the background luminance was 0.1% *(average of 3 trials for each intensity step)*. As with the recordings from biological photoreceptors these responses were highly non-linear and showed hyperpolarisation effects. Time of stimuli, shown below data traces, was 5ms.

Using similar techniques as above, the experiments were repeated on the hardware prototype circuit. Figure 4-4a shows the pulse responses of the prototype circuit against different input pulses when the LED was off between stimuli. The pulse responses were similar to the responses of the photoreceptors as shown in Figure 4-3a. Again, as the input pulse intensity increased, the peak response of the circuit increased as well. The peak output also tended to saturate as the pulse intensity got larger. Figure 4-4b shows that apart from a decrease in the response duration there were no significant changes with the overall shape of the circuit responses when a low level background illumination was introduced between stimuli.

Figure 4-4c shows the relative gain curves of the circuit. As with the biological results, the circuit had a higher relative gain when the background level was lower. Both of the gain curves start to meet at the point (10%) when the circuit reached the saturation threshold. Again, by normalising the pulse responses of the circuit, it was possible to evaluate the non-linearity of the circuit (Figure 4-4d). The output signals were monophasic when the input pulse intensities were low. As the pulse intensity increased, the signal outputs tended to produce a biphasic response and the hyperpolarised signals took hundreds of milliseconds to return to its resting potential (much longer compared to the actual photoreceptor responses). As with the biological data there was a small, but noticeable, change in the width of the responses as the input pulse intensity changed.

4.3.2 Step Response

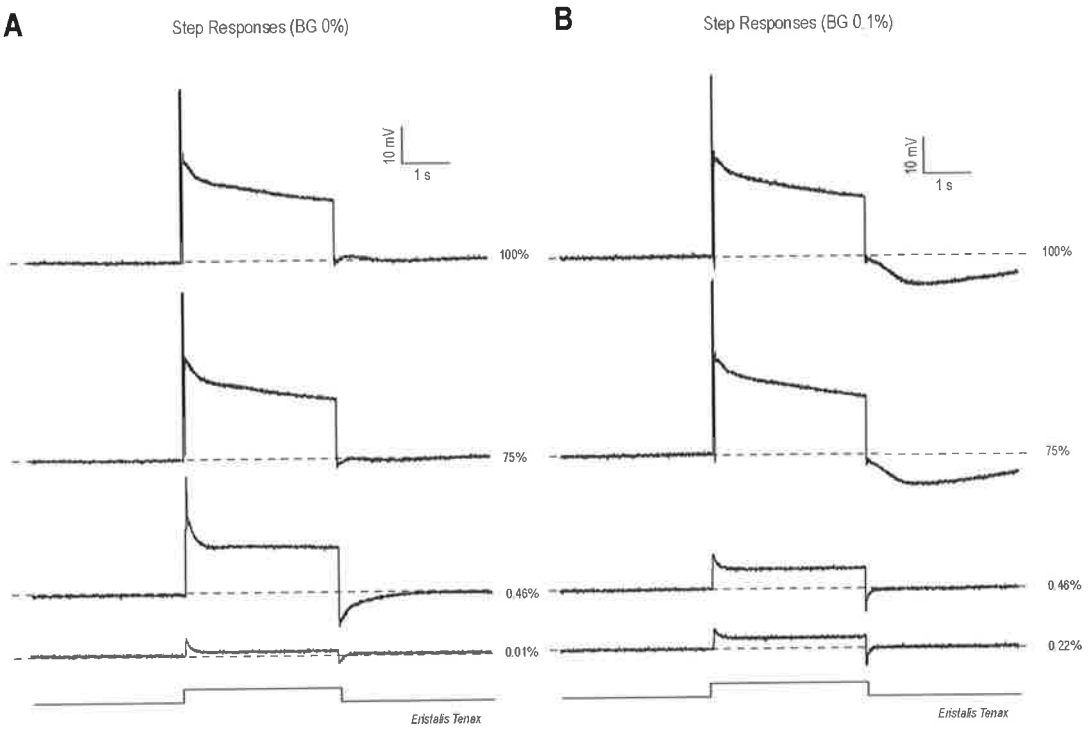

Figure 4-5: Step responses of the actual insect photoreceptor. A. Step responses of the insect photoreceptor cell at background 0% *(average of 5 trials for each intensity step, 1 cell).* The adaptive feature of the photoreceptor can be clearly seen during the onset of the stimulus. Lower intensity step responses have a higher adaptation rate (decay much faster) compared to the ones with a brighter intensity steps. B. Step responses of the insect photoreceptor cell at background 0.1% *(average of 3 trials for each intensity step, 1 cell).* Significant adaptation is observed even though the stimulus intensity is dim (0.22%). Huge post-stimulus hyperpolarisation effects (undershoots) occurred when the onset step intensities were large (75% and 100%). Time of stimuli, shown below data traces, was 3s.

The same stimuli used to generate pulse responses were used for step responses but the stimulus on time was increased from 5ms to 3s. Figure 4-5a shows the step responses of the photoreceptor cell. The cell was tested with steps of different brightness. Note that the cell adapted to the stimulus intensity during the stimulus period. The cell was initially adapted to 0% background intensity. As soon

as the stimulus started the output ramped to its maximum response followed by a period of adaptation. During the post-stimulus period, the cell response showed evidence of adaptation, significant hyperpolarisation (undershoot), even to the smallest stimuli.

Similar experiments were repeated in order to evaluate the rate of adaptation under different background lighting conditions. Figure 4-5b shows an example of one of these experiments. There were no obvious differences in the general shape of the response under 0% or 0.1% background levels.

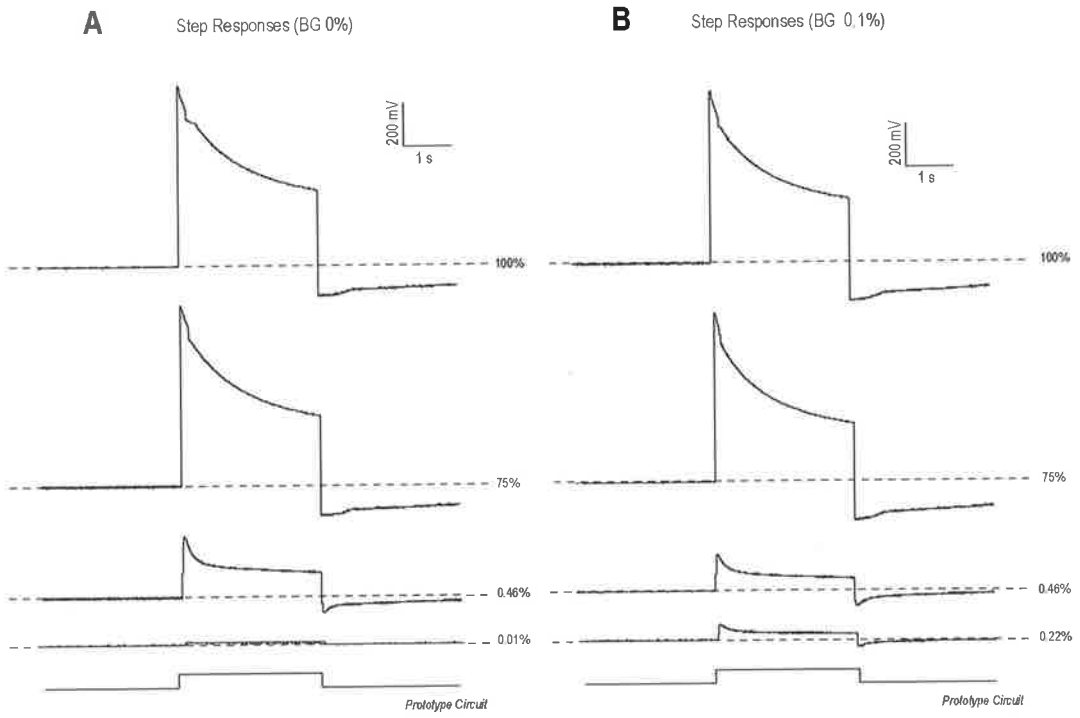

Figure 4-6: A. Step responses of the prototype circuit at background 0% *(average of 5 trials for each intensity step).* B. Step responses of the circuit at background 0.1% *(average of 3 trials for each intensity step).* As with the biological data (Figure 4-5) the rate of adaptation decreased with the size of the stimulus while hyperpolarisation after the cessation of the stimulus increased. Time of stimuli, shown below data traces, was 3s.

Again, the step response tests were repeated on the prototype circuit. Figure 4-6a shows the output step responses of the circuit at 0% background. The circuit responses were very similar to the actual neurobiological data collected (Figure 4-5a). The circuit responded to the constant input level by reducing the output level and also showed a hyperpolarisation when the stimulus was removed.

In order to further investigate the robustness of the circuit it was tested under different background lighting conditions. The pre- and post-stimulus LED intensity were set at 0.1% and the outputs are shown in Figure 4-6b. Notice that the outputs of the circuit were again very similar to the neurobiological data.

4.3.3 V LOG I

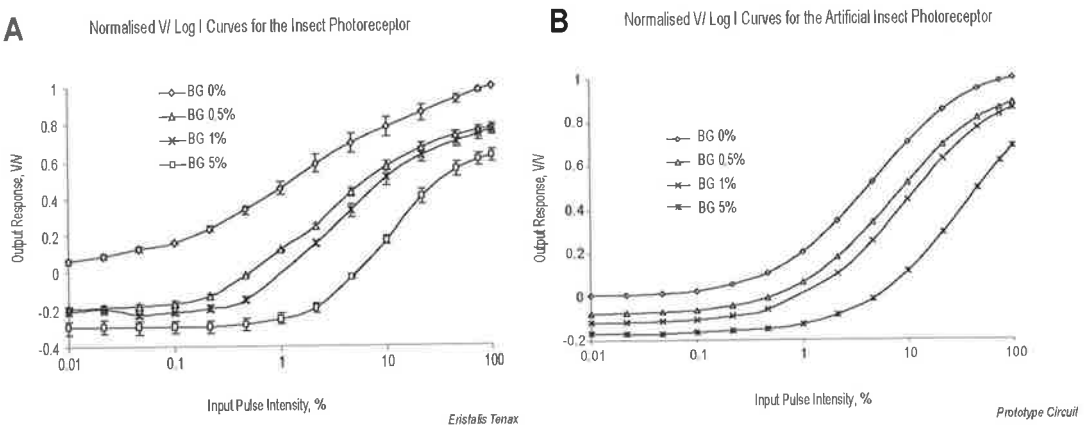

Figure 4-7: V Log I curves of the insect photoreceptor cells and prototype circuit. A. V LOG I curves of the insect photoreceptor cells: BG 0% (average of 4 cells – 3 trials per cell), BG 0.1% (averages of 6 cells – 3 trials per cell), BG 1% (average of 4 cells -3 trials per cell) and BG 5% (average of 4 cells – 3 trials per cell). Error bars show one standard error of the mean. B. V LOG I curves of the prototype circuit. Similar to the biological visual system responses, the V LOG I curves of the prototype circuit shift to the right and down as the background intensity increases. The responses are linearly related (1-2 log units) to the input pulse intensity up to a stimulus of approximately 1%. As the input pulse intensity increased from 1% to approximately 70%, the responses tended to behave logarithmically and, dependant on the background intensity, inputs beyond 70% resulted in a saturating output.

From the pulse responses obtained in the previous section, it was possible to characterise the cell responses by plotting the peak response of the cell, relative to the pre-stimulus mean, against the log of the corresponding input pulse intensity (V LOG I). Figure 4-7a shows the V LOG I curves of the insect photoreceptor. Note that the photoreceptor was a highly non-linear system. There were only minor changes with the peak magnitude when the input pulse intensities were very low. As the input pulse intensity reached a detection threshold, the cell started to respond logarithmically to the input signal (straight line on a log-scale) for approximately 2-3 log units, depending on the adaptation state. The cell then reached a

saturation level above which the sensitivity of the cell to increasing stimulus intensity reduced. Note also that the response curves shifted to the right and down as the background intensity increased. This was a consequence of the adaptation of the cell to the different background levels.

The same analysis was repeated on the circuit data and shown in Figure 4-7b. The circuit output showed similarities to the neurobiological data. The curves were shifted to the right and down as the background intensity increased. At any one adapting state, the prototype circuit has an effective visual information coding range of approximately 2-3 log units (similar to the neurobiological data recorded).

4.3.4 Frequency Response

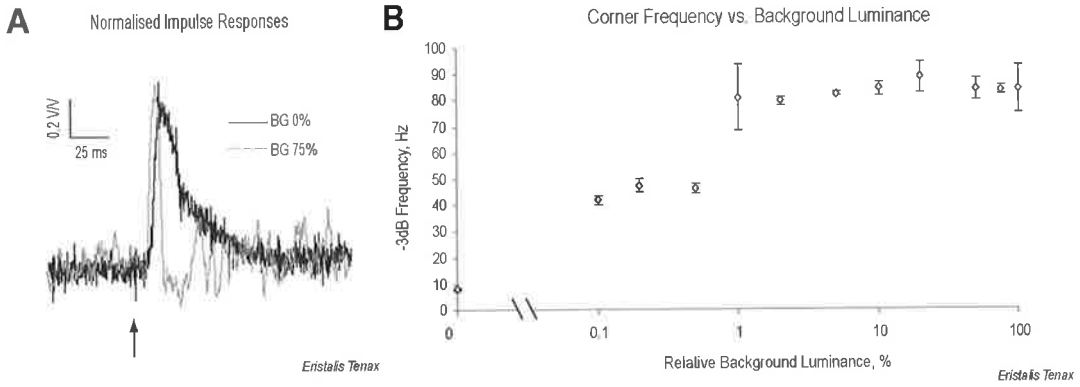

Figure 4-8: Frequency responses of the insect photoreceptor cells. A. Normalised impulse responses of the insect photoreceptor cell *(average of 10 trials for both intensity steps, 1 cell).* B. The calculated -3dB points (corner frequency) of the biological photoreceptor against the corresponding relative background luminance *(average of 3 cells).* Error bars show one standard error of the mean.

Figure 4-8a shows the normalised impulse responses at two different background adaptation states: 0% and 75%. The photoreceptor

responded much slower when the background luminance was at 0% (pulse width of 50ms) compared to when the background luminance was at 75% (pulse width of 7ms). Figure 4-8b shows the corner frequencies (3-dB point) of the cell against various background luminances. The corner frequency of the cell ranged from approximately 10Hz to 90Hz and the speed of roll-off in the cut-off region was indicative of a second order system (-40dB/decade), independent of the background luminance. The corner frequency of the cell increased non-linearly with the background luminance until a saturation point at a background of approximately 5%.

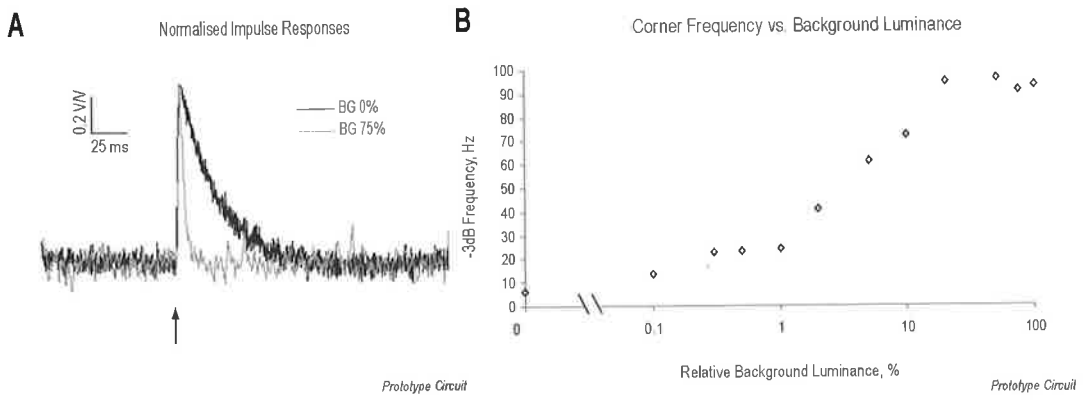

Figure 4-9: Frequency responses of the prototype circuit. A. Normalised impulse responses of the prototype circuit *(average of 20 trials for both intensity steps)*. B. This graph shows the calculated corner frequencies of the circuit against its corresponding relative background luminance.

Similar analysis was done on the impulse responses obtained from the prototype circuit, and is shown in Figure 4-9. The corner frequency range of the circuit was approximately the same as the biological photoreceptor. It was designed to be a second order low pass system. The circuit shows high non-linearity with the changes of the corner frequencies against various background luminance levels.

4.4 Discussions

We have presented an elaborated version of a hardware prototype circuit of a biological photoreceptor cell and described how the elaborated circuit has successfully mimicked most of the important characteristics of the cell. Although this paper only discussed the evaluations of the circuit against non-realistic conditions (steady-state impulse and step response tests), these tests were sufficient to permit the accurate design, implementation and tuning of all stages in the prototype circuit.

This elaborated artificial insect photoreceptor circuit was made as a more faithful mimic of the biological system than existing neuromorphic chip designs. Unlike many other designs this elaborated circuit is embedded with much more complicated features that mimics almost all features of biological photoreceptors.

The first feature is the soft saturation of the V LOG I curves. The elaborated circuit shows a significant saturation at the output when the input pulse intensity is high. This characteristic is a product of the final static non-linear stage (Naka-Rushton Stage). Instead of a hard saturation (Delbrück et al. 1996) this final stage smoothly saturates the output of the circuit in a similar way to the neurobiological data.

Another important feature, which has not been incorporated into any current neuromorphic designs, is the variable gain and corner frequency stage, which acts in a similar way to an automatic shutter in a digital system. At low light levels the gain of the system is increased and the corner frequency lowered (increasing integration time). Studies have shown that a variable corner frequency photoreceptor may improve the visual information coding in

biological visual systems (Weckström et al. 1995; van Hateren et al. 2001). This makes sense because under dark conditions the visual system has to slow down in order to allow time for a sufficient number of photons to enter the eyes for a reliable image to be formed (similar to conventional camera). By slowing down the system, and rejecting higher frequency components where there is little or no signal, the overall signal to noise ratio will increase; i.e. trade off between speed and signal-to-noise ratio. Similarly, when the background luminance is sufficiently high, the system is sped up in order to avoid early saturations and permit a more rapid response to stimuli.

Such a robust, elaborated adaptive artificial photoreceptor model not only provides a feasible front-end solution to many neuromorphic designs but it could also provide a reliable solution for many neurobiologists to use as a front-end for more elaborate systems which are designed to copy higher-order functions of the visual system such as the calculation of wide-field motion and the identification and tracking of targets.

Acknowledgements

We would like to thank the employees of the Botanic Gardens (Adelaide, Wittunga and Mt. Lofty), who had been very helpful during our fly-catching trips. This research was supported with a Linkage grant from the Australian Research Council, including a Post-Doctoral Fellowship for RSAB (LP0667744) and from US Air Force contracts F08630-02-C-0013 and FA9550-04-1-0283.

References

Baumann, F. (1975). Electrophysiological properties of the honey bee retina. The Compound Eye and Vision of Insects. London, Oxford University Press: 53-74.

Baumann, O. (2000). "Distribution of ryanodine receptor ca+21 channels in insect photoreceptor cells." The Journal of Comparative Neurology **421**: 347-361.

Delbrück, T. (1993). "Silicon retina with correlation-based velocity-tuned pixels." IEEE Trans. Neural Network **4**: 529-541.

Delbrück, T. and S. C. Liu (2004). "A silicon early visual system as a model animal." Vision Research **44**: 2083-2089.

Delbrück, T. and C. A. Mead (1996). Analog VLSI phototransduction by continuous time, adaptive, logarithmic photoreceptor circuits. Pasadena, California, California Institute of Technology Computation and Neural Systems Program: 30.

Dror, R. O., D. C. O'Carroll and S. B. Laughlin (2001). "Accuracy of velocity estimation by Reichardt Correlators." Optical Society of America **18**(2): 241-252.

Etienne-Cummings, R., S. Fernando, N. Takahashi, V. Shtonov, J. V. d. Spiegel and P. Mueller (1993). A new temporal domain optical flow measurement technique for focalplane VLSI implementation. Computer Architectures for Machine Perception.

Francheschini, N., J. M. Pichon and C. Blane (1992). "From insect vision to robot vision." Philosophical Transactions: Biological Sciences **337**(1281): 283-294.

Kramer, J., R. Sarpeshkar and C. Koch (1995). An analog VLSI velocity sensor. IEEE International Symposium on Circuits and Systems.

Kramer, J., R. Sarpeshkar and C. Koch (1997). "Pulse-based analog VLSI velocity sensors." IEEE Trans. Circuits and Systems II **44**: 86-101.

Laughlin, S. B. (1989). "A role of sensory adaptation in the retina." J. exp. Biol. **146**: 39-62.

Laughlin, S. B. and R. C. Hardie (1978). "Common strategies for light adaptation in the peripheral visual systems of fly and dragonfly." J. Comp. Physiol. **128**: 319-340.

Laughlin, S. B. and M. Weckström (1993). "Fast and slow photoreceptors - a comparative study of the functional diversity of coding and conductances in the diptera." J. comp. Physiol. A **172**: 593-609.

Liu, S. C. (1996). Silicon model of motion adaptation in the fly visual system. 3rd UCSD-Caltech Symposium on Neural Computation.

Liu, S. C. (1999). "Silicon retina with adaptive filtering properties." Analog Integrated Circuits and Signal Processing **18**: 1-12.

Matic, T. and S. B. Laughlin (1981). "Changes in the intensity-response function of an insect's photoreceptors due to light adaptation." J. comp. Physiol. A **145**: 169-177.

Moini, A., A. Bouzerdoum, K. Eshraghian, A. Yakovleff, X. T. Nguyen, A. Blanksby, R. Beare, D. Abbott and R. E. Bogner (1997). "An insect vision-based motion detection chip." IEEE Press **32**(2): 279-284.

Moini, A., A. Bouzerdoum, A. Yakovlev, D. Abbott, O. Kim, K. Eshraghian and R. Bogner (1996). An analog implementation of early visual processing in insects. Int. Symposium on VLSI Technology, Systems, and Applications.

Netter, T. and N. Francheschini (2002). "A robotic aircraft that follows terrain using a neuromorphic eye." IEEE Press **1**: 129-134.

Payne, R. and J. Howard (1981). "Response of an insect photoreceptor: a simple lognormal model." Nature **290**: 415-416.

Sarpeshkar, R., W. Bair and C. Koch (1993). "Visual motion computation in analog VLSI using pulses." Advances in Neural Information Processing Systems **5**: 781-788.

Sarpeshkar, R., J. Kramer, G. Indiveri and C. Koch (1996). Analog VLSI architectures for motion processing: from fundamental limits to system applications, Proceedings of the IEEE.

Shoemaker, P. A., D. C. O'Carroll and A. D. Straw (2005). "Velocity constancy and models for wide-field visual motion detection in insects." Biological Cybernetics **93**(4): 275-287.

Shoemaker, P. A., D. C. O'Carroll and A. D. Straw (2001). Implementation of Visual Motion Detection with Contrast Adaptation. Electronics and Structures for MEMS II, Adelaide, Australia, Proceedings of SPIE.

Tanner, J. and C. Mead (1988). "An integrated analog optical motion sensor." IEEE Press: 59-87.

van Hateren, J. H. and H. P. Snippe (2001). "Information theoretical evaluation of parametric models of gain control in blowfly photoreceptor cells." Vision Research **41**: 1851-1865.

van Hateren, J. H. and H. P. Snippe (2005). "Phototransduction in primate cones and blowfly photoreceptors: different mechanisms, different algorithms, similar response." J. Comp. Physiol. A **192**: 187-197.

Wallcott, B. (1975). Anatomical changes during light-adaptation in insect compound eyes. The Compound Eye and Vision of Insects. London, Oxford University Press: 20-33.

Weckström, M. and S. B. Laughlin (1995). "Visual ecology and voltage-gated ion channels in insect photoreceptors." Trends in Neurosciences **18**: 17-21.

Wuff, V. J. and W. J. Mueller (1975). The origin of the receptor potential of the lateral eye of Limulus. The Compound Eye and Vision of Insects. London, Oxford University Press: 37-52.

Yakovleff, A. J. S. and A. Moini (1998). "Motion perception using analog VLSI." Analog Integrated Circuits and Signal Processing **15**: 183-200.

5

Chapter 5: Response of a Neuromorphic Photoreceptor Model under Naturalistic Conditions

ENG-LENG MAH, RUSSELL SA BRINKWORTH and DAVID C. O'CARROLL

Discipline of Physiology, School of Molecular and Biomedical Science and the Centre for Biomedical Engineering, The University of Adelaide SA 5005, Australia.

Abstract

Phototransduction processes in fly photoreceptor cells are highly non-linear, displaying adaptation to background luminance, thus increasing the dynamic range of visual information perceived. Physiological studies suggest that this adaptive feature of the fly photoreceptor cells is capable of improving the effective dynamic range up to approximately 8 log units, depending on species. A number of neuromorphic models of insect visual systems have been proposed, with the front-end photodetector being a near linear input system. In this paper we analysed and evaluated the necessity of having a robust, elaborated adaptive photodetector model as the front-end of an artificial visual system. A neuromorphic model was used for comparison with neurophysiological recordings from fly photoreceptor cells. Two types of naturalistic images were used during experiments: (i) traditional (8-bit) natural scene panoramic images and (ii) high dynamic range (32-bit single precision floating-

point) natural scene panoramic images. The same ultra bright light emitting diode was used to playback the panoramic images as time series of intensities to both the fly photoreceptor and the neuromorphic model. Time and frequency domain analyses were used to compare the similarity of the neuromorphic model to the actual neurobiological data. To summarise the findings: (i) the neuromorphic model was a good mimic of actual photoreceptor cells under complicated naturalistic conditions, (ii) the neuromorphic model responded in an almost invariant way to large changes in image intensity (iii) the neuromorphic model had a larger signal to noise ratio than a simple linear model under low lighting conditions, (iv) varying the playback speed (relative motion) of the panoramas had no significant impact on the robustness of the neuromorphic model.

Key words: Insect Photoreceptor, Insect Visual System, Adaptive Photoreceptor, Neuromorphic, Bio-inspired Vision, Naturalistic Stimuli

Correspondence to: Eng-Leng Mah (email: eng.mah@adelaide.edu.au)

5.1 Introduction

Light intensities in real-world environments can vary considerably, especially during partially cloudy days. Despite the changes in surrounding light intensities, most animals are still able to navigate properly without experiencing significant problems. This compensation for varying light levels is not a conscious activity as visual systems have built-in light adaptation mechanisms to increase the effective range of perceived visual information (Baumann 1975; Laughlin et al. 1978; Matic et al. 1981; Fain et al. 2001; Silva et al. 2001). Insects in particular have naturally, throughout millennia of evolution, developed an elegant solution to

cope with high-bandwidth environments efficiently using their low-bandwidth visual systems. Physiological studies suggest that by having an adaptive mechanism animals, and insects, are able to increase their ability to visualise anything in a range of about 8 log units of intensity (Laughlin 1989). A number of researchers have modelled and implemented parts of insect visual systems, most notably the motion sensitive pathways, but many have neglected the importance of faithfully simulating earlier stages of visual processing, despite realising the fact that light adaptation occurs in the early stage of the insect visual pathway, i.e. photoreceptor stage (Kramer et al. 1995; Delbrück et al. 1996; Sarpeshkar et al. 1996; Liu 1999).

Without a good photoreceptor stage, the signals that propagate through the rest of the system might not produce a reliable output for the following higher order stages. For instance, the classic Reichardt Correlator model which uses linear detectors as the front-end to represent the photoreceptors poorly mimics the biological motion detectors as a velocity estimator, especially under dynamic (naturalistic) situations (Dror et al. 2001; Rajesh et al. 2004), while these authors showed that inclusion of some static nonlinearity to mimic some aspects of photoreceptor-like processing improved performance. Their models lacked the dynamic adaptation to luminance and contrast that has been shown to be necessary to mimic biological photoreceptor responses under similar conditions (van Hateren et al. 2001). Therefore, there is a need to devise a robust, elaborated front-end photodetector that properly mimics the biological photoreceptor cells that is robust in both the artificial and real-world environments.

It is impossible to conduct an *in-vivo* experiment on insect photoreceptor cells while having the insects manoeuvring freely in the natural environment, since all *in-vivo* recordings have to be done without any movements between recording apparatus and the insect brain. However, by having a reliable neuromorphic photoreceptor model, it is now possible to reliably predict the photoreceptor responses of a manoeuvring insect to the complex dynamic natural environment (Lindemann et al. 2005). The neuromorphic photoreceptor can be mounted on a robotic platform to manoeuvre around in the natural environment to collect photoreceptor data in real-time.

5.2 Methods

In this article, we have analysed and evaluated our elaborated neuromorphic photoreceptor model against 18 naturalistic scenes; five Low Dynamic Range (LDR) 8-bit panoramic images and thirteen High Dynamic Range (HDR) 32-bit panoramic images. Analysis shows that the neuromorphic model was a very close mimic of the biological photoreceptor cells in both the time (correlation) and frequency (coherence) domains. The neuromorphic model was tested for the effects of different maximum playback intensities (8-bit panoramas) and different playback speed (32-bit panoramas).

The 8-bit format LDR images were used in initial experiments. However, since the real-world luminance covers a much larger range, it is important that we be able to generate a system that realises a better representation of the real-world luminance. Playing back the luminance dynamic with only 256 steps can only produce a contrast between the dullest non-zero value and the brightest value

of 1:255, i.e. a poor representation of the real-world contrast. Since our system is capable of performing at a better dynamic range ($1:10^6$), later experiments were carried out using a set of 32-bit HDR panoramic images.

5.2.1 Stimuli Generation

The visual stimuli were presented to the fly photoreceptors and the neuromorphic model using an ultra bright green Light Emitting Diode (LED; Luxeon Star, Luxeon™). The LED was driven by a calibrated high current amplifier (350mA maximum current output) and the luminance level was fully controlled via a 16-bit data acquisition card (NI PCI6221, National Instruments™). The non-linear response of the LED with input voltage was recorded using a high precision photodiode (265, UDT Instruments™) and photodiode amplifier (PDA750, Terahertz Technology Inc™) combination. This transfer function was then used to produce a linearised response curve for the system. The maximum playback luminance of the LED was recorded to be approximately 70,000Cd/m^2 (100%), comparable to the luminance of the sky close to the sun on a bright day.

Due to the non-linear action of the LED close to threshold it was possible to accurately modulate extremely dim stimuli (0.0001%) at the lower end while still being able to deliver very bright stimuli. The usable dynamic range was six log units (120dB), which is greater than that permitted by a 16-bit linear system which would have a range of 4.8 log units (96dB). The LED was electrically isolated using an optical fibre core light guide to eliminate electrical noise interferences. A high precision 5-axis Cardan-Arm system was used to move the light source during experiments. The tip of the light-

guide was placed close enough to the detector under test (either biological or artificial) to fill its acceptance angle. In other words, the LED was effectively an extended source. But since the stimuli played out through it had been sampled in a manner that takes into account the normal optics and sampling of the fly eye, we can use this approach to reconstruct the scene in two-dimensions as encoded by the eye.

5.2.2 Panoramic Images - Generation

Two sets of images were used during experiments: (i) 8-bit LDR panoramic images. (ii) 32-bit HDR panoramic images. The images were captured using a high resolution digital camera (Nikon D-70) mounted on a panoramic tripod head, with the centre of rotation aligned with the lens nodal point. Images were taken at 30^{o} increments and a panorama stitching software was used to stitch the images together to complete the whole 360° horizontal field of view. Windy days were avoided during image capture in order to minimise any movements or changes to the scene settings because any differences between the adjacent images could introduce stitching artifacts. Figure 5-1 further illustrates the methodology discussed above.

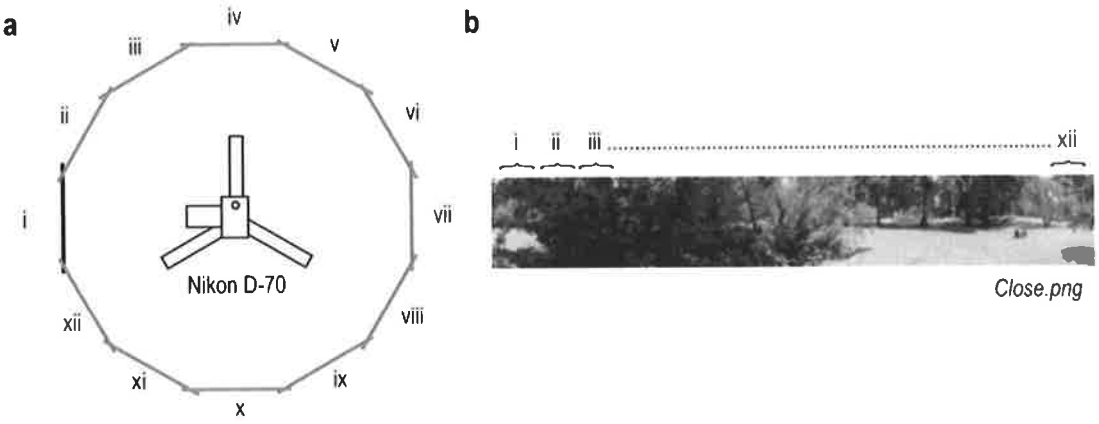

Figure 5-1: Panoramic image generation setup. Twelve images (i – xii) were taken using a digital camera mounted on a panoramic tripod *(left)*. All the images were stitched together to form a complete 360° (horizontal) panorama *(right)*.

More effort was spent generating the high dynamic range images in order to better represent the real-world luminance. Similarly to the 8-bit images, several images were taken before stitching them together to form a panoramic image. However, instead of just a single shot per 30°, three shots of the same scene were taken at a time with different shutter speeds. The camera was preset to an f-stop number of eleven and the first shutter speed was adjusted such that the brightest part of the scene did not saturate the camera's dynamic range. The two subsequent shots of the same scene were taken using progressively faster shutter speeds. A total of 12x3 shots were taken per panoramic image and all of the shots were saved as .NEF (raw format). NEF images were converted to 16-bit TIFF format in Photoshop, but left in a raw (unprocessed) state for subsequent processing. One panorama was constructed for each shutter speed using PTGui software and all the processes and output were kept at 16-bit format. The non-linear encoding of luminance by the camera was corrected (Debevec et al. 1997) and the images combined and converted to 32-bit floating point using a custom program written in LabVIEW®.

8-bit Panoramic Images

All the 8-bit panoramic images were scaled to 1000x150 pixels (360x54 deg). In order to closely mimic the optical characteristics of a fly, the panoramic images were then pre-blurred with a 1° half-width Gaussian function in Photoshop. 36 rows were sampled during experiments to mimic an inter-receptor angle of 1.3° (Stavenga 2003; Straw et al. 2006). Only the green channel of the images was presented since the majority of the photoreceptors are green sensitive (Smakman et al. 1986). Figure 5-2 further illustrates the procedures discussed above.

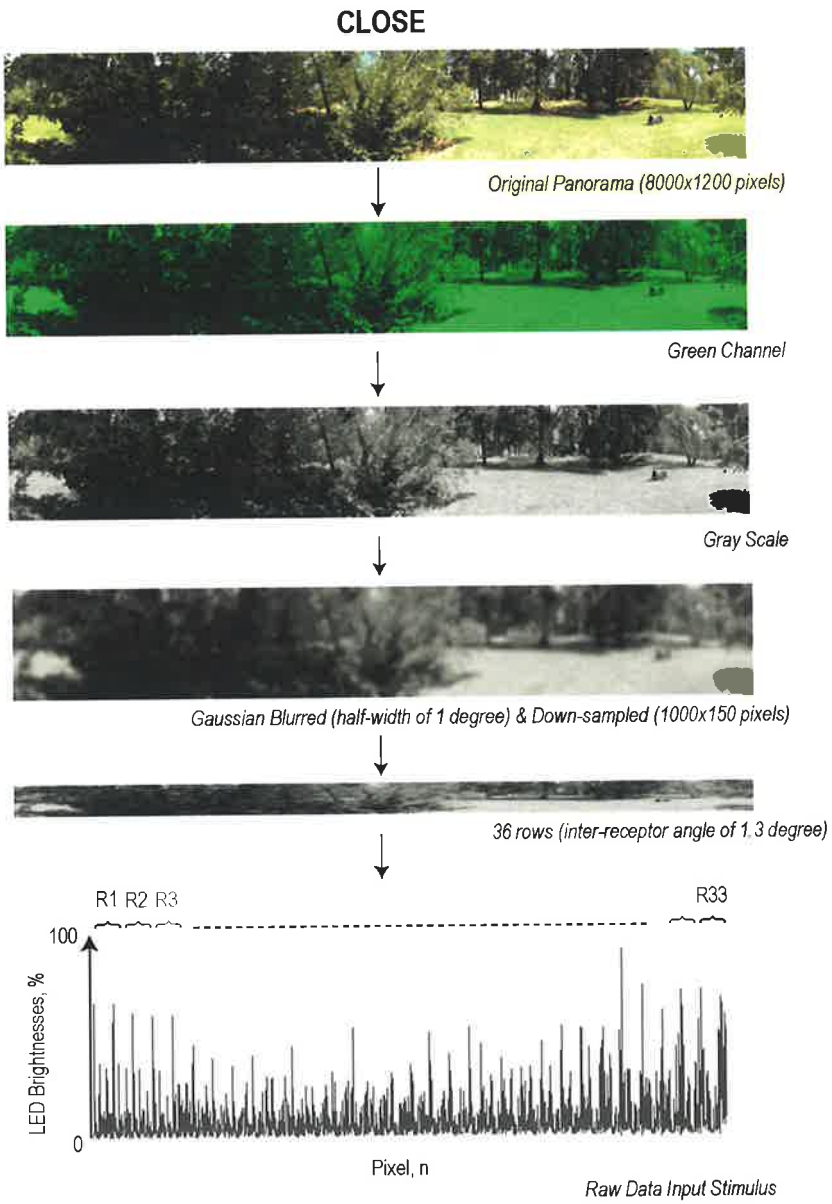

Figure 5-2: 8-bit panoramic image generation. The original images were taken in a full colour format and they were stitched together to form a full colour panorama as shown (8000x1200 pixels). Since the flies photoreceptors are green colour sensitive, the panorama was deliberately filtered in Photoshop to only keep the information from the green channel. The panorama was then converted to the grey scale format for better representation on the screen. A half-width of 1° Gaussian blur was applied to the grey-scaled panorama to emulate the optical blur of the insects' eyes. The panorama was down-sampled and converted to a natural time series of intensities. R1 to R36 were the rows of the down-sampled panorama and they were played from the left to the right of the panorama during experiments, i.e. a spinning drum effect.

For this paper, we used five different 8-bit panoramas. Each of the panoramas was played back at eight different maximum intensities in order to thoroughly evaluate the artificial circuit under various luminance conditions: 0.1%, 0.5%, 1%, 5%, 10%, 30%, 50% and 100%. The panoramas were displayed at 1kHz, i.e. simulating a rotational speed of 360°/s.

32-bit Panoramic Images

The HDR panoramas were scaled to 8000x1600 pixels (360x72 deg) and had a 1.4° half-width Gaussian blur, which matches the size of the receptors in the bright zone of *Eristalis tenax* (Stavenga 2003). In order to emulate an inter-receptor angle of 1° (Straw et al. 2006), the panoramas were converted to 8000x62 and the first row played twice to reduce start-up noise (onset saturation due to low luminance pre-adaptive states). Note that the inter-receptor angle of the 32-bit panoramas was based on the horizontal measurement on a hex-sampled grid. Hence, the vertical distance had a factor of 1/cos (30°) and it must be included for the above calculations of resolutions to be correct (Figure 5-3).

The HDR panoramas were played back at real-world luminance levels and various speeds: 45°/s, 90°/s, 180°/s, 360°/s, 720°/s and 1440°/s.

Hexagonal Representation of Flies Compound Eyes

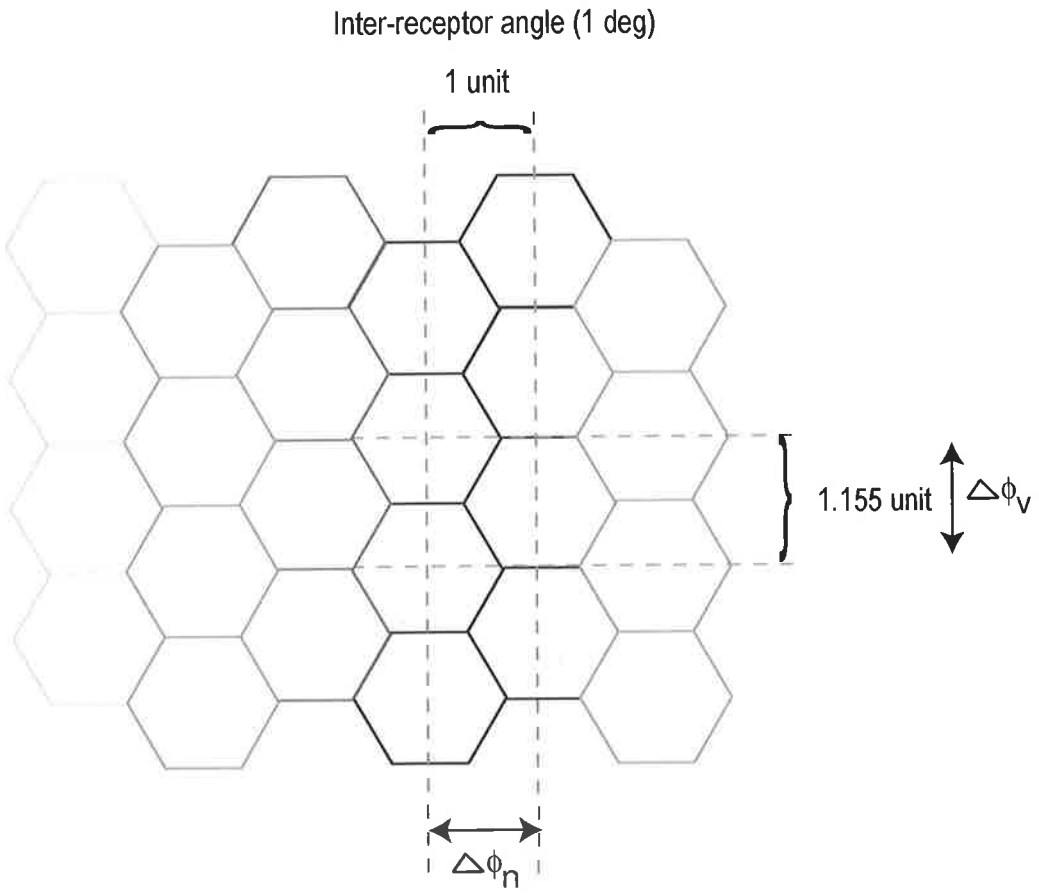

Figure 5-3: Hexagonal representation of fly's compound eye where each hexagonal box represents a single facet lens. 1° inter-receptor angle was used to calculate the amount of rows of the panorama required for experiments.

5.2.3 Electrophysiological Recordings

A number of electrophysiological experiments were conducted to evaluate the responses of biological photoreceptors to the stimuli. All experiments were recorded in the fronto-dorsal "bright-zone" (Straw et al. 2006) photoreceptors of intact hoverflies (*Eristalis tenax*). Since photoreceptors are temperature sensitive (Tatler et al. 2000), temperature was controlled and maintained in the range 23-25°C. Individual photoreceptor cells were penetrated with a manipulated

micropipette filled with 2.0M KCl, with a resistance of 100-200MΩ. The microelectrode was connected to a pre-amplifier (BA1S npi) and the amplified output was connected to a high precision 50Hz filter (Hum Bug, Quest Scientific) to eliminate unwanted power line interference. The output of the Hum Bug was monitored using a digital oscilloscope (TDS210, Tektronix™). Results were recorded using the 16-bit data acquisition card system (NI PCI6221, National Instruments™) and custom software written in LabVIEW®.

5.2.4 Neuromorphic Modelling and Recordings

The neuromorphic model was designed and implemented using electronic discrete components available off the shelf. The neuromorphic model was built on breadboards for testing and evaluation purposes. Initial modelling was done using Matlab & Simulink and DXP simulation suite software. A working model was then used as a basic model to implement the neuromorphic model which consisted of a cascade of several dynamic and static non-linear stages to mimic the response of a true biological photoreceptor (Mah et al. 2006) (Chapter 3).

Stimuli similar to those used during electrophysiological recordings were applied to the prototype circuit to obtain results for comparison purposes. An amplified photodiode (TSL251) was used as the light detector for the neuromorphic model. Data were recorded using the 16-bit data acquisition card system and custom software written in LabVIEW®.

5.2.5 Data Analyses

Mathematical approaches were used to evaluate the similarity between the biological photoreceptors and artificial photoreceptor circuit in both time (correlation) and frequency (coherence) domains. Averages were obtained from data with multiple trials and 95% confidence interval was used to statistically measure the error margin. Both analyses were performed using custom software written in LabVIEW®.

Panoramic Images – Reconstruction

All the results obtained during experiments were resynthesised and rescaled (1000x150 for the LDR panoramas and 1000x200 for the HDR panoramas) from the neuronal recordings using a custom program written in LabVIEW® for image reconstruction.

Noise Limit

A Fast Fourier Transform (FFT) was used to measure the noise limit for all data collected from the 8-bit panoramas. Since the data were sampled at 1kHz, it was reasonable to assume that the wide-band signal which becomes discernable as a plateau region near the Nyquist limit (i.e. 500Hz) was white noise. Thus, the average power spectra of the frequencies ranging from 450-500Hz were measured to determine the mean noise level (dB) for that particular panorama scene. The upper bound of this noise level (at mean + 95% CI of the mean) was then used as a point to statistically ($p>0.05$) determine the noise-limit frequency of any power spectra obtained from the experiments, i.e. the noise-limit frequency of the recording was located at the point where the recorded spectrum rose above this

upper bound curve. Any regions of the spectrum below this level can be considered to be noise.

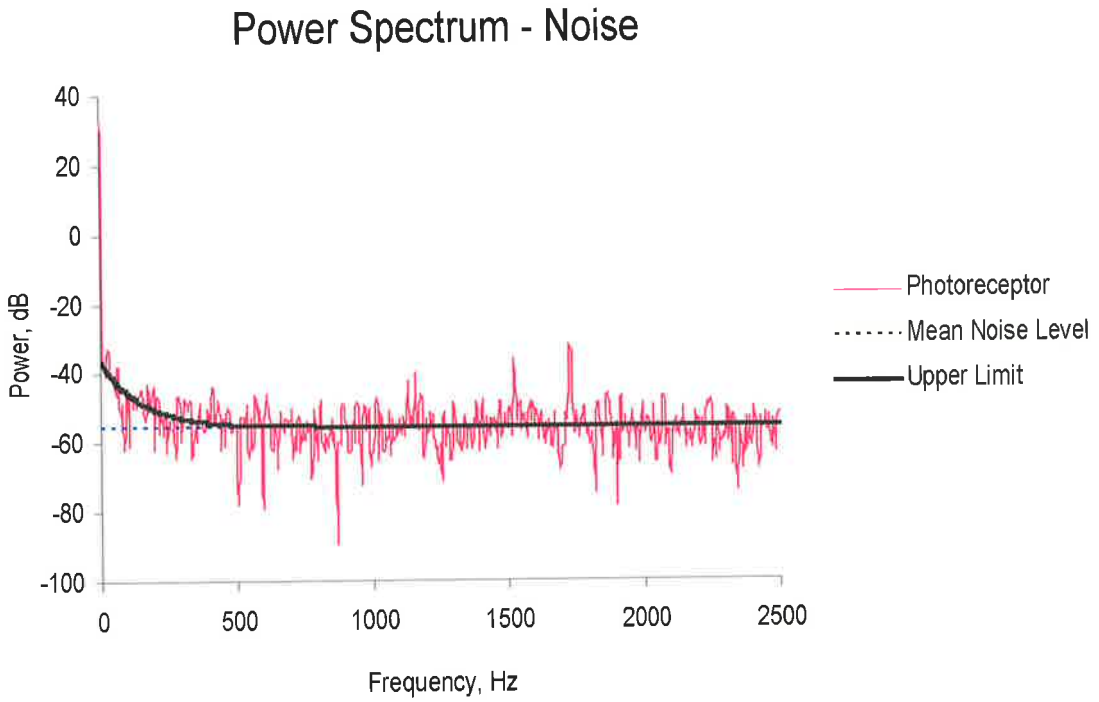

Figure 5-4: Power spectrum of the noisy biological photoreceptor response to a stimulus with an intensity equal to the median intensity of a scene *(Barr-Smith)* from a 32-bit panorama. The upper limit (mean+95% CI of the mean) curve was fitted to the spectrum, clearly showing the departure from the mean noise level at lower frequencies

A similar method was applied to measure the noise limit for the 32-bit panorama power spectra, which were sampled at 5kHz. However, to determine the white noise level for the 32-bit panoramas, a recording was made to measure the response of the biological photoreceptor to a stimulus equal to the median intensity of one of the thirteen panoramic images *(Barr-Smith)*. It was found that the resulting noise power spectrum exhibited a non-linear curve at lower frequencies, instead of a constant value. As a result of this, an upper bound curve was fitted to the spectrum to obtain the noise upper bound (Figure 5-4). This fitted curve was then used to determine the

noise-limit frequency in the 32-bit panorama spectra in a similar manner as with the 8-bit recordings.

Peak Value, Average Passband and Corner Frequency

Since it would be difficult to visually measure the performance of the non-linear photoreceptor circuit against the linear system or the actual biological photoreceptors, three important parameters (peak value, average passband and corner frequency) were obtained from the analysed coherence curves as illustrated in Figure 5-5. The peak value was taken as the maximum coherence value of the curve and the corner frequency was measured when the coherence value was 0.7. The average passband was calculated by averaging the coherence values when the power spectrum was above a defined noise-limit frequency (obtained from the power spectrum curve).

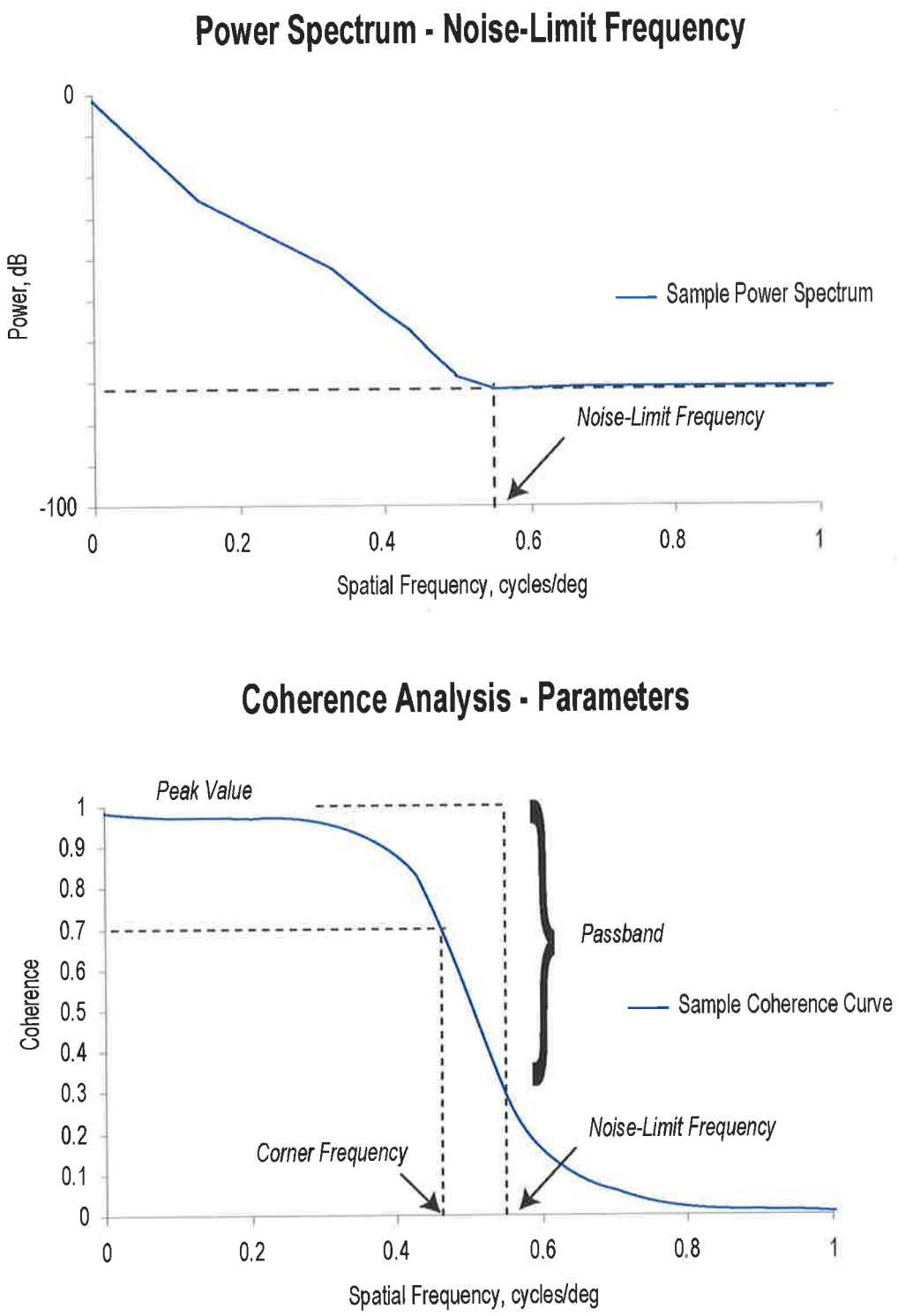

Figure 5-5: Coherence analysis parameters. The maximum value of the curve was assigned as the peak value parameter. The corner frequency was located where the coherence value was at 0.7. The average passband was obtained by averaging the coherence values between the frequency band of 0 and noise-limit frequency.

5.3 Results

5.3.1 8-bit Images

Figure 5-6 shows the reconstructed images from the output responses of both the biological and artificial non-linear photoreceptors to one scene played back at a variety of luminance levels. Notice that the output images for both were very dim when the maximum playback intensities were very low (0.1% and 0.5%). As the intensity increased, the images became more visible as the contrast of the images was greatly enhanced. More details of the images were observed after being processed by the photoreceptors. The darker bits of the image were amplified and the brighter parts darkened. Similar output responses were observed for the other 4 panoramas ***(Appendix: Figure A1-4)***

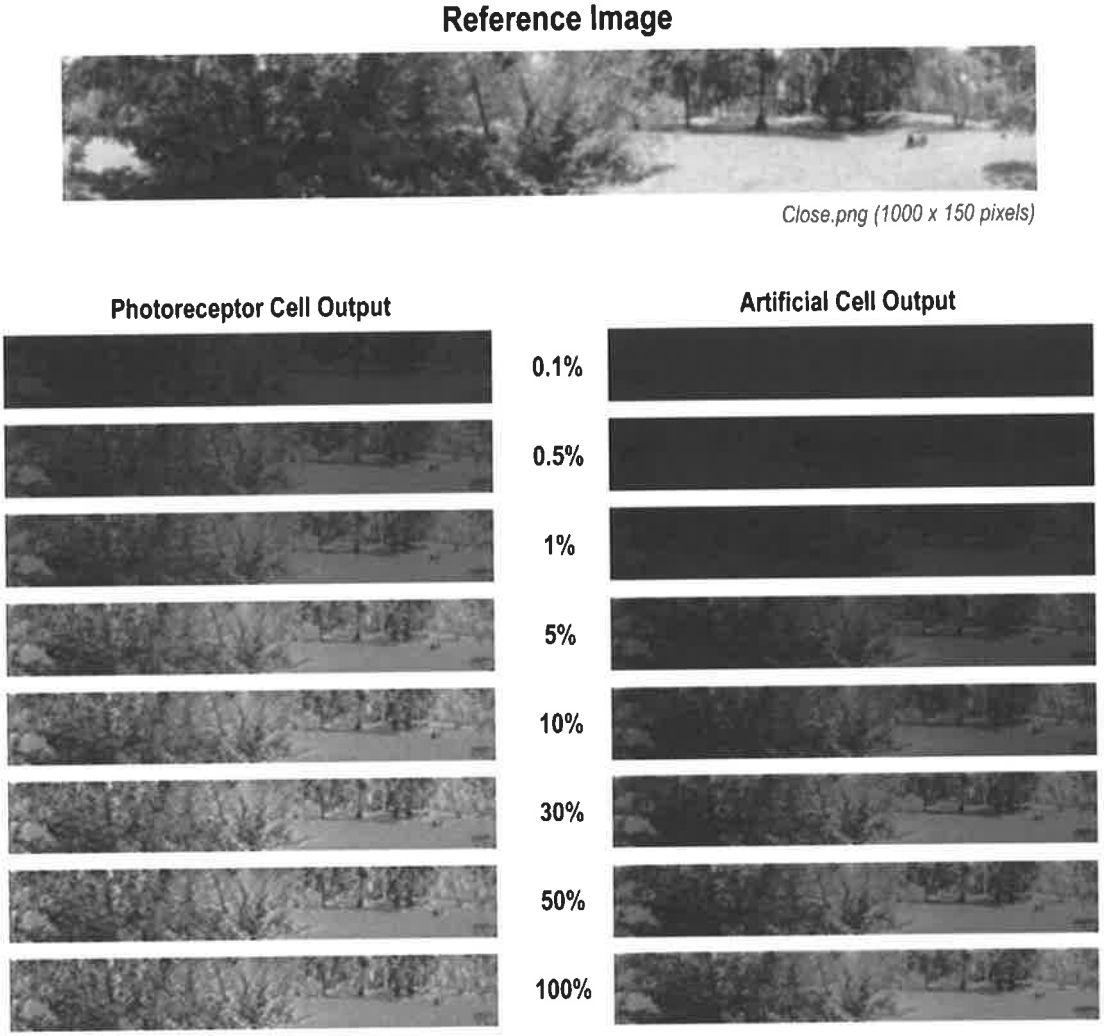

Figure 5-6: Reconstructed output images from both the actual biological photoreceptors *(average of 4 trials)* and the artificial photoreceptor *(no repeats)* at several maximum brightness playbacks – 0.1%, 0.5%, 1%, 5%, 10%, 30%, 50% and 100%. The image at the top of the figure was used as a reference for all mathematical analyses.

Power Spectrums

Figure 5-7 shows the power spectra of the photoreceptor output images to a single LDR scene at various maximum playback intensities. The power spectrum curves shifted closer to that of the reference image curve as the maximum playback intensity increased, i.e. more details from the panoramas were captured by both the

biological photoreceptors and the artificial photoreceptor as the playback intensity increased. Notice also that the power spectrum curves for the circuit were generally weaker compared to the biological output during dim playback intensities (0.1%, 0.5%, 1% and 5%). This may due to the imperfect matching of the circuit corner frequency to the actual biological photoreceptors. As the intensity increased (10%, 30%, 50% and 100%), the power spectrum curves of the biological photoreceptors and the circuit became similar. The curves also tended not to shift that much as both the biological and artificial photoreceptors reached their saturation level.

Figure 5-8 shows the average power spectra of all five images at various intensities. Again, the power spectrum curves shifted to the right as the playback intensity increased. The power spectrum curves for the artificial photoreceptor were lower compared to the actual biological photoreceptors during dim intensity playbacks (0.1%, 0.5%, 1%, 5% and 10%). As the playback intensity increased, both of the curves tended to saturate at the same level.

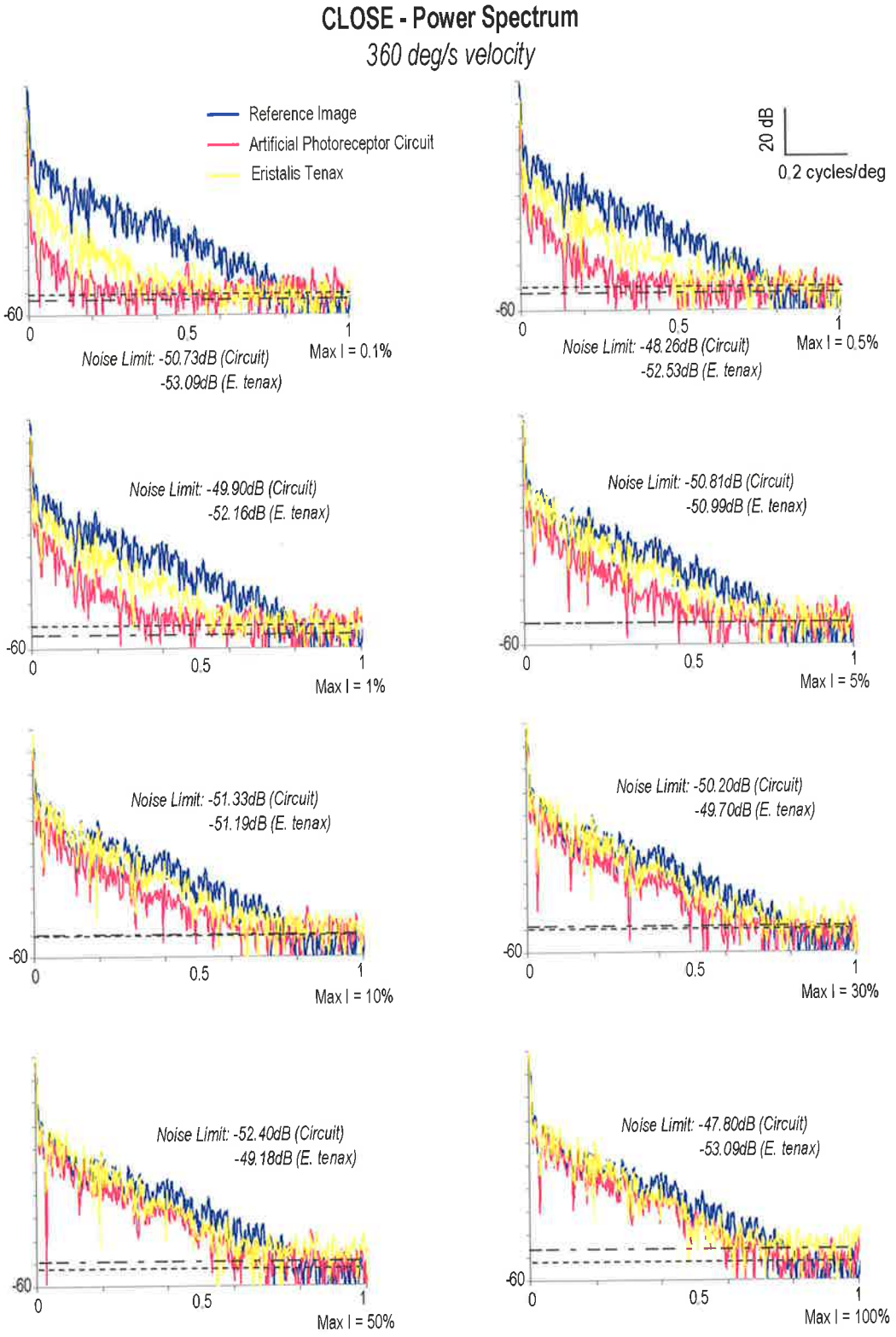

Figure 5-7: Power spectra under various maximum playback intensities (0.1%, 0.5%, 1%, 5%, 10%, 30%, 50% and 100%). The dotted lines on the graphs were used as a noise level indication where anything below the line was considered noise.

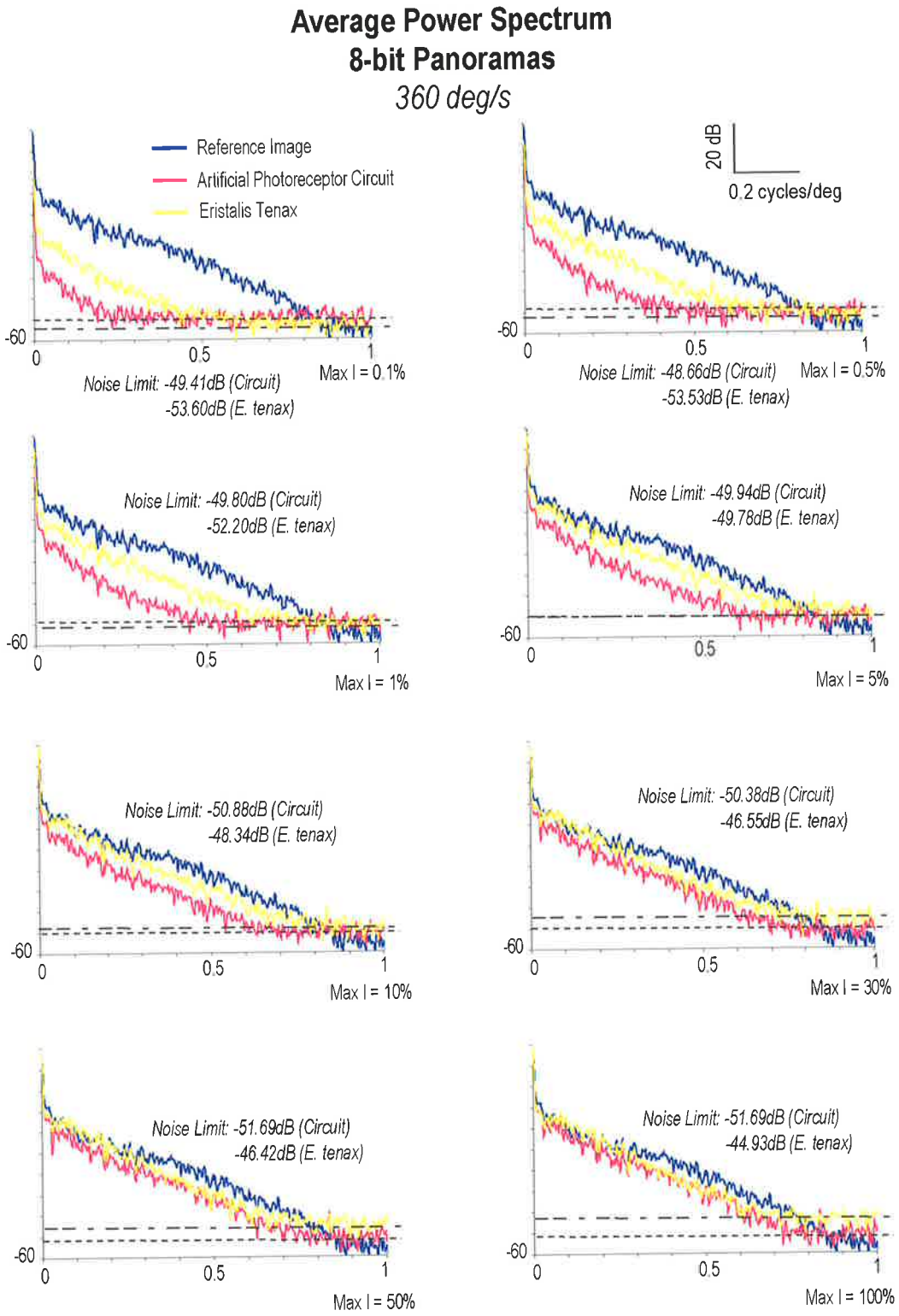

Figure 5-8: Average power spectrums from five panoramic images (8-bit) under various maximum playback intensities (0.1%, 0.5%, 1%, 5%, 10%, 30%, 50% and 100%). The dotted lines on the graphs were used as a noise level indication where anything below the line was considered noise.

Correlation Analyses

Figure 5-9 shows the average correlation analysis between the artificial insect photoreceptor and the actual biological photoreceptor cells. A linear system was used as an experimental control. The artificial photoreceptor showed a great correlation to the biological cells for all the panoramic images with majority of them having an average r^2 value of greater than 0.8 (better than the linear system which had $r^2 < 0.7$). The artificial photoreceptor had an average (for all light levels except 0.1%) 18.92% improvement in the correlation coefficient over the simple linear system. Also note that the artificial photoreceptor was mimicking the biological photoreceptor optimally for all five images where the maximum playback intensity was at 1% with an average $r^2=0.892\pm0.028$ (mean ± 95% CI of the mean) compared to the linear system with an average $r^2=0.835\pm0.039$. However, the correlations tended to depreciate as the maximum playback intensity increased.

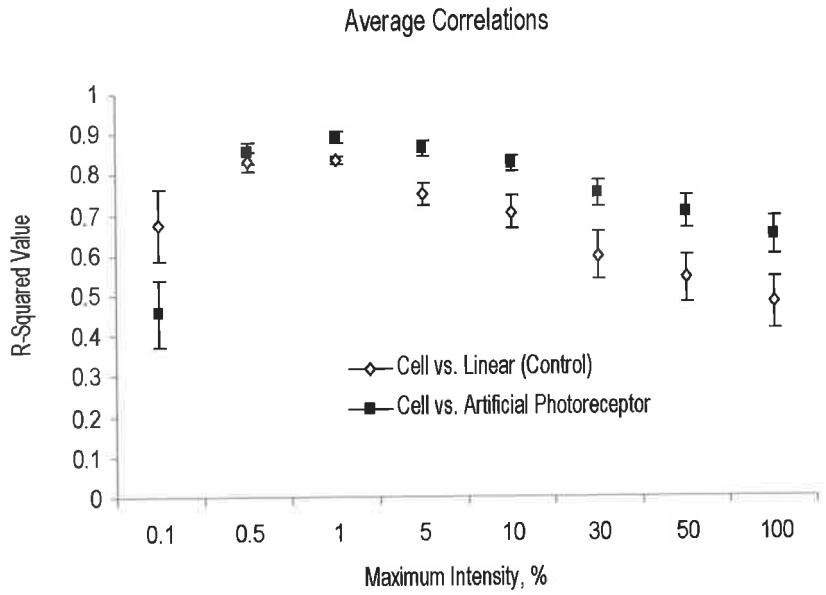

Figure 5-9: Average correlation of the output of the actual biological photoreceptor cells *(average of 5 r^2 values from five different images under the same maximum playback intensity; 4 trials each)* against the artificial insect photoreceptor circuit *(no repeats)*. Error bars show the standard errors.

The correlation of the artificial non-linear photoreceptor response to the biological photoreceptor was always higher than for the linear system except at the playback intensity of 0.1%. In this instance the artificial photoreceptor was incapable of demonstrating a good correlation (r^2=0.456±0.231) with the biological photoreceptors compared to the linear system (r^2=0.673±0.213), likely due to noise at the input to the system caused by the use of a linear photodiode (TSL 251).

Coherence Analyses

Figure 5-10 shows the coherence analysis output of an image (Close.png) against various maximum playback intensities. Notice that the coherence curves were shifted to the right as the playback intensity increased. At low intensity (0.1%), the artificial photoreceptor was highly cohered (> 0.7) with the biological photoreceptors and had a corner spatial frequency of approximately 0.1cycles/°. As the maximum playback intensity increased, the artificial photoreceptor became highly cohered with the biological photoreceptors for a larger range of spatial frequencies. However, as the maximum playback intensities were beyond 5-10%, the curves tended not to shift any further (saturated). The corner spatial frequency of the saturated curves was at approximately 0.5cycles/° for this particular image.

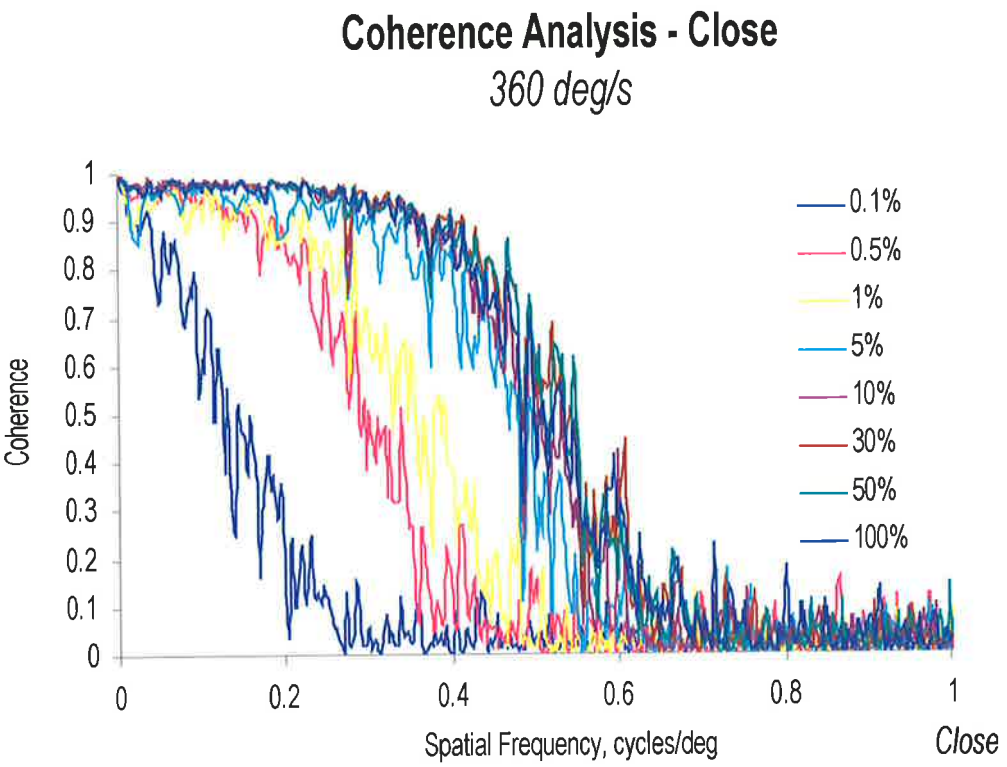

Figure 5-10: Coherence analysis between the actual biological photoreceptor cells *(4 trials)* and the artificial photoreceptor circuit *(no repeats)* at various maximum intensity playbacks.

Figure 5-11 shows the output of two important analysed parameters: average passband coherence values and average corner frequencies from the five different panoramas. Notice that the overall average passband coherence values (Figure 5-11a) of the linear photodiode against biological photoreceptors were lower compared to the average coherence values of the artificial photoreceptor, i.e. the photoreceptor circuit was performing robustly under all the playback intensities. Note that the photoreceptor circuit performed its best during the 5% maximum intensity playback with average passband value of 0.847±0.026 CI. The lowest average passband value calculated for the photoreceptor circuit against biological photoreceptors was 0.707±0.046 CI at the playback intensity of 0.1%.

The low average passband values (in general) for the linear photodiode system against the biological photoreceptor strengthen the fact that the photoreceptor circuit was mimicking the actual biological photoreceptors better than the simple linear system. Notice that the lowest average passband values for the linear system was 0.655±0.044 CI at playback intensity of 0.1% while the highest was 0.769±0.028 CI at 50% maximum intensity playback.

The average corner spatial frequencies (Figure 5-11b) for both the linear photodiode and artificial photoreceptor tended to increase as the maximum playback intensities increased, i.e. the coherence curves were shifted to the right as the playback intensities increased. They both saturated at approximately 0.45cycles/° during high intensity playback (beyond 5-10%).

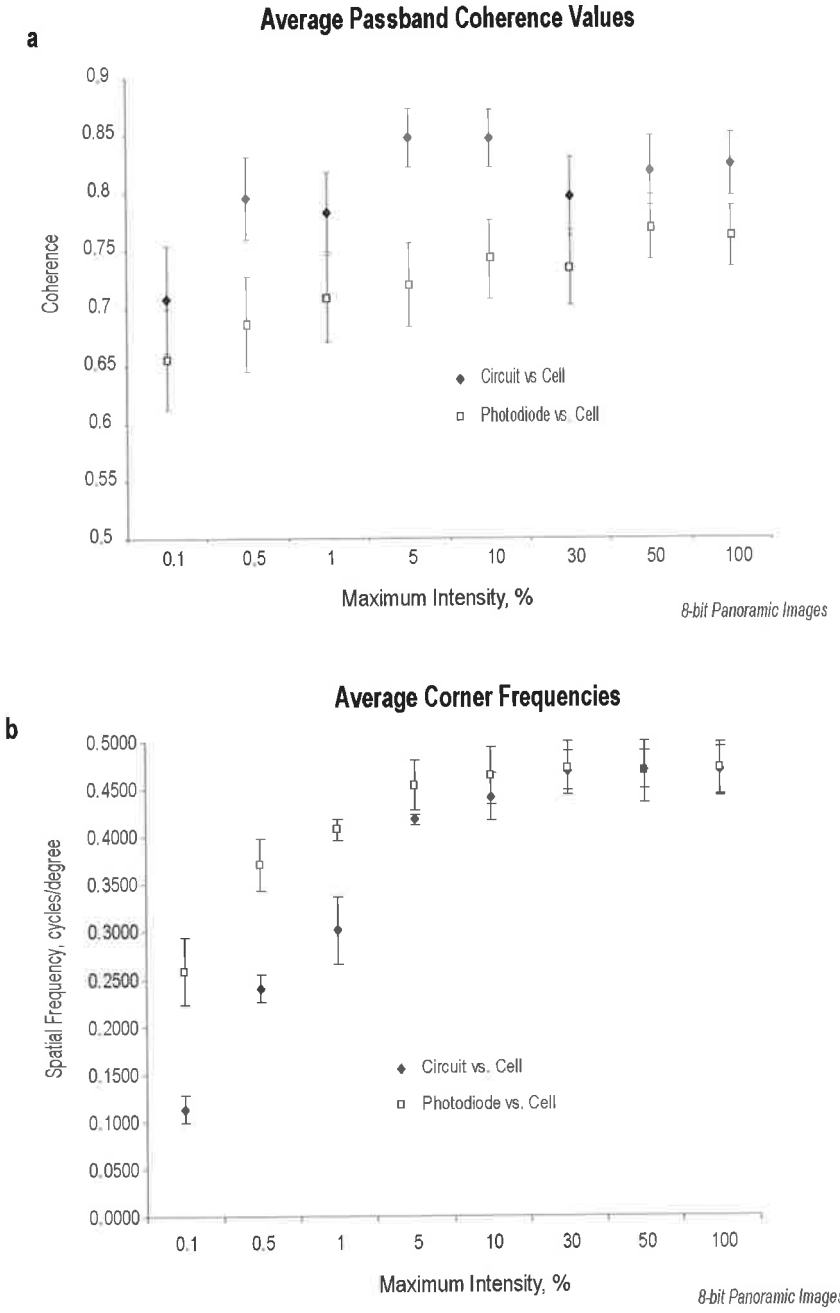

Figure 5-11: Coherence analysis parameters of the 8-bit panoramic images. a. Average passband values calculated from the coherence analyses of the 8-bit images for both the photoreceptor circuit and linear photodiode against actual biological photoreceptors *(averages of 5 mean values from 5 different images under the same playback intensity; 4 trials each).* Error bars show the 95% confidence interval. b. Average corner frequencies from the coherence analyses for both the photoreceptor circuit and linear photodiode against actual biological photoreceptors *(averages of 5 mean values from 5 different images under the same playback intensity; 4 trials each).* Error bars show the 95% confidence interval.

5.3.2 32-bit Images

The following figure shows the reconstructed images of both the recorded biological photoreceptors output and the artificial photoreceptor output (Figure 5-12). Notice that as the playback speed increased, the images seen by both the biological photoreceptors and the artificial photoreceptor were blurred (360°/s, 720°/s and 1440°/s). Similar output responses were observed for the rest of the 12 panoramas ***(Appendix: Figure A5-16).***

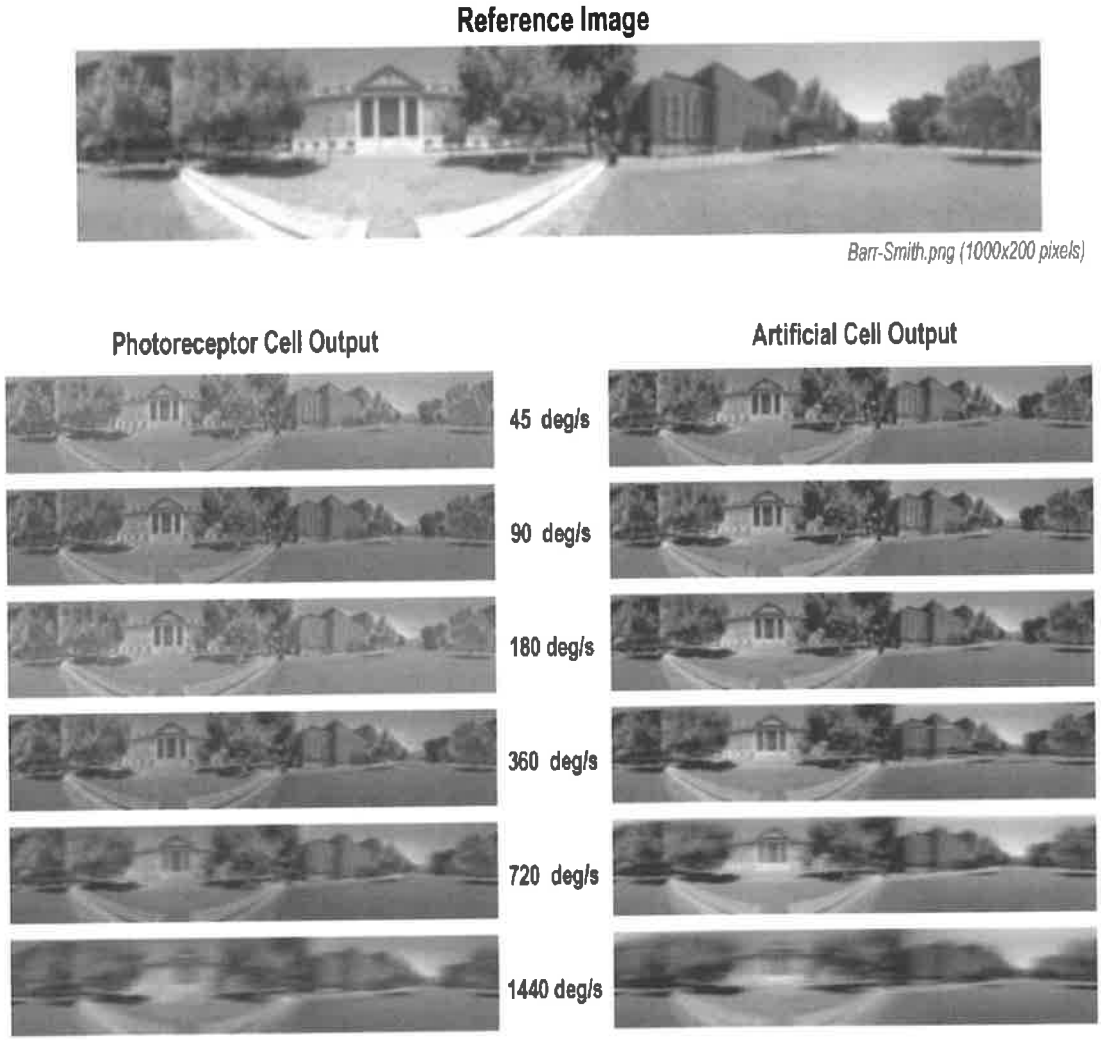

Figure 5-12: Reconstructed output images from both the actual biological photoreceptors *(average of 4 trials)* and the prototype circuit *(no repeats)* at several playback speeds – 45°/s, 90°/s, 180°/s, 360°/s, 720°/s and 1440°/s. The image at the top of the figure was used as a reference for all mathematical analyses.

Power Spectrum

Figure 5-13 shows the average power spectrums of 13 different images at the 6 different speeds: 45°/s, 90°/s, 180°/s, 360°/s, 720°/s and 1440°/s. According to the power spectrum curves, the artificial photoreceptor output shared a very similar output energy level with the biological photoreceptors output. As the speed of the panorama playback increased, the energy at high spatial frequency for both the artificial photoreceptor and the biological output decreased. At the lowest speed (45°/s), the power spectrum curves for both the artificial photoreceptor and biological cells were saturated at the noise-limit-frequencies of 1.836cycles/° and 0.683cycles/°, respectively. The saturation point decreased as the speed increased with a minimum saturation point of 0.317cycles/° (artificial photoreceptor) and 0.283cycles/° (biological cells) at the playback speed of 1440°/s.

The power spectra of the photodiode output (linear system) were used as the control to the experiments. Note that, as the playback speed increased, both the power spectra from the photoreceptor circuit and biological photoreceptors tended to shift to the left, away from the linear system power spectra. In other words, high spatial frequency components of the panoramic images were filtered by the non-linearities of the biological and artificial photoreceptors as the playback speed increased.

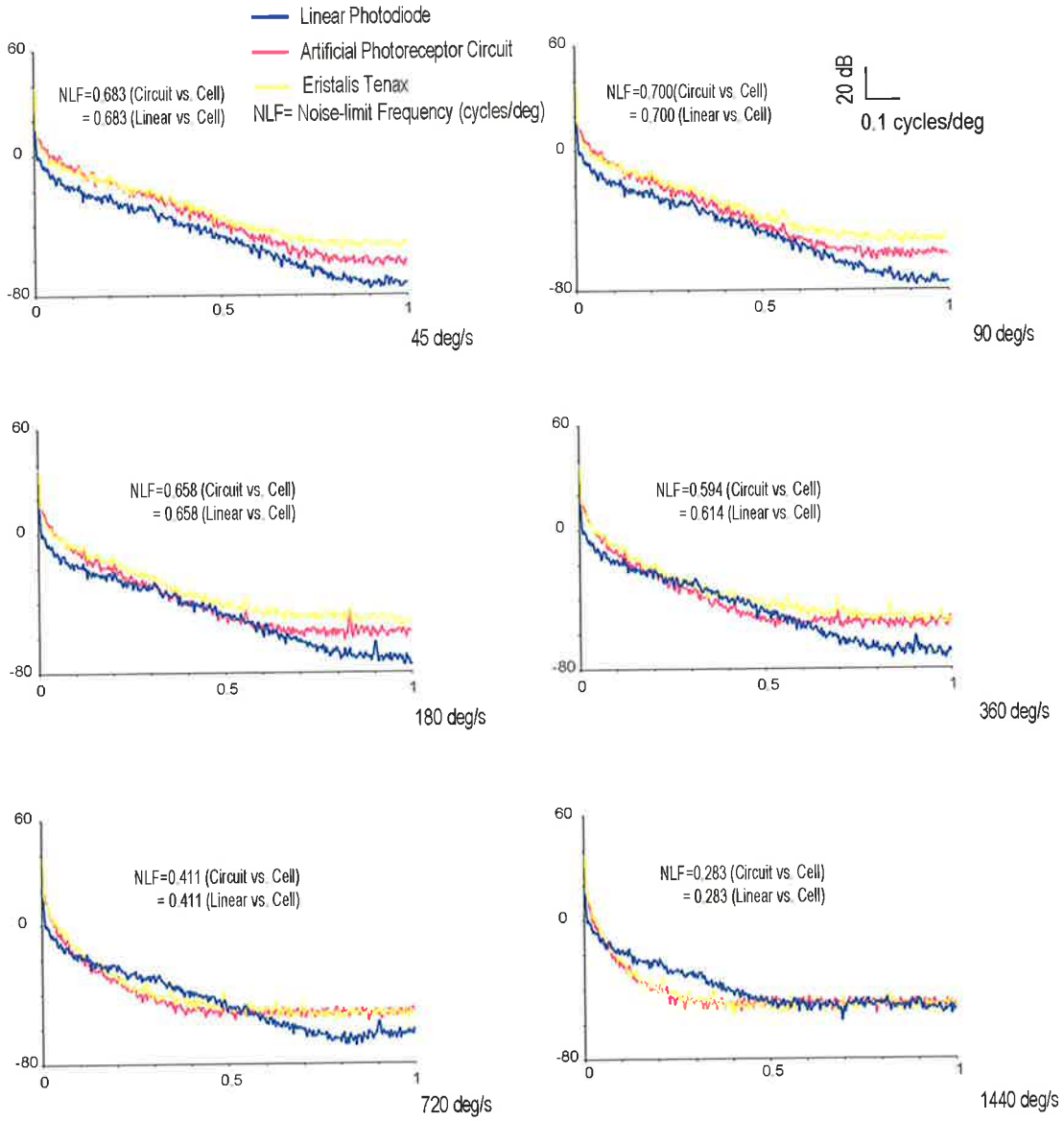

Figure 5-13: Average power spectrums from thirteen panorama images (32-bit) under various playback speeds (45°/s, 90°/s, 180°/s, 360°/s, 720°/s and 1440°/s).

Correlation Analysis

Figure 5-14 shows the average correlation analyses between the artificial photoreceptor and the actual biological photoreceptor cells.

Again, a linear system was used as a control experiment. The artificial photoreceptor showed an excellent correlation to the biological cells for all the panoramic images and had an average r^2 value > 0.8 (greater than the linear system – approximately 0.6). Also notice that the artificial photoreceptor was mimicking the biological photoreceptors optimally for all the 13 images when the playback speed was at 90°/s with an average $r^2=0.862\pm0.049$. However, the correlations tended to depreciate as the playback speed increased, i.e. the similarity between the artificial photoreceptor the actual biological photoreceptors in the time domain decreased as the playback speed increased. This was because as the playback speed increased, the long time constant decaying of the biological photoreceptors became significantly slower as compared to the adaptation rate of the artificial photoreceptor.

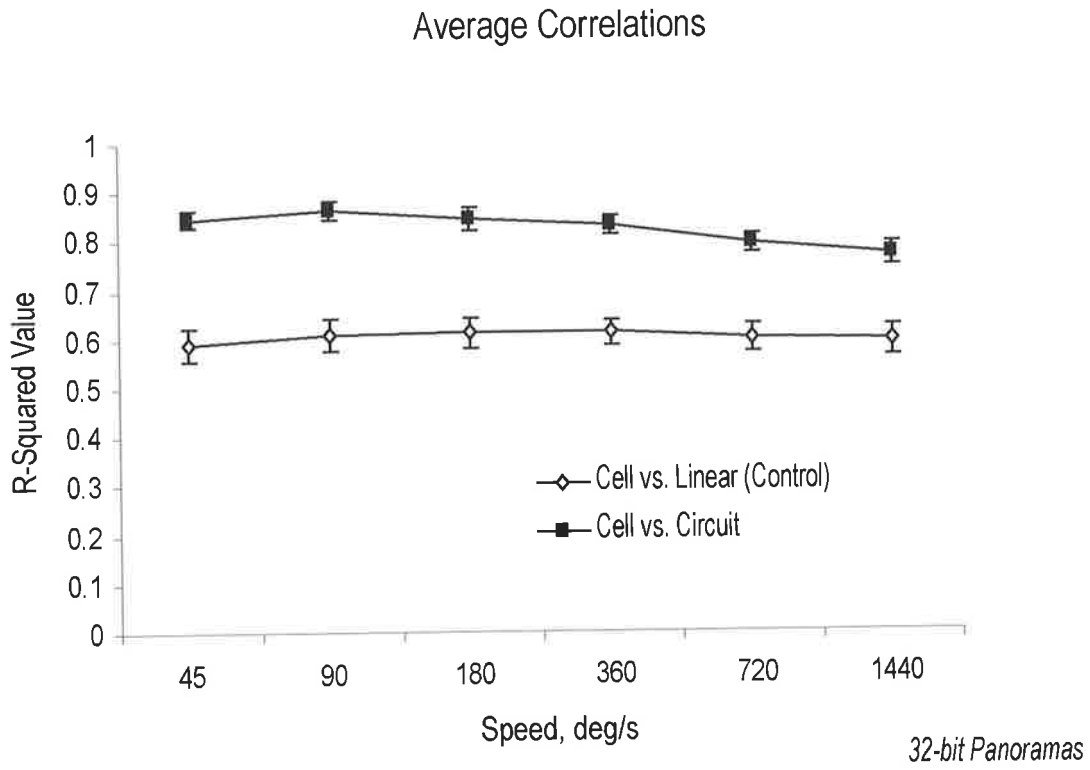

Figure 5-14: Average correlations of the actual biological photoreceptor cells *(average of 13 r^2 values from 13 different images under the same playback speed; 4 trials each)* against the artificial insect photoreceptor circuit *(no repeats)*. Error bars show the standard errors. The 13 different panoramic images (32-bit quality) that were used to test and evaluate both the actual photoreceptor and the artificial circuit were *Barr-Smith, Block, Botanic, Bushes, Car Park, Close, Creek Bed, Lab, Mt Lofty, Outdoor, Rock Garden, Shadow and Tree.*

Coherence Analysis

Figure 5-15a shows the average passband values for the artificial photoreceptor and linear photodiode against the actual biological photoreceptors of 13 different panoramas. Again, the average passband values for the artificial photoreceptor against the actual biological photoreceptors were higher for all playback speeds as compared to the simple linear system. However, as the playback speed increased, the average passband values for both the biological photoreceptors and artificial photoreceptor decreased. For the

artificial photoreceptor, the maximum average passband was measured at 0.735±0.035 CI during the playback speed of 45°/s while the minimum was measured at 0.316±0.068 CI during the playback speed of 1440°/s. As for the linear system, the values measured for the average passband were smaller as compared to the artificial photoreceptor. The lowest point measured from the linear photodiode curve was at 0.274±0.060 CI during the highest playback speed (1440°/s), while the highest point measured was at 0.529±0.024 CI during the playback speed of 45°/s.

Figure 5-15b shows the average corner frequencies from the same 13 images. The corner frequencies for both the artificial photoreceptor and linear photodiode decreased as the playback speed increased with average corner frequency ranging from 0.49 cycles/° at 45°/s to 0.066cycles/° at 1440°/s for the artificial photoreceptor and 0.36 cycles/° at 45°/s to 0.055cycles/° at 1440°/s for the linear photodiode. The percentage of difference between the average corner frequencies of the artificial photoreceptor and the linear photodiode had became less significant as the playback speed increased.

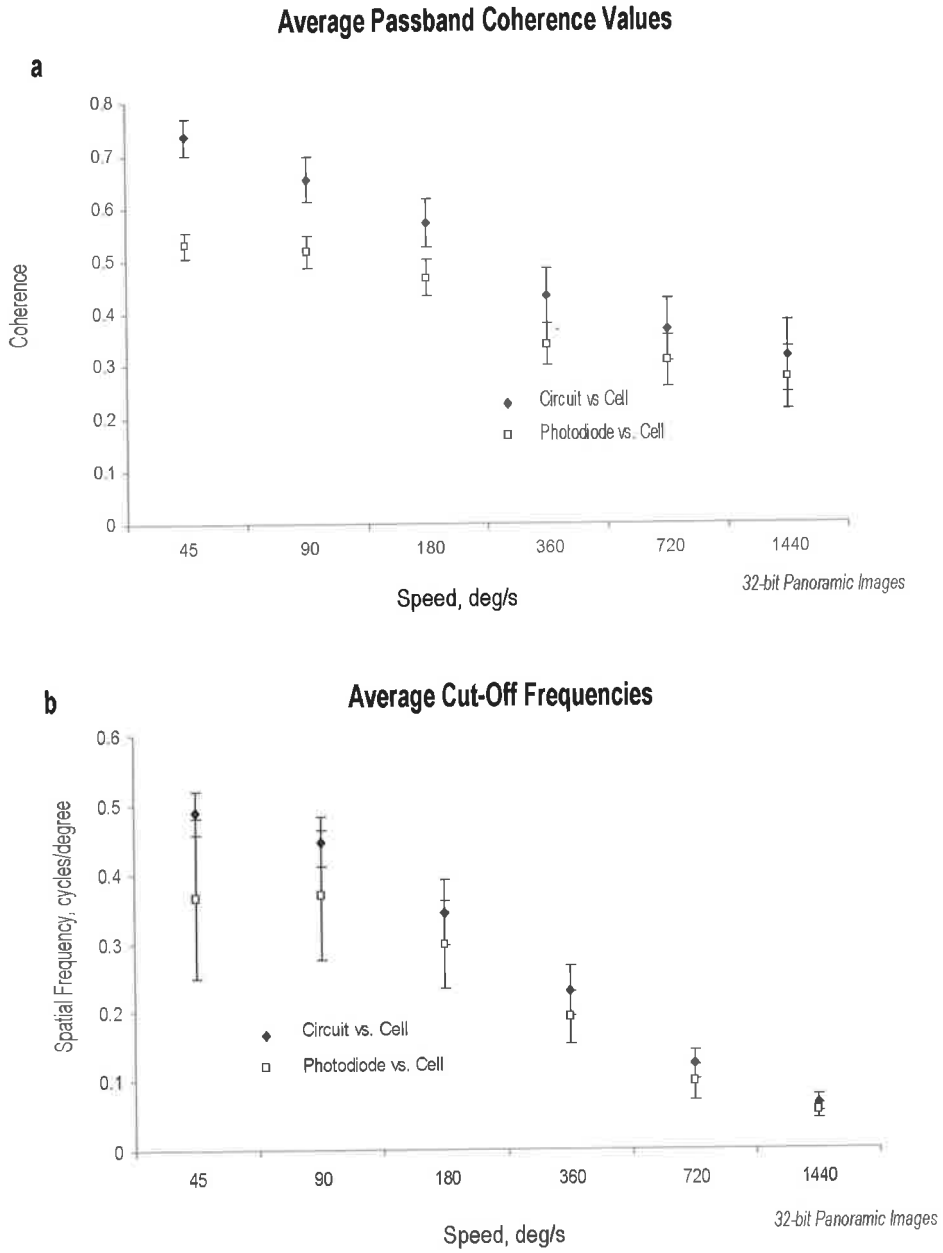

Figure 5-15: Coherence analysis parameters of the 32-bit panoramic images. a. Average passband values calculated from the coherence analyses of the 32-bit images for both the photoreceptor circuit and linear photodiode against actual biological photoreceptors *(averages of 13 mean values from 13 different images under the same playback intensity; 4 trials each).* Error bars show the 95% confidence interval. b. Average corner frequencies from the coherence analyses for both the photoreceptor circuit and linear photodiode against actual biological photoreceptors *(averages of 13 mean values from 13 different images under the same playback intensity; 4 trials each).* Error bars show the 95% confidence interval.

5.4 Discussion

The mathematical analyses, both in the time (correlation) and frequency (coherence) domains have shown that our artificial photoreceptor was a good mimic of actual photoreceptor cells under complicated naturalistic conditions. The artificial photoreceptor responded in an almost invariant way to large changes in image intensity. The adaptive non-linear features (automatic gain control and variable corner frequency) that were implemented in the artificial photoreceptor had endowed the artificial photoreceptor with a greater signal to noise ratio than a simple linear model under low lighting conditions. Also, various speed playbacks (relative motion) of the HDR panoramas were used to thoroughly evaluate of the artificial photoreceptor. Such variations in speed have been shown to have no significant impact on the robustness and reliability of the artificial photoreceptor, in spite of the minor decrease in the r^2 values as the playback speed increased as shown in Figure 5-14. By having a robust artificial photoreceptor, researchers are now able to reliably collect data that was impossible to obtain electrophysiologically of the biological photoreceptors for an extensive period of time. The collected data can be used as input stimuli for better evaluating and investigating higher order neurons models.

5.4.1 Effects of Light Level

Insect photoreceptor cells are responsible for transmitting light information into electrical signals for higher order cells in the insect visual pathway before reaching the brain as visual interpretations (Carlson et al. 1979). Many researchers have directly modelled the photoreceptor cells with a linear light detector since the main characteristic of a light detector is to convert photon energy to

electrical signal. However, numerous studies have suggested that insect photoreceptors are not just a simple linear light detector (Wallcott 1975; Payne et al. 1981). Results from the current experiments have clearly shown that our artificial photoreceptor is a better mimic to the biological photoreceptors compared to the simple linear detector.

Insect photoreceptors are highly non-linear, displaying adaptation to light and background luminances (Baumann 1975; Laughlin et al. 1978; Matic et al. 1981; Laughlin et al. 1993). Studies suggest that adaptation mechanisms are naturally equipped to maximise visual information perceived (Snyder et al. 1976; Laughlin 1989; van Hateren 1992). Input light signals to the photoreceptors will be automatically readjusted based on its current states of adaptation. Input signals that are too bright will be reduced and vice versa, i.e. an automatic gain control system. Such a mechanism is mainly due to the anatomical changes and photochemical processes in the photoreceptor cells, which take place during light-adaptation (Wallcott 1975). Thus, even extremely dim intensity playbacks between 0.1% and 0.5% (Figure 5-2) were enough to stimulate the biological photoreceptors. The photoreceptors automatically adapted to such dim playbacks and readjusted their gain by amplifying the input light signals for better visual information coding. The artificial photoreceptor, equipped with similar adaptive mechanisms, shows high correlation with the biological photoreceptors for various maximum playback intensities except during extreme conditions such as 0.1%. For this case, the artificial photoreceptor was unable to perform that well due to the insufficient gain settings of the circuit during low lighting conditions and the limitations of the signal to noise ratio of the photodetector (TSL 251) used in the circuit.

Changes in the maximum intensity of the playbacks did not only change the gain settings of the photoreceptors. Experimentation has also suggested that insect photoreceptor cells exposed to different lighting conditions will have different frequency responses (Laughlin et al. 1993). Insect photoreceptors, which are approximated as second order low pass filters, change their frequency response ranges by shifting their corner frequencies non-linearly (Mah et al. 2005). Such effects can be evidenced from the output power spectrum curves of both the biological photoreceptors and the artificial photoreceptor (Figure 5-7). During dim playbacks (0.1% and 0.5%), the corner frequencies of the photoreceptors were low, hence only allowing the low frequency signals to pass through. As the maximum playback intensity increased, the photoreceptors increased their frequency ranges and allowed more signals to propagate through. According to our previous studies, *Eristalis tenax* has photoreceptors with a corner frequency range from approximately 10Hz to 90Hz and they started to saturate at the maximum corner frequency at approximately 3500 cd/m^2 (Mah et al. 2006). Such saturation effects can be clearly observed on the power spectrum curves in Figure 5-7, where there are no significant changes to the power spectrum curves as the playback intensities exceed 5%. However, notice that the power spectrum curves of the circuit reached saturation at a slightly different point. The artificial photoreceptor started to saturate at approximately 10% maximum intensity playback. This was because the frequency response of the circuit was limited by physical components.

Because of the changes of the corner frequency of the system, the coherence curves of the systems also had to change accordingly. During dim playbacks, the coherence curve had a much lower corner frequency compared to brighter intensity playbacks because the

systems had already filtered out the higher frequencies. Thus, the coherence curves shifted to right as the intensity increased.

5.4.2 Effects of Speed

Photoreceptor cells are capable of sampling light information at a temporal corner frequency ranging from 10Hz to 90Hz, depending on their light adaptation state (Mah et al. 2006). The temporal properties of a photoreceptor are functionally related to its spatial properties through image velocities. When an image moves, the higher spatial frequencies generate the higher temporal frequencies. For a given image velocity, high spatial frequencies will be lost if the temporal frequencies they generate are too fast for the photoreceptor to code (Snyder et al. 1977). As the playback speed increased, the higher spatial frequencies were lost due to the temporal limitation of the photoreceptors. The photoreceptors were incapable of resolving most of the details of the panoramas due to the small amount of energy at high spatial frequencies. The reconstructed output images thus appeared to be blurry (see Figure 5-14).

As mentioned, the artificial photoreceptor was implemented and equipped with all the adaptive non-linear features of a photoreceptor cell. Thus, the outputs of the artificial photoreceptor showed great similarity with the biological photoreceptors. The power spectrum curves for both the biological photoreceptors and the artificial photoreceptor shifted to the left as the playback speed increased. Such shifts led to the decrease in the corner frequency of the coherence curves (see Figure 5-15b).

How could these non-linearities make a better front-end for high-order processing tasks? Under low background lighting, insect

photoreceptors increase their gain in order to amplify the bad lighting conditions for better information coding. However, increasing the gain of the photoreceptors might be detrimental due to the photon bump noise. We believe this is why dark-adapted photoreceptors have a lower corner frequency response compared to the light-adapted ones - in order to eliminate unwanted high frequency noise, i.e. to increase the signal to noise ratio. Information that has been effectively compressed through the non-linearities of the photoreceptors is then transmitted to limited bandwidth higher order neurons such as motion sensitive neurons and small target neurons to perform specific tasks.

Acknowledgements

We would like to thank the employees of the Botanic Gardens (Adelaide, Wittunga and Mt. Lofty), who had been very helpful during our fly-catching trips. This research was supported with a Linkage grant from the Australian Research Council, including a Post-Doctoral Fellowship for RSAB (LP0667744) and from US Air Force contracts F08630-02-C-0013 and FA9550-04-1-0283.

References

Baumann, F. (1975). Electrophysiological properties of the honey bee retina. The Compound Eye and Vision of Insects. London, Oxford University Press: 53-74.

Carlson, S. D. and C. Chi (1979). "The functional morphology of the insect photoreceptor." Ann. Rev. Entomol. **24**: 379-416.

Debevec and Malik (1997). Recovering High Dynamic Range Radiance Maps from Photographs. SIGGRAPH '97: 369-378.

Delbrück, T. and C. A. Mead (1996). Analog VLSI Phototransduction by Continuous-time, Adaptive, Logarithmic Photoreceptor Circuits. Pasadena, California Institute of Technology-Computation and Neural Systems Program: 23.

Dror, R. O., D. C. O'Carroll and S. B. Laughlin (2001). "Accuracy of velocity estimation by Reichardt Correlators." Optical Society of America **18**(2): 241-252.

Fain, G. L., H. R. Matthews, M. C. Cornwall and Y. Koutalos (2001). "Adaptation in vertebrate photoreceptors." Physiological Reviewss **81**(1): 117-151.

Kramer, J., R. Sarpeshkar and C. Koch (1995). An analog VLSI velocity sensor. IEEE International Symposium on Circuits and Systems.

Laughlin, S. B. (1989). "A role of sensory adaptation in the retina." J. exp. Biol. **146**: 39-62.

Laughlin, S. B. and R. C. Hardie (1978). "Common strategies for light adaptation in the peripheral visual systems of fly and dragonfly." J. Comp. Physiol. **128**: 319-340.

Laughlin, S. B. and M. Weckström (1993). "Fast and slow photoreceptors - a comparative study of the functional diversity of coding and conductances in the diptera." J. comp. Physiol. A **172**: 593-609.

Lindemann, J. P., R. Kern, J. H. van Hateren, H. Ritter and M. Egelhaaf (2005). "On the computations analyzing natural optic flow: Quantitative model analysis of the blowfly motion vision pathway." Journal of Neuroscience **25**(27): 6435-6448.

Liu, S. C. (1999). "Silicon retina with adaptive filtering properties." Analog Integrated Circuits and Signal Processing **18**: 1-12.

Mah, E. L., R. S. A. Brinkworth and D. C. O'Carroll (2005). Bio-inspired analog circuitry model of insect photoreceptor cells. SPIE, Brisbane.

Mah, E. L., R. S. A. Brinkworth and D. C. O'Carroll (2006). "Implementation of an elaborated neuromorphic model of a biological photoreceptor." Biological Cybernetics **submitted on Dec 2006**.

Matic, T. and S. B. Laughlin (1981). "Changes in the intensity-response function of an insect's photoreceptors due to light adaptation." J. comp. Physiol. A **145**: 169-177.

Payne, R. and J. Howard (1981). "Response of an insect photoreceptor: a simple lognormal model." Nature **290**: 415-416.

Rajesh, S., D. C. O'Carroll and D. Abbott (2004). Effects of nonlinear elaborations on the performance of a Reichardt correlator. BioMEMs and Nanotechnology, Proceedings of the SPIE.

Sarpeshkar, R., J. Kramer, G. Indiveri and C. Koch (1996). Analog VLSI architectures for motion processing: from fundamental limits to system applications, Proceedings of the IEEE.

Silva, G. A., J. R. Hetling and D. R. Pepperberg (2001). "Dynamic and steady-state light adaptation of mouse rod photoreceptors *in vivo*." Journal of Physiology **534**(1).

Smakman, J. G. and D. G. Stavenga (1986). "Spectral sensitivity of blowfly photoreceptors: dependence on waveguide effects and pigment concentration." Vision Research **26**(7): 1019-1025.

Snyder, A. W., S. B. Laughlin and D. G. Stavenga (1976). "Information Capacity of Eyes." Vision Research **17**: 1163-1175.

Snyder, A. W., D. G. Stavenga and S. B. Laughlin (1977). "Spatial information capacity of compound eyes." J. comp. Physiol. A **116**: 183-207.

Stavenga, D. G. (2003). "Angular and spectral sensitivity of fly photoreceptors. I. Integrated facet lens and rhabdomere optics." Journal of Comparative Physiology A **189**: 1-17.

Straw, A. D., E. J. Warrant and D. C. O'Carroll (2006). "A 'bright zone' in male hoverfly (Eristalis tenax) eyes and associated faster motion detection and increased contrast sensitivity." Journal of Experimental Biology **209**: 4339-4354.

Tatler, B., D. C. O'Carroll and S. B. Laughlin (2000). "Temperature and the temporal resolving power of fly photoreceptors." Journal of Comparative Physiology A **186**(4): 399-407.

van Hateren, J. H. (1992). "A theory of maximising sensory information." Biological Cybernetics **68**: 23-29.

van Hateren, J. H. and H. P. Snippe (2001). "Information theoretical evaluation of parametric models of gain control in blowfly photoreceptor cells." Vision Research **41**: 1851-1865.

Wallcott, B. (1975). Anatomical changes during light-adaptation in insect compound eyes. The Compound Eye and Vision of Insects. London, Oxford University Press: 20-33.

6

Chapter 6: Neuromorphic Photoreceptor Model Maximises Information for Higher Order Neurons

ENG-LENG MAH, RUSSELL SA BRINKWORTH and DAVID C. O'CARROLL
Discipline of Physiology, School of Molecular and Biomedical Science and the Centre for Biomedical Engineering, The University of Adelaide SA 5005, Australia.

Abstract

A faithful neuromorphic model of the biological photoreceptor cell has been designed and implemented using standard analogue discrete electronic components. This analogue neuromorphic model has been thoroughly tested and evaluated against actual photoreceptor cells of the hoverfly, *Eristalis tenax* using high dynamic range movie stimuli. Correlation and coherence analyses show that the analogue circuit is an excellent mimic of the biological photoreceptors with an r^2 value of 0.890±0.030 (mean±standard deviation). We then show how the early visual processing actually maximises the transmission of visual information through the limited-bandwidth higher order neuron channels in the insect visual pathway. A simple linear model was used as a control in the experiments. Snap shots from the movie showed that the early visual processing had compressed without loss of salience and hence the loss of visual information after transmission to the higher order

neurons was minimised. Significant improvements were observed through the whole movie as compared to the simple linear model. Such a robust, reliable neuromorphic model could be beneficial to many applications such as target tracking, motion detector and surveillance systems.

Key words: Insect Photoreceptor, Insect Visual System, Adaptive Photoreceptor, Neuromorphic, Bio-inspired Vision

Correspondence to: Eng-Leng Mah (email: eng.mah@adelaide.edu.au)

6.1. Introduction

Biological visual processing involves complex, highly non-linear photochemical processes that are significantly challenging to model compared to a linear system, yet many engineers, being aware of the elegant solutions that nature may provide, are taking inspiration from biological systems in developing "neuromorphic" models (Delbrück et al. 1996; Liu 1996; Moini et al. 1996; Sarpeshkar et al. 1996; Kramer et al. 1997; Delbrück et al. 2004). For instance, the aerobatic manoeuvring capabilities of the hoverfly, *Eristalis tenax*, which are directly due to having an "intelligent" visual system, provide a bio-inspired solution to many potential real-world applications such as collision avoidance, unmanned aerial vehicle (UAV) and motion detector systems.

Physiological studies suggest that non-linearities of the biological visual processing are evident even at the earliest stage of visual processing in the visual pathway – the photoreceptor cells (Baumann 1975; Wallcott 1975; Payne et al. 1981; Baumann 2000). Theory and modelling have shown that the non-linearities that occur in the early visual processing are responsible for maximising the visual information transmitted via the limited-bandwidth higher order

neurons in the visual pathway (Snyder et al. 1976; Snyder et al. 1977; van Hateren 1992). However, many bio-inspired models have completely neglected the importance of having a reliable, good front-end processing stage. Take for instance the classic Reichardt Correlator model (motion sensitive), which only uses a linear front-end system at the early visual processing. Despite responding well to standard characterised stimuli, this model has been shown to be inferior under complicated naturalistic stimuli (Dror et al. 2001; Rajesh et al. 2004). A neuromorphic motion detector chip designed by Delbrück and Mead (1996) is another example of bio-inspired model that uses a non-faithful model of the phototransduction stage as the front-end of the visual processing. Although the chip has been tested and proven to operate under characterised stimuli such as pulse and step tests, it has yet to be demonstrated to perform under complex dynamic naturalistic stimuli.

Therefore, we have designed and implemented an elaborated photoreceptor circuit that faithfully mimics the biological photoreceptors (Mah et al. 2006). The photoreceptor circuit consists of several non-linearities stages that is derived and fine tuned from electrophysiological experiments. We also built an additional circuit to mimic the insect large monopolar cell and cascade it to the output of the photoreceptor circuit in order to demonstrate and evaluate the importance of having a robust, reliable photoreceptor stage as the front-end processing for higher order neuron designs.

6.2 Methods

6.2.1 Stimuli Generation (Movie)

"Moving" Scene - High Dynamic Range Movie

A specialised high precision monochrome 14-bit video camera (XCD-V50, Sony™) was used to pre-record the movie (naturalistic scenes). The video camera, which was equipped with green channel filter (N52-534, Edmund™) and 90° wide angle lens (TF2.8DA-8, Fujinon™), was mounted on a robotic platform and the movements of the robot were fully controlled using a wireless remote control. Video images were streamed at 25 frames/s to a laptop using the firewire IEEE1394 output port of the video camera. The video camera was programmed to alter the shutter speed after each frame (total of 5 shutter speeds used) thus increasing the dynamic range of the images captured at the expense of temporal resolution, providing detail in both the dark and light parts of the scene. A custom LabView® software was used to communicate with an external data acquisition card in order to acquire all the video images.

The camera was mounted on top of the robot in order to avoid having the robot appear in the area of interest of the video camera. Below the camera was a counter balance system in order to reduce vibrations during video recording. A pair of optical encoders was mounted on both sides of the wheels to transduce the motion of the wheels. This was particularly useful for regeneration of the path travelled by the robot during video recording session.

The recorded video images were Gaussian blurred with half width of 1.4° in LabVIEW® based on the average facet diameter of 40μm in order to mimic the optical properties of the compound eyes

(Stavenga 2003; Straw et al. 2006). Figure 6-1 shows how the video images were finalised as a natural time series of intensities (NTSI) for visual experiments.

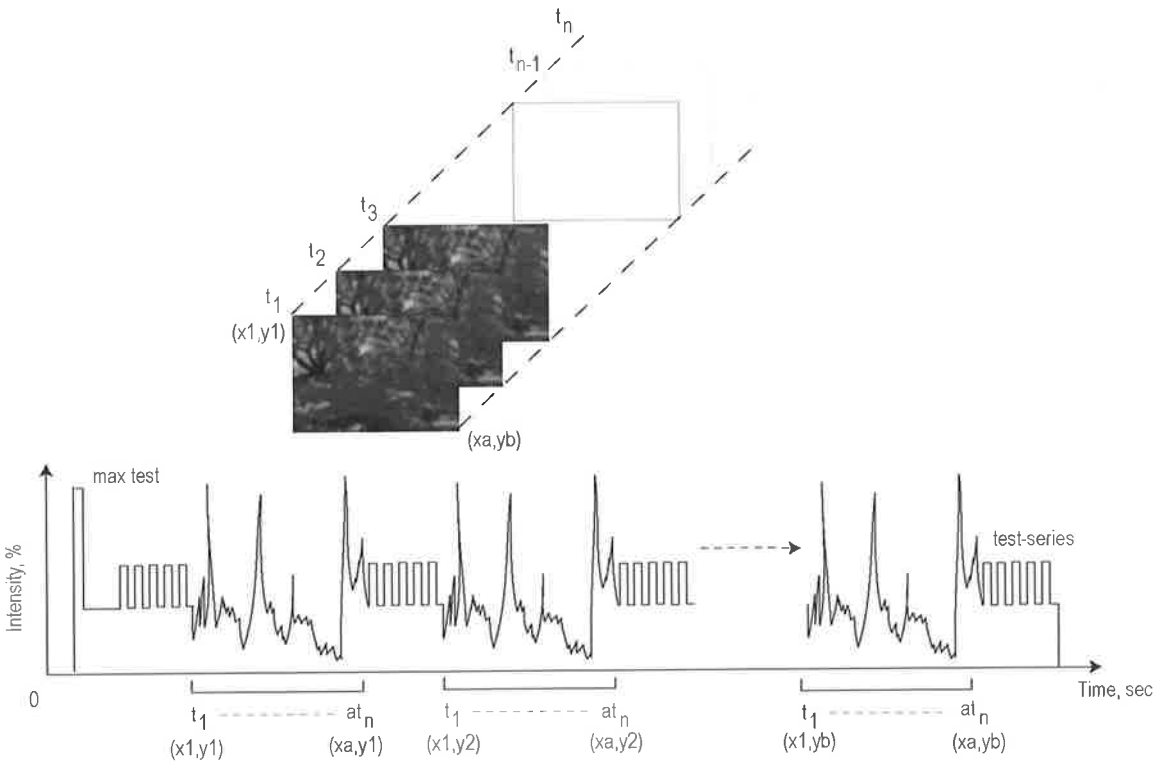

Figure 6-1: Construction of the natural time series of intensities. Each frame of the movie had a*b pixels and each pixel that went through time t_1 to t_n formed a pixel-time series. The pixel-time series were played back by stitching the back of the series to the front of the next series and in between each column of the pixel-time series were some test-series (square waves) to assure the quality of the recordings. The maximum test was only done once in the whole movie playback in order to measure the maximum response of the biological cell or the artificial photoreceptor.

The recorded movie was played back in a vertical raster fashion starting from the top left pixel. Since the starting scene of the movie was approximately the same as the ending scene of the movie, each pixel through time, or known as the pixel-time series, was connected front-to-back to form a long time series of intensities for visual

experiments and test-series (square waves) was placed in between each column of the pixel-time series for offline quality assurance purposes.

"Stationary" Scene

A digital camcorder (Sony DCR-TRV15E) was mounted on a tripod stationarily to record the movie at 25 frames/s. We then deliberately changed the brightness of the movie (offline) into 6 intensity bands (100%, 50%, 1%, 1%, 50% and 100%) to create extreme luminance conditions. Again, the recorded movie was played back in a vertical raster fashion starting from the top left pixel as described in the previous section.

6.2.2 Data Reconstruction

All the raw data recorded from the visual experiments were saved in a special custom format in LabView® and the data were reconstructed back to images using custom software written in LabView®. The images were then compiled to form a movie sequence using QuickTime® Pro.

6.2.3 Large Monopolar Cell Circuit Design

This circuit was a temporal model of a Large Monopolar Cell of the insect visual pathway and did not incorporate any of the known spatial processing. The circuit model was designed based on the current existing literature (James 1990). The model was sufficient to highlight the performance of the photoreceptor circuit against a simple linear phototransduction system in maximising visual information transmitted. Figure 6-2 shows the schematic diagram of the LMC circuit. The circuit consisted of a multiplication stage, a Naka-Rushton stage, a variable high-pass filter stage, and a high-

pass control stage. The multiplication stage was used to square the output of the photoreceptor.

An additional offset of approximately 0.1V was introduced to eliminate the possibility of having a negative voltage enter the multiplication stage since the multiplier chip (AD633JN, Analog Devices) used was only capable of operating in the positive region. A and B were both amplifier stages with gain factors of 10 and 2.72 respectively.

The output of the multiplier stage was then fed into the Naka-Rushton stage using the following equation,

$$NROut = \frac{A*(B*PhotoOut+offset)^2}{(k+A*(B*PhotoOut+offset)^2)} \qquad \textbf{(Eq 6-1)}$$

where k=0.03V. The Naka-Rushton stage was designed and implemented using a standard divider chip (AD734AQ, Analog Devices). Output from the Naka-Rushton stage was then fed into the first order variable high-pass filter where the frequency response of the filter, F_{VHP} was automatically controlled by the high-pass control stage based on the mean luminance measured at that time. The variable high-pass filter was designed in such a way that the -3dB point of the filter frequency response (corner frequency) increased non-linearly as the mean background luminance increased (Equation 6-2), similar to the biological responses (Laughlin et al. 1993). The -3dB point stopped changing (saturated) at approximately 10Hz when the mean background luminance was greater than 700cd/m^2. The final output was then inverted using a standard unity gain inverting amplifier stage.

$$F_{VHP} = \frac{1}{60x10^{-6}\pi R_{vac}} \qquad \textbf{(Eq 6-2)}$$

Where $R_{vac} = 3.09x10^{29}\exp(-38.12CS) - 5.658x10^{22}\exp(-27.56CS)$ **(Eq 6-3)**

$$CS = 1.487 + 1.970V_{photo} \qquad \textbf{(Eq 6-4)}$$

$$V_{photo} = \frac{Bv}{1750} \qquad \textbf{(Eq 6-5)}$$

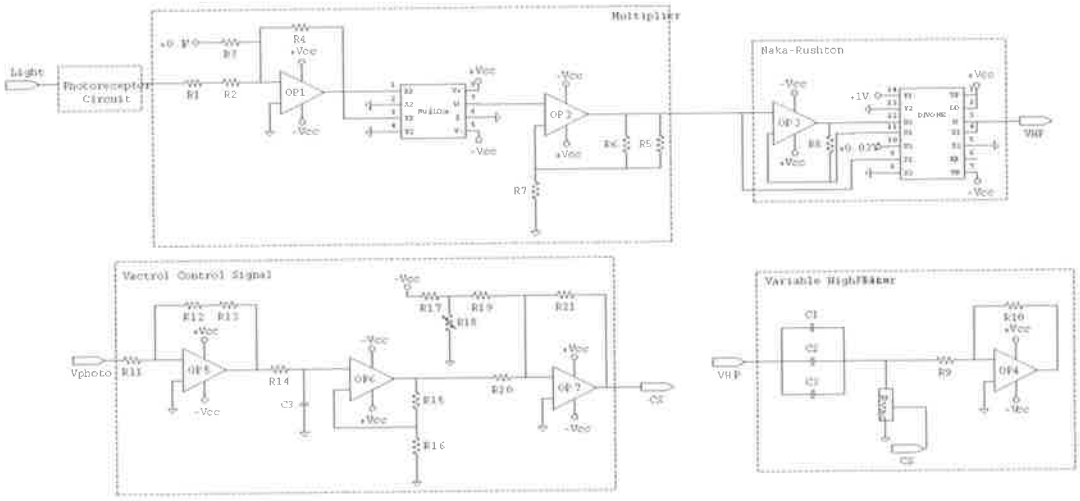

Figure 6-2: A schematic diagram of a second order neuron circuit. The output signal from the photoreceptor circuit was cascaded to the second order neuron circuit. The luminance (Bv, in cd/m^2) was averaged to obtain the background value. The vactrol control signal stage fully controls the frequency response of the variable high pass filter was dependent on this background luminance.

6.2.4 Data analyses

Correlation and coherence analyses were used to measure the performance of the photoreceptor circuit against biological photoreceptors under both time and frequency domains. The analyses were done on each pixel time-series of the high dynamic

range movie and results were averaged along all pixels (90 x 58 pixel time-series). All results are given as mean ± SD.

Coherence Significance Levels

From the coherence analyses, we were able to calculate the significance level (95% CI) of the coherence curve using the equation 6-6.

$$c^2 = 1 - \alpha^{\left(\sqrt{\left(\frac{1}{n-1}\right)}\right)} \qquad \textbf{(Eq 6-6)}$$

Where c is the coherence value, α is the confidence interval value and n is the amount of sample. Since we were working on 90 x 58 pixel time-series, the 95% CI of the coherence curve has a value of 0.024.

Contrast Metric

A contrast metric was chosen as the measure of how detectable the target was in the scene. The size of the target in the scene was approximately two pixels by one pixel. A background area was defined around the target, with a perimeter of two pixels from the target (28 nearest-neighbouring pixels). A basic contrast metric would be to compare the mean intensities of the target (μ_{tgt}) and background (μ_{bkg}) areas. However, to help account for the target being detectable due to its internal structure, a root sum of squares (RSS) method was used, which makes use of the variance of the target (σ^2_{tgt}) as given by Equation 6-7.

$$RSS = [(\mu_{tgt} - \mu_{bkg})^2 + \sigma^2_{tgt}]^{1/2} \qquad \textbf{(Eq 6-7)}$$

6.2.5 Electrophysiological recording

Electrophysiological recordings were done intracellularly, with a manipulated micropipette filled with 2.0 M KCI was inserted into the brain of an intact fly to record its neuronal activities. Experiments were done in a dark room with the controlled temperature range of 23-25°C. Results were recorded using a 16-bit data acquisition card system (NI PCI6221, National Instruments™) and custom software written in LabVIEW®.

6.3 Results

6.3.1 Correlation Analysis

The average neuronal data (3 trials) acquired from the intact flies were pre-analysed in order to make sure of their consistency. Correlation analyses were performed between the trials with r^2=0.910±0.046 for N1 and N2, r^2=0.915±0.047 for N1 and N3, and r^2=0.913±0.057 for N2 and N3.

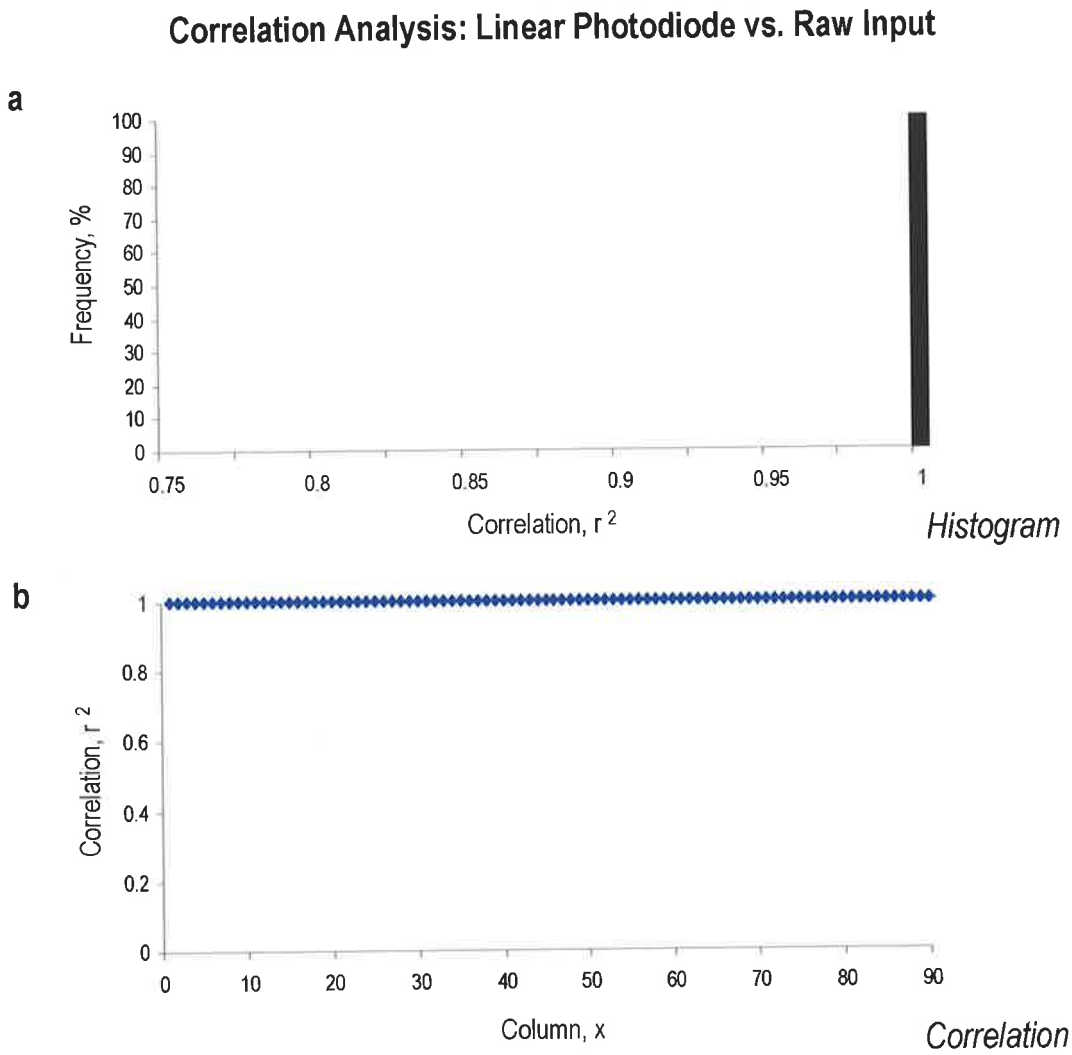

Figure 6-3: Correlation analysis for the linear photodiode against raw input. a. Histogram of the overall correlation of 90x58 pixel-time series for the linear photodiode system against raw input *(n=1)*. b. Average correlation output (58 rows) of the linear photodiode against raw input for 90 columns *(n=1)*.

In order to make sure that the stimuli were generated accordingly, a comparison between the raw input data and the linear photodiode output were performed. Figure 6-3a shows the histogram of the analysed correlation value for the linear photodiode output against raw input data of the stimuli. Note that the histogram shows that the correlation value was at 1 at all the time, i.e. the photodiode had generated the desired stimuli playback for all the 90x58 pixel-time series.

Figure 6-3b shows average correlation values of 58 rows for each column, for 90 columns in total. The results demonstrate strong correlation between the linear photodiode output and the raw input data of the stimuli throughout the whole 90x58 pixel-time series. Again, this indicates that the photodiode was operating satisfactorily.

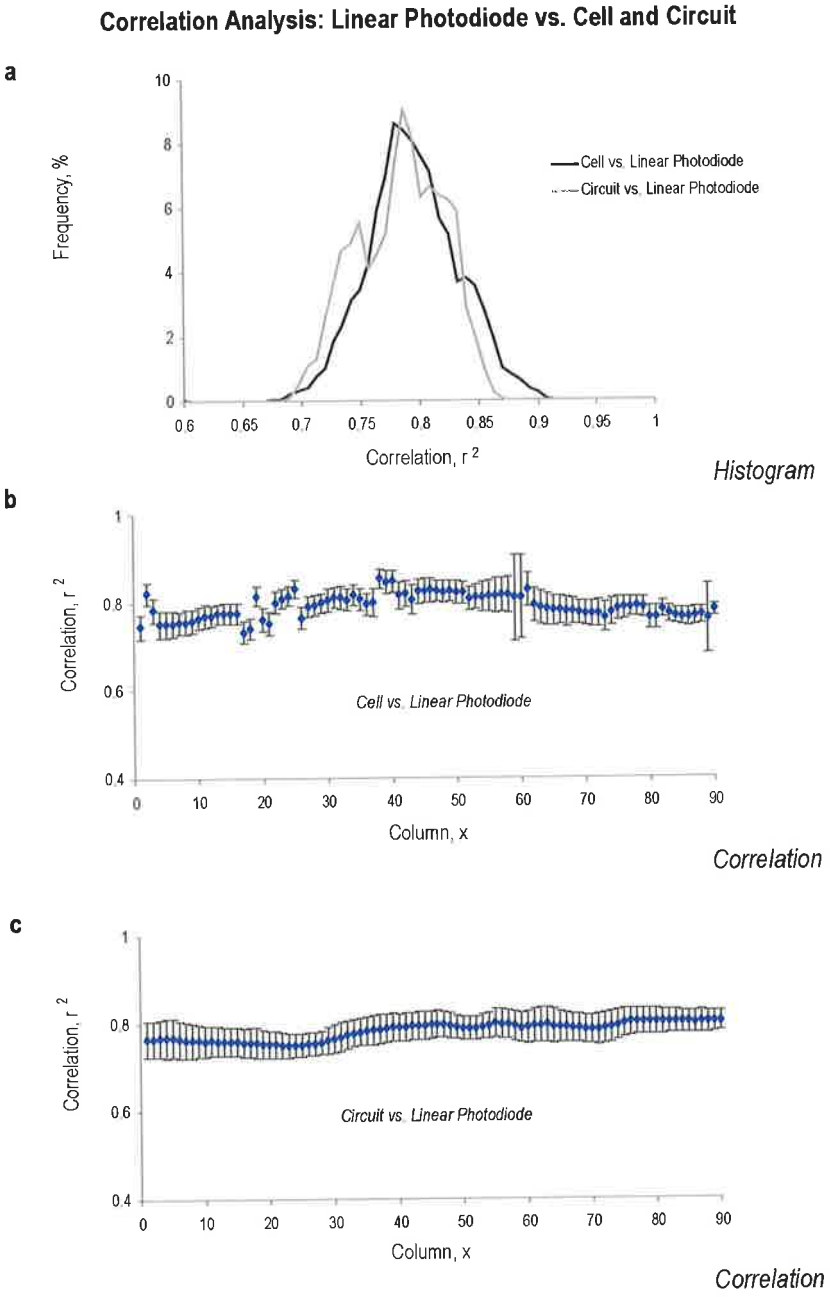

Figure 6-4: Correlation analysis for the linear photodiode against biological cells and circuit. a. Histogram of the overall correlation of 90x58 pixel-time series for the linear photodiode system against photoreceptor circuit *(n=1)* and actual biological photoreceptor cells *(n=3, 30 cells, 12 animals)*. b. Average correlation output (58 rows) of the linear photodiode against actual biological photoreceptor cells for 90 columns *(n=3, 30 cells, 12 animals)*. c. Average correlation output (58 rows) of the linear photodiode against photoreceptor circuit for 90 columns *(n=1)*. Errors bars indicate the standard deviations.

Figure 6-4a shows the histogram of the analysed correlation data between the linear photodiode system and photoreceptors (both biological and artificial circuit). For the biological photoreceptor cells, the peak of the histogram distribution occurred at 8.58% of the time with r^2 value of 0.780. The maximum and minimum r^2 values were calculated to be 0.903 and 0.137 respectively. With a very similar histogram distribution, the photoreceptor circuit was performing at maximum r^2 value of 0.864 and minimum at r2 value of 0.685. The peak of the histogram distribution occurred at 9.02% of the time with r^2 value of 0.788.

Again, correlation values for each column were averaged and unlike the results in Figure 6-3b, the analysed results show in Figure 6-4b demonstrate significant differences between the linear photodiode system and the biological photoreceptor cells, in which the average r^2 value across the whole 90x58 pixel-time series was at 0.791±0.042.

Figure 6-4c shows the detailed average correlation output of each individual column for the linear photodiode system against photoreceptor circuit. The average r^2 value for all the individual pixel-time series was calculated to be 0.781±0.037. Note that there are obvious fluctuations at the analyses output for the biological photoreceptors compared to those in Figure 6-4b. This was because the biological recordings were done in a separate cells and animals.

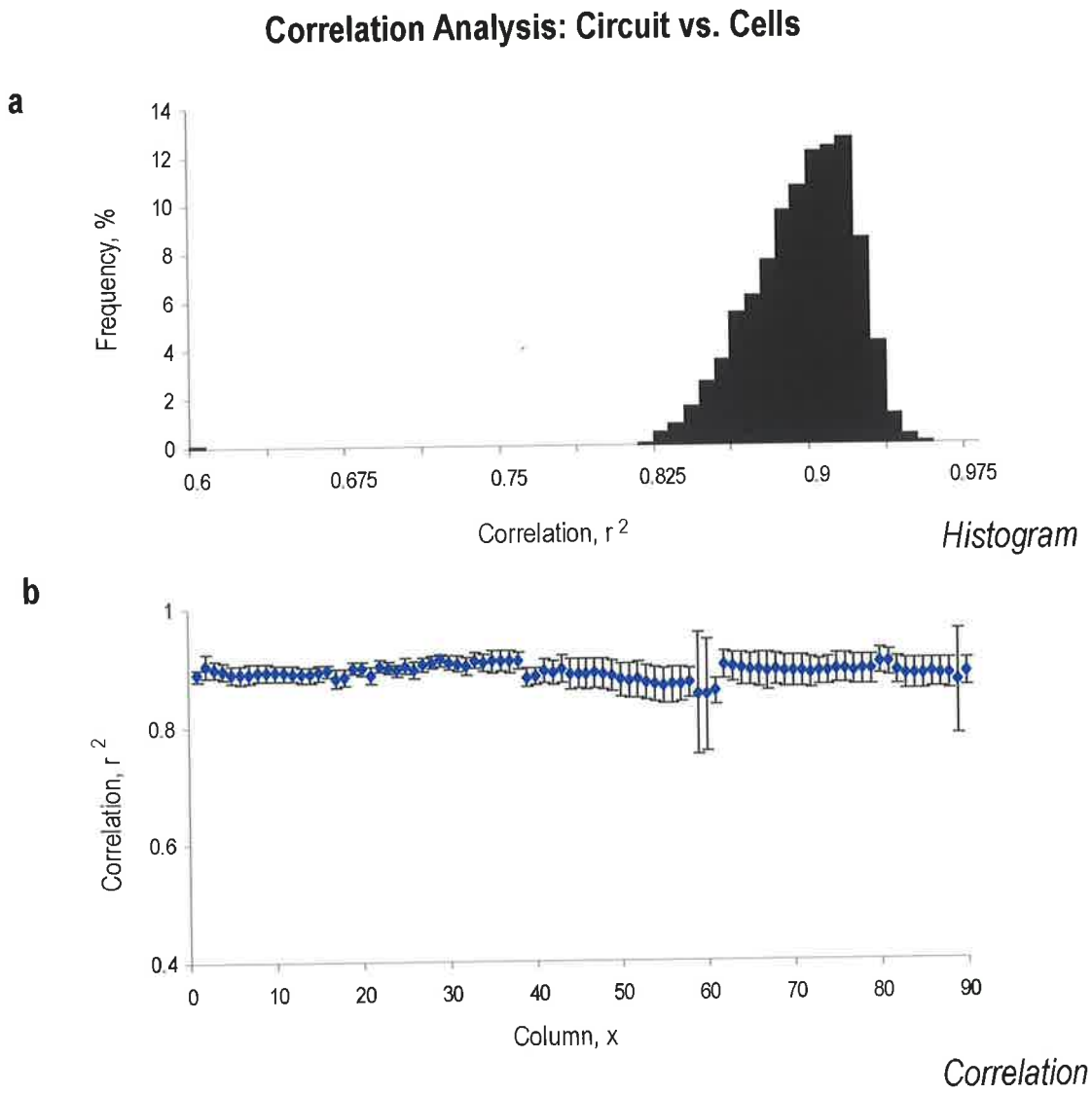

Figure 6-5: Correlation analysis for the photoreceptor circuit against biological cells. a. Histogram of the average correlation. b. Average correlation output (58 rows) of photoreceptor circuit against biological photoreceptor cells output for 90 columns. b. Average correlation output (58 rows) of the non-linear photoreceptor circuit against actual biological photoreceptor cells for 90 columns *(n=3, 30 cells, 12 animals)*. Error bars indicate the standard deviations.

All the previous correlation analyses have shown how the linear photodiode differs from both the biological photoreceptor cell and the non-linear photoreceptor circuit. Figure 6-5a shows the histogram of the analysed correlation value of the photoreceptor circuit against actual biological photoreceptor cells. Notice that the distribution of

the histogram is very different compared to the results shown previously. The overall data was centred at a higher correlation value, which leads to higher median value of 0.894. The maximum and minimum values were calculated to be 0.950 and 0.109 respectively. The peak of the histogram distribution occurred at 12.32% of the time with r^2 value of 0.915.

Figure 6-5b shows the detailed average correlation values for each individual column of the movie. It has a maximum r^2 value of 0.853±0.021 and a minimum r^2 value of 0.733±0.025. Unlike the previous results shown in Figure 6-4b and 6-5c, the average correlation values for all 90 columns of the pixel-time series are generally higher. Not only that, there were also more obvious fluctuations in the data simply because the data used in the analyses were recorded of a few different cells and animals.

6.3.2 Coherence Analysis

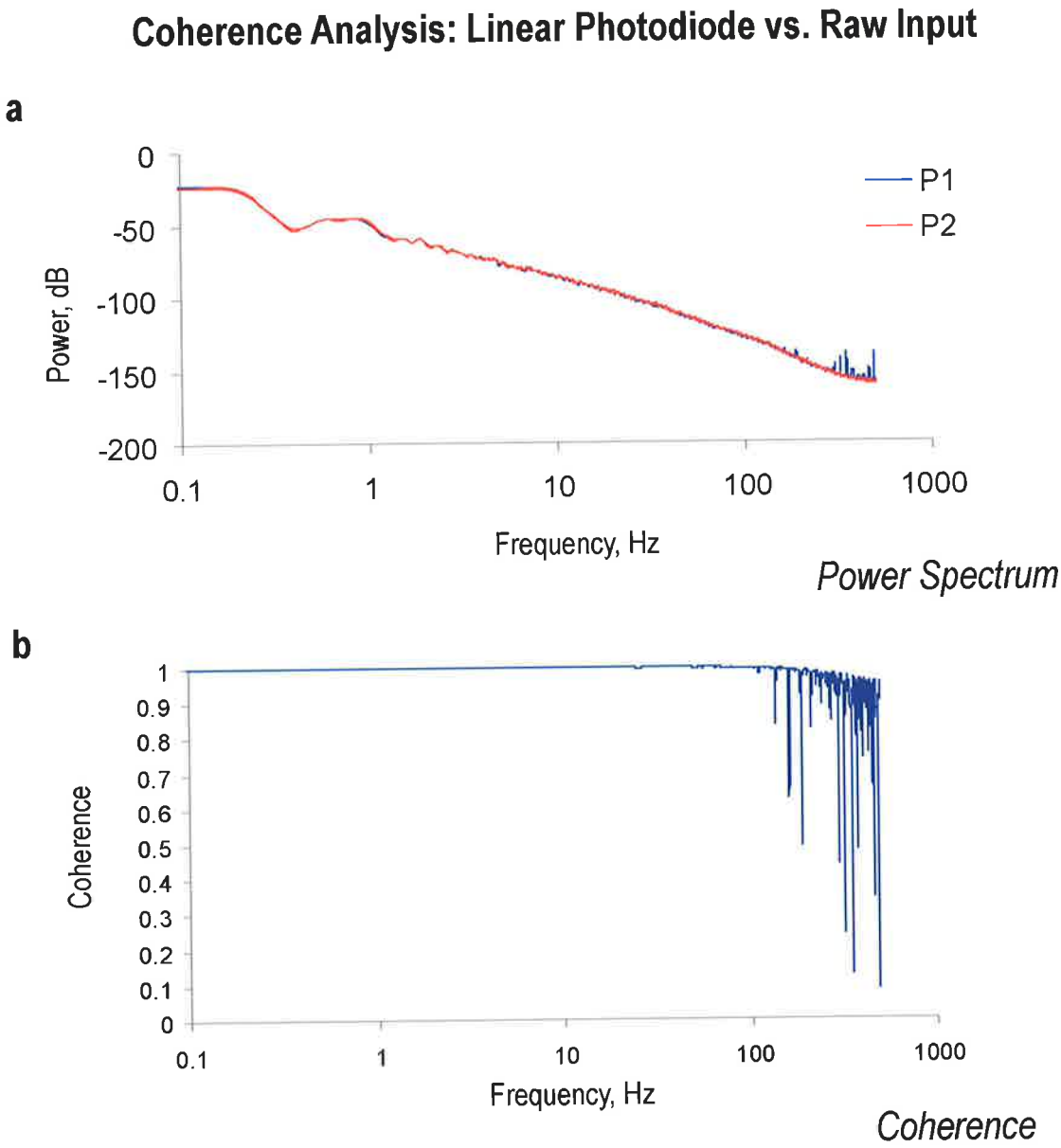

Figure 6-6: Coherence analysis for the linear photodiode against raw input. a. Normalised power spectrum curves of the linear photodiode system (P1) and raw input (P2). b. Coherence curve of the linear photodiode system against raw input data.

Figure 6-6a shows the power spectrum analysis curves of the linear photodiode system and raw data stimuli. The blue curve, P1 represents the power spectrum curve of the linear photodiode system and the red curve, P2 represents the power spectrum curve

of the raw input stimuli. There are no significant differences between these two curves, indicating that the linear photodiode system reproduced the raw input stimuli very closely in the frequency domain throughout the frequency range of interest, despite a few noisy spikes in the blue curve at high frequencies which may very well be due to interference noise from the data acquisition method.

The coherence analysis for both the linear photodiode system and the raw data stimuli is illustrated on the coherence curve shown in Figure 6-6b. Again, because of the close similarity between the linear photodiode system output and the raw input stimuli in the frequency domain, the coherence value is unity for most of the frequency range.

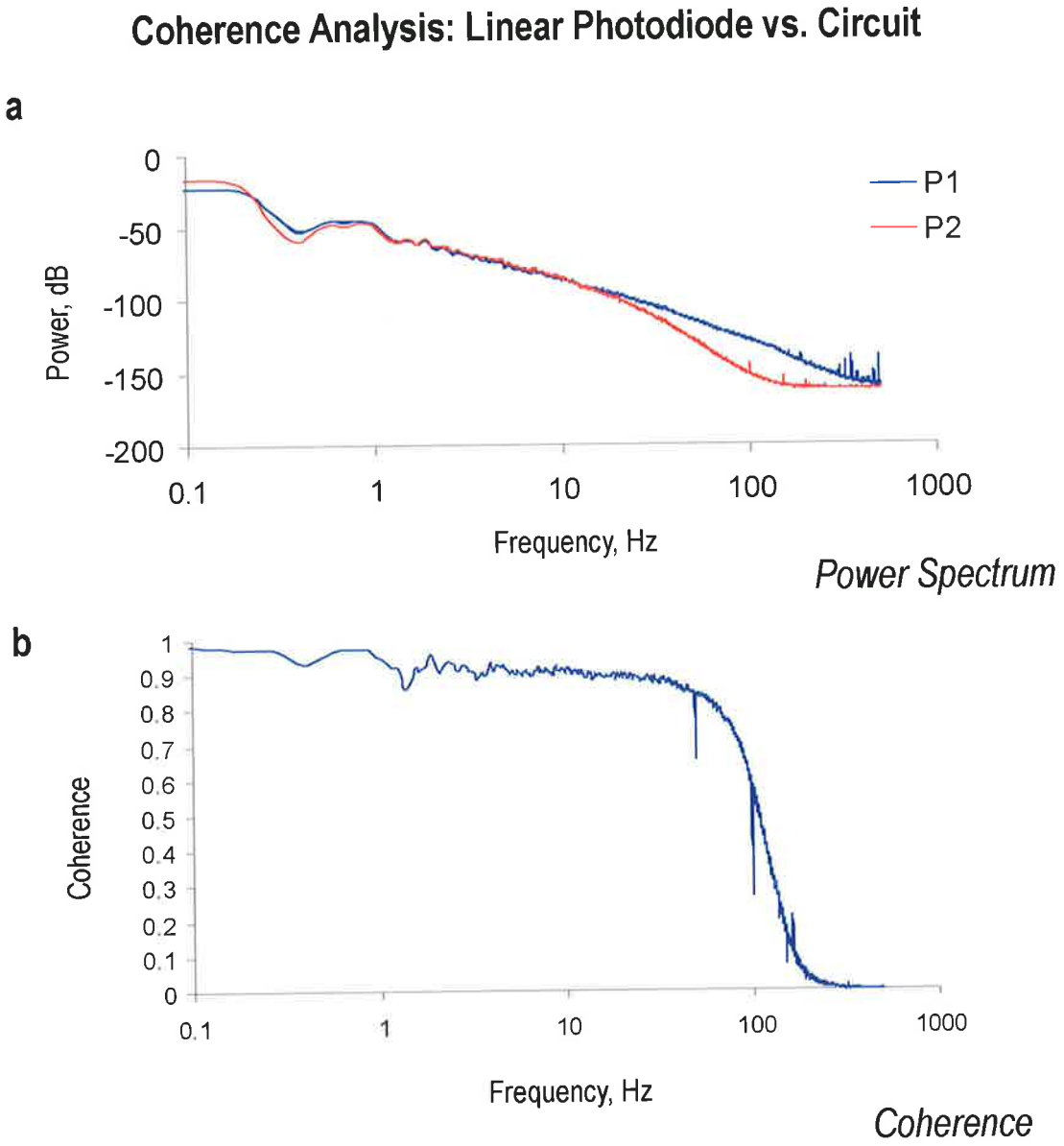

Figure 6-7: Coherence analysis for the linear photodiode against photoreceptor circuit. a. Normalised power spectrum curves of the linear photodiode system (P1) and photoreceptor circuit (P2) b. Coherence curve of the linear photodiode system against photoreceptor circuit.

Figure 6-7a shows the normalised power spectrum curves of the linear system and the adaptive photoreceptor circuit (P1 and P2). Both the curves show the 1/f function as expected from a complex natural scene (Simoncelli et al. 2001). Most of the power was

concentrated at the low frequencies. The maximum and minimum power measured were −16.55dB and −162.20dB (noise limit) respectively.

Figure 6-7b shows how similar the linear photodiode system is to the raw input data in frequency domain. The coherence curve indicates that the linear photodiode system was very similar for frequency range from 0.1Hz to 100Hz with a maximum coherence value of 0.995. The coherence curve rolled off as the frequency increased with a corner frequency of approximately 87Hz. Any coherence values above 200Hz exceeded the minimum significance limit (Equation 6-6) of the curves.

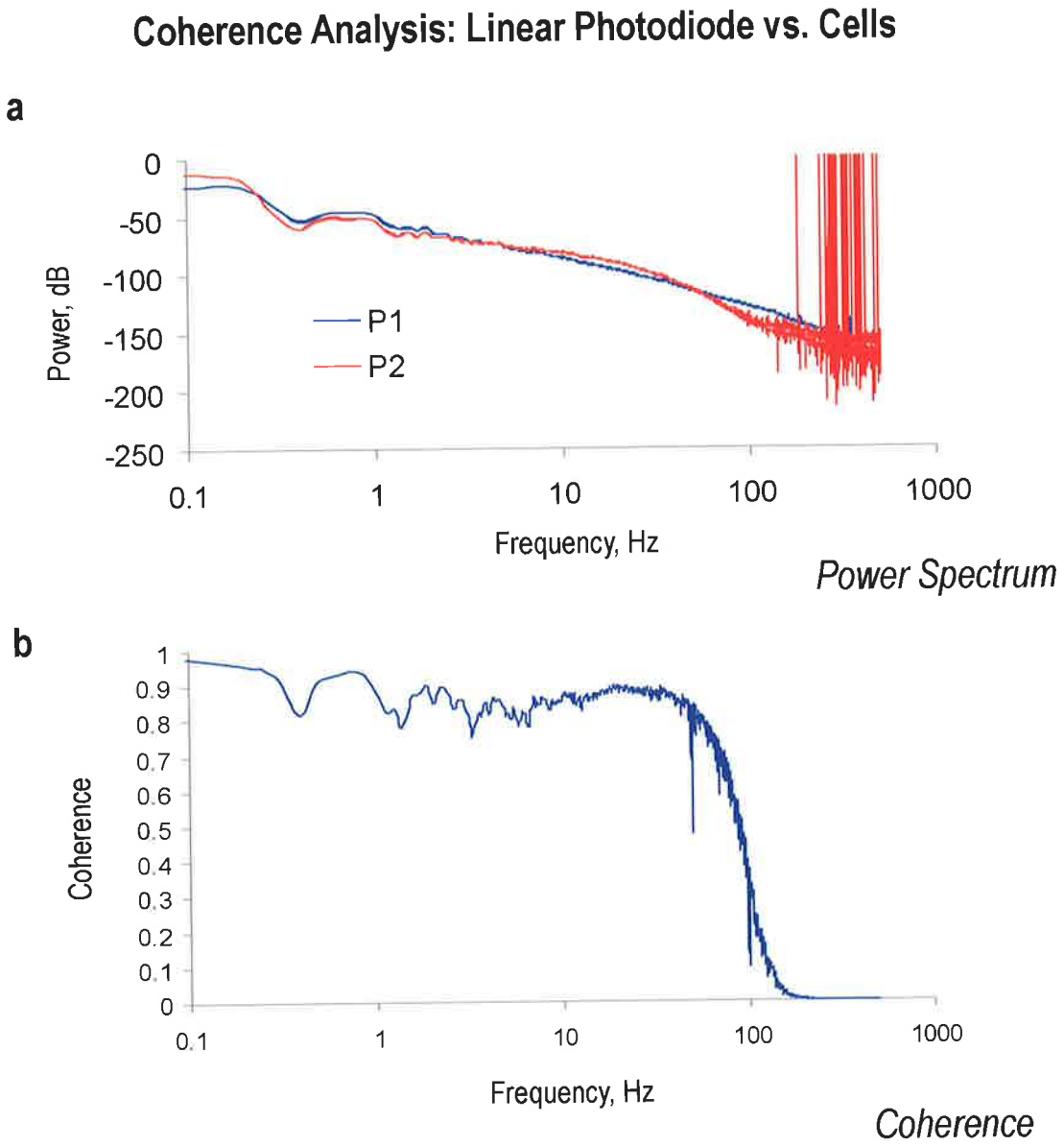

Figure 6-8: Coherence analysis for the linear photodiode against biological cells. a. Normalised power spectrum curves of the linear photodiode system (P1) and actual biological cells (P2) b. Coherence curve of the linear photodiode system against actual biological cells.

Figure 6-8a shows the power spectrum curves for both the linear photodiode system and the average biological photoreceptor cells output. The actual biological cell output showed relatively higher power at the low frequency compared to the linear photodiode system. As the frequency increased beyond 0.2Hz, the cell output dropped down below the linear photodiode system at approximately

5dB differences until 2-3Hz. Beyond 3Hz, the cells tended to have a stronger power output compared to the linear photodiode system and at about 150Hz and beyond, the power spectrum of the cells started to pick up some noise spikes. Such interference has no significant impact to our results since the frequency of interest for our experiments is way below the noise limit.

Figure 6-8b shows the coherence analysis curve of the linear photodiode system against the actual biological cells output. Because the biological cells output were highly non-linear, the coherence values obtained throughout the whole frequency range of interest were not close to one. The coherence curve started to roll off as the frequency increased with the corner frequency of 72Hz. The maximum coherence value measured was 0.9801 (at 0.0971Hz). Note that there is a spike at approximately 50Hz, which was due to the Hum Bug noise filtering system used in the recording equipment. Any coherence values above 149.71Hz exceeded the minimum significance limit (Equation 6-6) of the curves.

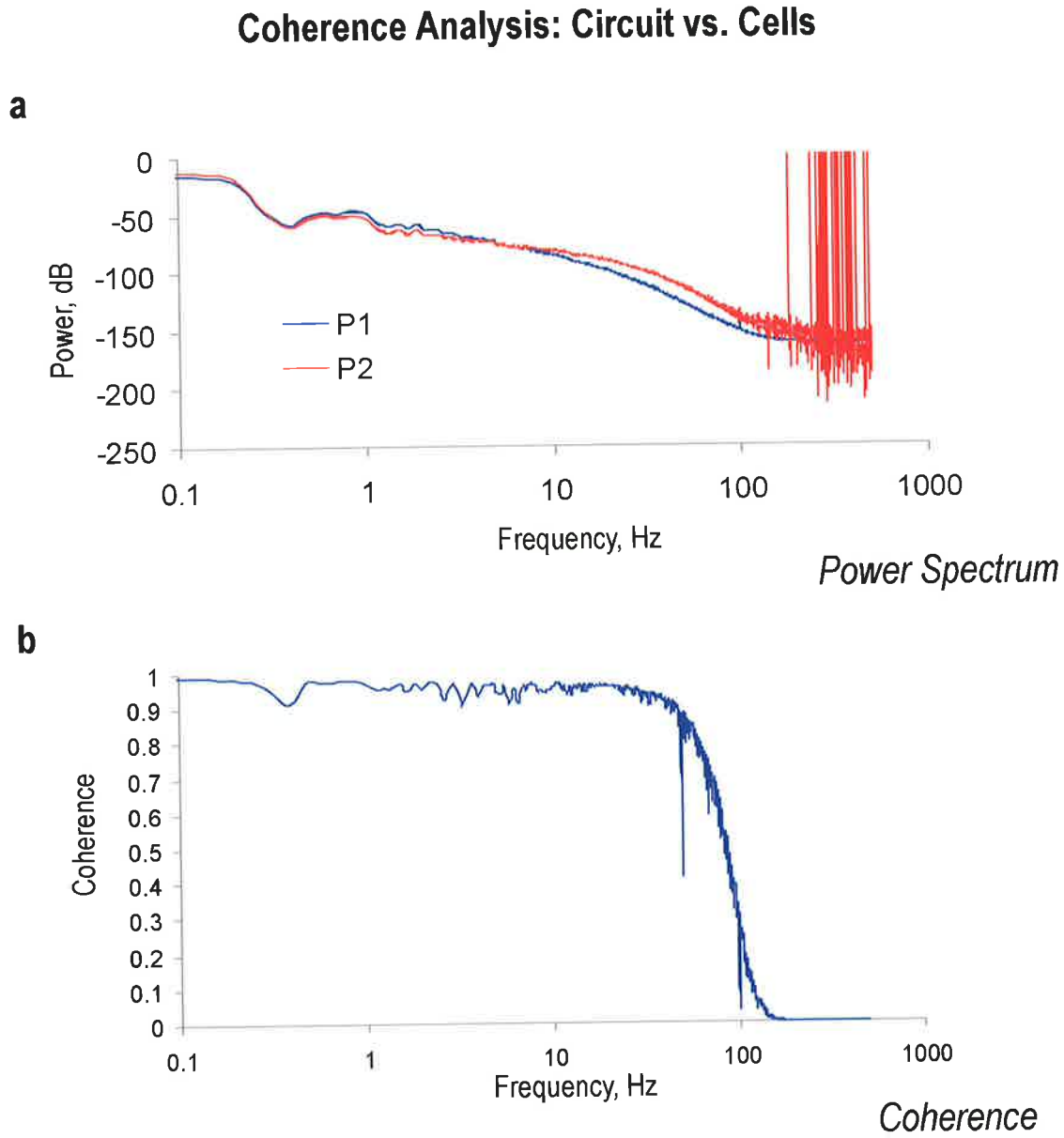

Figure 6-9: Coherence analysis for the photoreceptor circuit against biological cells. a. Normalised power spectrum curves of the photoreceptor circuit (P1) and actual biological cells (P2). b. Coherence curve of the photoreceptor circuit against actual biological cells.

The normalised power spectrum curves, P1 and P2 shown in Figure 6-9a represent the energy curves for both the photoreceptor circuit and the biological photoreceptor cells respectively. Both of the curves shared a very similar power spectrum curves up to approximately

10Hz, in which the biological photoreceptor cells tended to have higher energy (approximately 10dB more) to code high frequencies. Again, noise interference is observed in the power spectrum curve of the biological photoreceptor cells after 150Hz.

Because the photoreceptor circuit was a faithful design of the real biological photoreceptor cells, the average coherence value measured in the curve shown in Figure 6-9b are generally above 0.9. The coherence curve started to roll-off as the frequency increased with the corner frequency of approximately 73Hz. Any coherence values above 134.66Hz exceeded the minimum significance limit (Equation 6-6) of the curves. Again, there was a noise spike at 50Hz that was mainly due to the electrical interference from the Hum Bug.

6.3.3 Higher Order Neuron Experiment

"Moving" Scene

Figure 6-10 shows a collage of a single snap shot (frame #8123) from a 10 second movie (playback speed of 1kHz) that was presented to both the linear photodiode circuit and the adaptive photoreceptor circuit, the outputs of which were cascaded to the LMC circuit model for comparison purposes ***(refer to supplementary material in the CD)***. The top left section of the figure shows the input stimuli of the experiment. The input stimuli were fed to the non-linear photoreceptor circuit (top right) and the corresponding output was transmitted through the LMC circuit. Note that the resulting output of the LMC circuit (bottom right) had clearly spotted the 'small target' in the scene (circled in red), despite the tiny size of the target.

This can be compared to the output of the LMC circuit which employed the linear photodiode as the front end of visual processing

(bottom left), which poorly highlighted the small target that was deliberately integrated in the stimuli scene. Not only was it hard to discern the small target in the scene, the output did not seem to contain much of the other salient features in the scene such as trees and shadows.

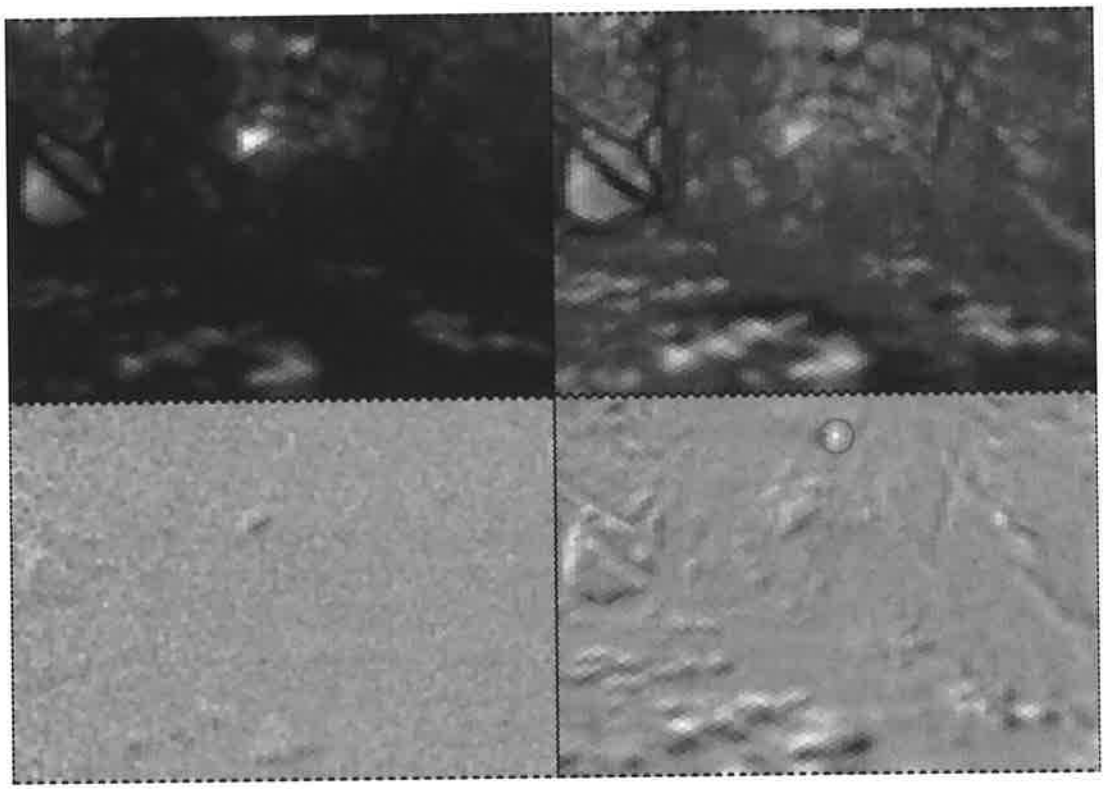

Figure 6-10: Frame #8123 – A collage snapshot of an outdoor movie. The top left section represents the input stimuli and the top right shows the output response of the photoreceptor circuit. Both bottom left and right represent the second order neuron circuit (LMC) output that had the linear photodiode and non-linear photoreceptor circuit as input, respectively.

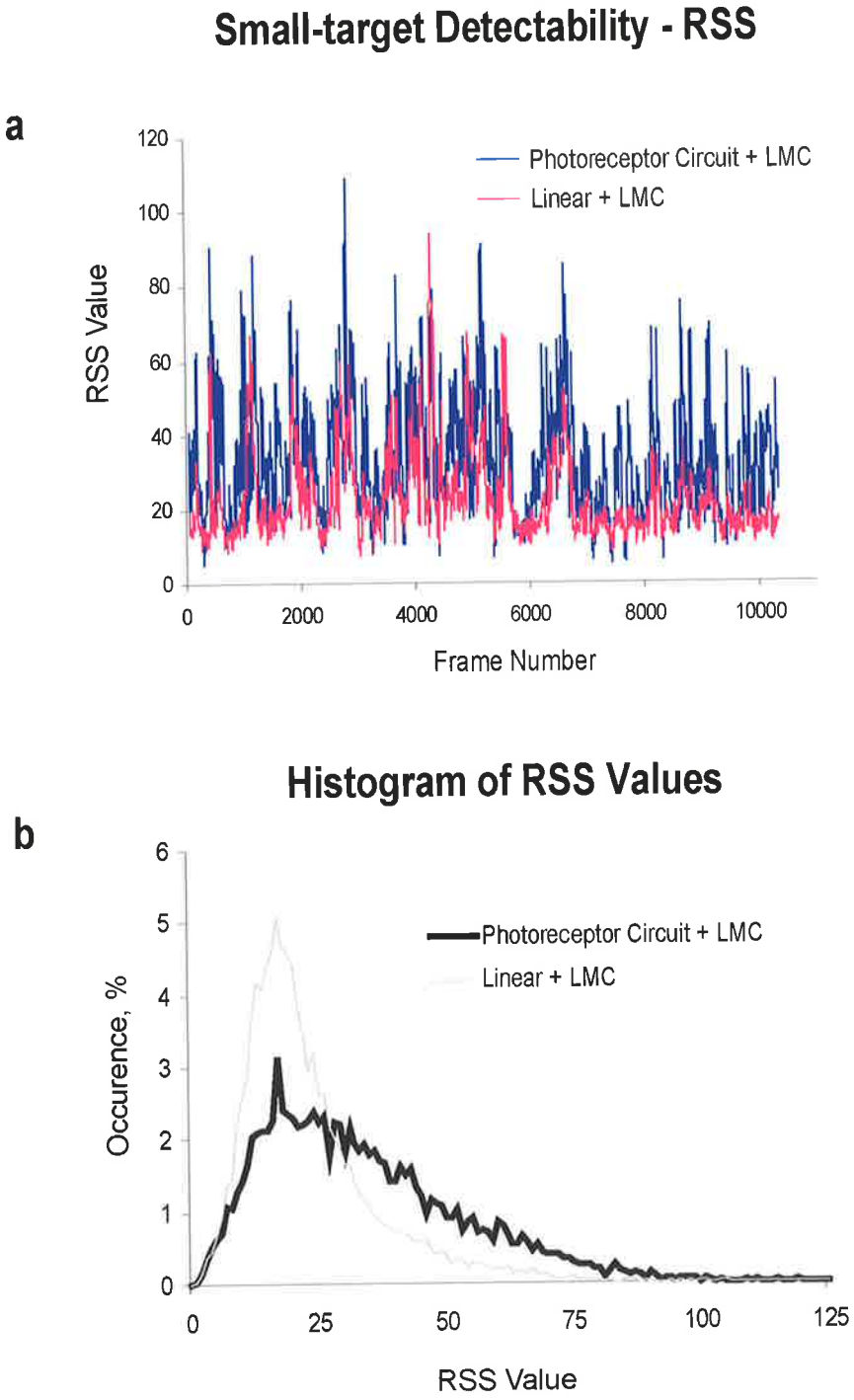

Figure 6-11: Performance comparison between the output of the non-linear + LMC and linear + LMC. a. Contrast metric (RSS value) between the target and the local surround (next-nearest neighbours) for both the non-linear photoreceptor + LMC and linear + LMC. The data was smoothed by using zero-phase 11 frames of moving averages filter for display purposes. b. Histograms of the non-linear photoreceptor + LMC against the linear + LMC, with a bin size of 1.

As can be seen from Figure 6-11a, the detectability of the small target throughout the duration of the scene was generally improved when the non-linear photoreceptor was used at the front-end to the LMC circuit as compared with a linear photoreceptor.

This is more clearly illustrated in the histogram of RSS values (Figure 6-11b). The modal value for both photoreceptors was found to be 17. The histogram for the non-linear photoreceptor exhibits a lower frequency of RSS values around this modal value, instead having a much greater proportion of frames with high RSS values of 28 and above. The mean improvement in RSS value over the linear photoreceptor was 75.5 %. This improvement is also reflected in the higher median RSS value of 29.26 and maximum value of 121 obtained with the non-linear photoreceptor as compared with a median of 19.45 and a maximum of 105 obtained with the linear photoreceptor.

"Walking" Scene

The experiments were repeated with a different movie scene ***(refer to supplementary material in the CD)***. Figure 6-12 shows a collage snapshot of a movie (playback speed of 400Hz) where 2 people were walking towards the middle of the scene and one of them attempted to hide behind the tree trunk. The scene was deliberately programmed to have several bands of maximum intensity playback (100%, 50%, 1%, 1%, 50% and 100%) in order to demonstrate an extreme lighting condition and how our non-linear adaptive photoreceptor circuit provides better visual information to higher order neurons as compared to the simple linear photodiode system.

Figure 6-12: Frame #850 – A collage snapshot of an outdoor movie with camera mounted stationary on a tripod. Top left section represents the input stimuli with variable bands of maximum playback intensities (100%, 50%, 1%, 1%, 50% and 100%). The top right section shows the output from the photoreceptor circuit. The output of the photoreceptor was cascaded to the LMC circuit and the result is shown in the bottom right section. The bottom left section is a result from the LMC circuit that was cascaded with the linear photodiode as the front-end detector.

Again, note that with the linear photodiode system as the front-end of the visual processing, no information was captured by the LMC circuit, particularly in the darkest area, 1% (bottom left). However, the LMC output (bottom right) employing the non-linear adaptive photoreceptor circuit as the front-end (top right) demonstrated its capability to compress visual information elegantly before transmitting them to the higher order neuron to process. Note that even in the darkest area of the scene, the LMC circuit was capable of highlighting the two people in the middle.

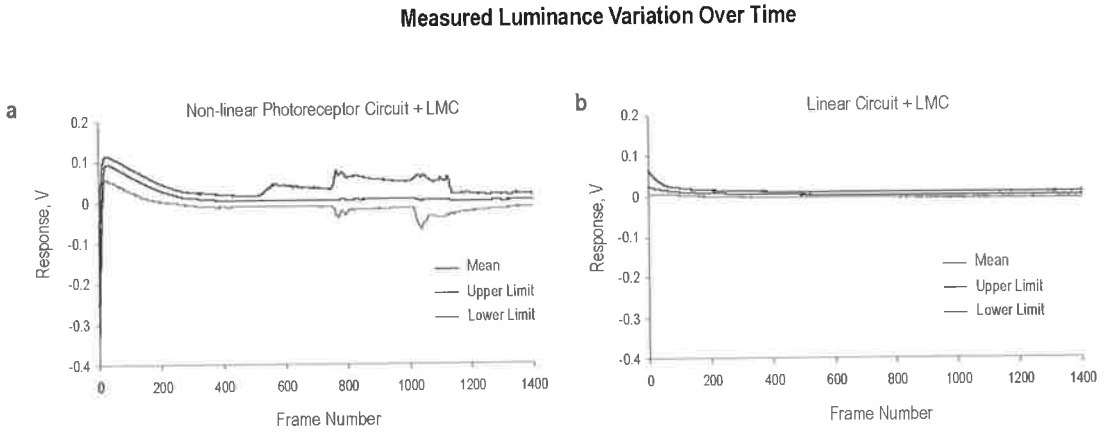

Figure 6-13: Measured luminance variation over 1400 frames that were played back at 400Hz, with traces of 2.5 percentile and 97.5 percentile also shown, representing the lower and upper limits respectively of a 95% CI around the mean. The mean values were calculated only from the middle part of all the frames (1% intensity bands). a. The output of the LMC circuit that had the non-linear photoreceptor circuit as the front-end of visual processing. b. The output of the LMC circuit that had the linear photodiode circuit as the front-end of visual processing.

To further investigate the benefits of having the non-linearities of the photoreceptors at the front-end of visual processing, the mean values of the LMC responses were calculated for each frame of the played back movie. Figure 6-13a shows the measured mean luminance of the LMC output that had a non-linear photoreceptor cascaded at the front-end stage of visual processing, together with the upper and lower limits of a 95% CI interval around the mean. Note that during the first 400 frames of the movie, the mean values increased sharply followed by a gradual decay, with similar behaviour in both the upper and lower limit curves. Unlike the mean values curve, which remained approximately constant (0V) for the rest of the frames, the upper value curve showed significantly larger variation in the scene starting from frame number 530. This was when the person approaching from the left entered the middle part of the scene and caused an increase in the standard deviation.

Notice that there was no obvious change to the lower limit curve simply because the person who entered the scene from the left mainly caused depolarisations at the output of the LMC circuit.

The second person entered the scene from the right, starting at frame number 754. At this point, the upper limit curve once again starts to rise due to the increase of luminance variations in the scene. At about the same time, the lower limit curve starts to have some changes simply because the second person creates some hyperpolarisations responses at the output of the LMC circuit. When both people walked away from the middle part of the scene, the amount of luminance variations decreased and thus the difference between the limit curves and the mean curve decreased accordingly.

The benefits of having a non-linear stage at the front-end of visual processing can be clearly seen when the results in Figure 6-13a are compared to the results in Figure 6-13b, in which a linear photodiode circuit was used as the front-end to the LMC circuit. Both the lower and upper limit curves show no obvious fluctuations around the mean value curve. In other words, the LMC circuit did not detect any person walking into the scene throughout the whole movie.

4.4 Discussions

Biological visual processing involves complex non-linearities, which theory and modelling have suggested are responsible for maximising visual information perceived in the real-world environment (Snyder et al. 1976; Snyder et al. 1977; van Hateren 1992). The neuromorphic model that we designed and implemented has clearly demonstrated how the non-linear compression stage evident in early

visual processing (photoreceptor cells) actually does assist in optimising the visual information prior to transmitting it to the limited-bandwidth higher order neuron channels. Even though biological visual processing, especially in insects such as flies, has relatively low visual resolution compared to that in humans, it is still capable of resolving visual information due to nature's "intelligent" compression technique. Such a biological compression technique would no doubt provide an elegant solution to many current existing surveillance camera systems.

Acknowledgements

We would like to thank the employees of the Botanic Gardens (Adelaide, Wittunga and Mt. Lofty), who have been very helpful during our fly-catching trips. This research was supported with a Linkage grant from the Australian Research Council, including a Post-Doctoral Fellowship for RSAB (LP0667744) and from US Air Force contracts F08630-02-C-0013 and FA9550-04-1-0283.

References

Baumann, F. (1975). Electrophysiological properties of the honey bee retina. The Compound Eye and Vision of Insects. London, Oxford University Press: 53-74.

Baumann, O. (2000). "Distribution of ryanodine receptor ca+21 channels in insect photoreceptor cells." The Journal of Comparative Neurology **421**: 347-361.

Delbrück, T. and S. C. Liu (2004). "A silicon early visual system as a model animal." Vision Research **44**: 2083-2089.

Delbrück, T. and C. A. Mead (1996). Analog VLSI Phototransduction by Continuous-time, Adaptive, Logarithmic Photoreceptor Circuits. Pasadena, California Institute of Technology-Computation and Neural Systems Program: 23.

Dror, R. O., D. C. O'Carroll and S. B. Laughlin (2001). "Accuracy of velocity estimation by Reichardt Correlators." Optical Society of America **18**(2): 241-252.

James, A. C. (1990). White-noise studies in the fly lamina, Australian National University: 191.

Kramer, J., R. Sarpeshkar and C. Koch (1997). "Pulse-based analog VLSI velocity sensors." IEEE Trans. Circuits and Systems II **44**: 86-101.

Laughlin, S. B. and M. Weckström (1993). "Fast and slow photoreceptors - a comparative study of the functional diversity of coding and conductances in the diptera." J. comp. Physiol. A **172**: 593-609.

Liu, S. C. (1996). Silicon model of motion adaptation in the fly visual system. 3rd UCSD-Caltech Symposium on Neural Computation.

Mah, E. L., R. S. A. Brinkworth and D. C. O'Carroll (2006). "Implementation of an elaborated neuromorphic model of a biological photoreceptor." Biological Cybernetics **submitted on Dec 2006**.

Moini, A., A. Bouzerdoum, A. Yakovlev, D. Abbott, O. Kim, K. Eshraghian and R. Bogner (1996). An analog implementation of early visual processing in insects. Int. Symposium on VLSI Technology, Systems, and Applications.

Payne, R. and J. Howard (1981). "Response of an insect photoreceptor: a simple lognormal model." Nature **290**: 415-416.

Rajesh, S., D. C. O'Carroll and D. Abbott (2004). Effects of nonlinear elaborations on the performance of a Reichardt correlator. BioMEMs and Nanotechnology, Proceedings of the SPIE.

Sarpeshkar, R., J. Kramer, G. Indiveri and C. Koch (1996). Analog VLSI architectures for motion processing: from fundamental limits to system applications, Proceedings of the IEEE.

Simoncelli, E. P. and B. A. Olshausen (2001). "Natural image statistics and neural representation." Annual Review of Neuroscience **24**: 1193-1216.

Snyder, A. W., S. B. Laughlin and D. G. Stavenga (1976). "Information Capacity of Eyes." Vision Research **17**: 1163-1175.

Snyder, A. W., D. G. Stavenga and S. B. Laughlin (1977). "Spatial information capacity of compound eyes." J. comp. Physiol. A **116**: 183-207.

Stavenga, D. G. (2003). "Angular and spectral sensitivity of fly photoreceptors. I. Integrated facet lens and rhabdomere optics." Journal of Comparative Physiology A **189**: 1-17.

Straw, A. D., E. J. Warrant and D. C. O'Carroll (2006). "A 'bright zone' in male hoverfly (Eristalis tenax) eyes and associated faster motion detection and increased contrast sensitivity." Journal of Experimental Biology **209**: 4339-4354.

van Hateren, J. H. (1992). "A theory of maximising sensory information." Biological Cybernetics **68**: 23-29.

Wallcott, B. (1975). Anatomical changes during light-adaptation in insect compound eyes. The Compound Eye and Vision of Insects. London, Oxford University Press: 20-33.

7

Chapter 7: Conclusion

Biological visual systems are highly non-linear, displaying adaptation to background luminance. Theories and models have suggested that these complex non-linearities which occur at the very beginning of the visual system pathway (photoreceptor cells) not only provide an "intelligent" compression technique for the high bandwidth visual information received by the photoreceptor, but at the same time assist in the processing of information in higher order neurons (Snyder et al. 1977; Laughlin et al. 1978; Laughlin 1989; van Hateren 1992; van Hateren 1992; van Hateren 1992; Brenner et al. 2000). This represents a key feature in the biological visual systems of insects which allows them to achieve excellent performance with limited-bandwidth neuronal channels. By developing and implementing a neuromorphic model for a biological photoreceptor I have shown that these advantages can be realised in practical applications.

This study makes significant contributions in the area of insect visual system modelling, including the design, construction and testing of a working neuromorphic photoreceptor circuit, the development of experimental equipment to obtain high quality biological photoreceptor recordings and confirm the validity of the neuromorphic circuit, and the investigation of the effectiveness of

photoreceptor non-linearities in assisting information processing in higher order neurons.

7.1 Neuromorphic Photoreceptor Circuit Design

The main objective of this project was to implement a neuromorphic model of a biological photoreceptor cell based on the mathematical model proposed by van Hateren and Snippe (2001) with additional elaborations to better mimic the actual biological photoreceptors. The prototype neuromorphic circuit was constructed on breadboards using discrete electronic circuit components. This neuromorphic circuit has the capability to accept light input that is as bright as real-world luminance and at the same time perform very similarly to the actual biological photoreceptor. An amplified photodiode (TSL 251), which had an output range of 0-4V was used as the light detector for the photoreceptor circuit. Accordingly, the photoreceptor circuit was designed and implemented to accept voltage ranging from 0-4V, with an output voltage of 0-1V. A preliminary design of the circuit using printed circuit board technology indicates that the overall circuit size could be minimized, mainly using surface mount components. This analog circuit would not only have low power consumption but at the same time can be made portable for outdoor experiments.

7.2 Construction of Experimental Equipment

The real-world environment presents very high dynamic range (HDR) visual information. Thus, it was vital that the circuit design be evaluated against the actual biological photoreceptors using high quality 32-bit HDR scenes. During the experiments on the biological and artificial photoreceptor cells, artificial natural scenes comprised of high dynamic range images were applied as stimuli, using a light

emitting diode (LED). In order to properly reproduce the dynamic range of the real-world luminance, a high current LED driver was custom-built to drive a green Luxeon Star LED and calibrated to be able to produce light intensities ranging from 0 cd/m^2 to 70000 cd/m^2. Unlike other commercially available LED drivers, this high current LED driver system was fully dimmable, providing stable, flicker-free output even at low light intensities. This was vital in performing high quality visual experiments, particularly since a dependable low intensity light source was required to accurately characterize the frequency response of the photoreceptor in a dark-adapted state.

7.3 Biological Photoreceptor Features

The photoreceptor characteristics of the fly *Eristalis tenax* are properly illustrated in Chapter 4 of this thesis, in particular the relationship between the corner frequencies of the photoreceptors and the background luminance. The corner frequency increased non-linearly as the background luminance increased from 10Hz and tended to saturate at approximately 90Hz when the background luminance was above 3500cd/m^2. This well-defined steady-state characteristic of the biological photoreceptor allowed us to further enhance the circuit design to closely mimic the biological photoreceptor. This additional elaboration to the circuit successfully demonstrated the practicality of a variable corner frequency system that was dependent on the background luminance.

This feature was important as studies have indicated that a variable bandwidth system allows the insect to maximize the signal to noise ratio of the visual information. In a dark background, the biological photoreceptors are very sensitive to light due to the increase in

photoreceptor gain. Even extremely low intensity stimuli between 70cd/m^2 are sufficient to stimulate the photoreceptors. As a result of this, they are very likely to pick up high frequency noise/interference such as photon noise. Thus, in order to ensure that the photoreceptors perform optimally, they sacrifice their signal bandwidth by reducing their corner frequency and hence achieve a higher signal-to-noise ratio in the perceived visual information. Conversely, because it is very unlikely that the photoreceptors will pick up any high frequency noise during a light-adapted state, the photoreceptors increase their corner frequencies for better bandwidth performance. By implementing this feature in a neuromorphic model, it is possible to develop an automatic gain control that is optimised in an information theoretical sense.

7.4 Photoreceptor Circuit Performance

In order to fine tune the neuromorphic circuit and evaluate it against the actual biological photoreceptor cells, steady-state analyses were performed on both the circuit and the actual photoreceptors. Since it was practically impossible to perform any *in-vivo* experiments outdoors, all electrophysiological recordings were done in the laboratory, with a simple linear photodiode output used as an experimental control.

The measured corner frequency of the circuit varied with background intensity from 10Hz to 90Hz, closely matching the experimental results obtained from the biological photoreceptor. The V Log I curves also exhibited the expected adaptive characteristic. Correlation and coherence analyses showed that the circuit was capable of emulating the biological photoreceptor faithfully in both

time and frequency domains, with an r^2 value of 0.890±0.030 (mean ± standard deviation) based on high dynamic range stimuli.

Despite the high level of correlation, there were minor differences between the response of the biological photoreceptor and that of the photoreceptor circuit. Under extremely low intensity conditions such as a luminance of 70cd/m^2, the performance of the photoreceptor circuit suffered from insufficient gain. This was found to be due to the limitations of the components themselves, in particular the signal-to-noise ratio of the photodetector used (TSL 251), which was the lowest-noise cost-effective component available. Additionally, the photoreceptor circuit corner frequency saturated at a slightly higher background intensity as compared with the biological photoreceptor. This was because we had no control over the non-linear characteristic of the light-dependent resistor component used. While it may be possible to incorporate additional circuitry to compensate for or minimize this minor discrepancy, a decision was made not to do so as this would potentially involve greatly increased design complexity and thus development time.

7.5 Benefits of Non-linear Photoreceptor Features

Since the implemented photoreceptor circuit was found to be a faithful mimic of the actual photoreceptor cells, the circuit was used to study the response of the photoreceptors in a naturalistic moving scene. To investigate the theory that the non-linear attributes of photoreceptors improve the quality of visual processing in higher order neurons, the performance of the adaptive non-linear photoreceptor circuit was compared with a simple linear detector. This was accomplished by feeding the visual signal from a real scene through the photoreceptor circuit prior to transmission to a second

order neuron, which was implemented in this project by a circuit mimicking the large monopolar cell (LMC) in the insect visual pathway.

The results showed that there were significant improvements to the visual information at the LMC output when the photoreceptor circuit was used as the front-end of the visual processing unit as compared to having a simple linear detector. A small target that was deliberately integrated into the naturalistic scenes was easily picked out by the photoreceptor circuit + LMC, which may explain how a low resolution hoverfly has the capability to detect its prey in a cluttered background as recently demonstrated for higher order neurons (Nordström et al. 2006). Additionally, under extreme lighting conditions such as the one demonstrated in Chapter 6, the LMC output managed to pick out movements that occurred even in the darkest area of the scene.

7.6 Future Work and Potential Applications

The neuromorphic circuit was implemented purely to investigate the feasibility of designing and implementing a circuit based on a biological photoreceptor. Thus, some parts of the circuit design may be not optimized or even not required for certain applications. Ultimately, implementing the photoreceptor circuit on a chip using VLSI technology would offer increased portability and open up many potential applications.

One obvious potential real-world application that arose from this project was to use a multi-pixel photoreceptor circuit as the front-end for surveillance camera systems. The pixel-by-pixel adaptation of insect eyes provides a solid solution to many existing problems in the standard surveillance camera system, especially when extreme

lighting conditions are encountered in the scene, such as sun flare and headlight flare. In situations like these, existing cameras with global automatic gain control will adjust the gain of the entire scene, causing loss of important details in other parts of the scene. However, by having pixel-by-pixel adaptation in the front-end of the camera, scenes with features that are too bright will not experience any detrimental effects in other parts of the scene. This is because each pixel has its own built-in automatic gain control system.

The superior performance of the photoreceptor circuit due to its intrinsic logarithmic coding and other adaptive non-linear attributes makes it a desirable option as the front-end for other artificial systems which perform tasks such as tracking and motion detection. The potential for fast and robust response could be beneficial in military applications such as visual target-tracking in missile guidance or other weapon systems.

Aside from industry-related applications, a portable unit based on the photoreceptor circuit could allow greater flexibility in collecting experimental data for further studies in insect vision. Since it has been shown to faithfully reproduce the characteristics of the biological fly photoreceptors, it can be used to obtain a reliable set of data for evaluating or benchmarking models of higher order neurons. Similarly, it may find use as an educational tool to aid in demonstrating certain characteristics of the insect visual system.

References

Brenner, N., W. Bialek and R. R. de Ruyter van Steveninck (2000). "Adaptive rescaling maximizes information transmission." Neuron **26**: 695-702.

Laughlin, S. B. (1989). "A role of sensory adaptation in the retina." J. exp. Biol. **146**: 39-62.

Laughlin, S. B. and R. C. Hardie (1978). "Common strategies for light adaptation in the peripheral visual systems of fly and dragonfly." J. Comp. Physiol. **128**: 319-340.

Nordström, K., P. D. Barnett and D. C. O'Carroll (2006). "Insect detection of small targets moving in visual clutter." PLoS Biol. **4**(3): e54.

Snyder, A. W., S. B. Laughlin and D. G. Stavenga (1977). "Information capacity of eyes." Vision Research **17**: 1163-1175.

van Hateren, J. H. (1992). "Real and optimal neural images in early vision." Nature **360**: 68-69.

van Hateren, J. H. (1992). "Theoretical predictions of spatiotemporal receptive fields of fly LMCs, and experimental validation." Journal of Comparative Physiology A **171**: 157-170.

van Hateren, J. H. (1992). "A theory of maximizing sensory information." Biol. Cybern. **68**: 23-29.

van Hateren, J. H. and H. P. Snippe (2001). "Information theoretical evaluation of parametric models of gain control in blowfly photoreceptor cells." Vision Research **41**: 1851-1865.

Appendix

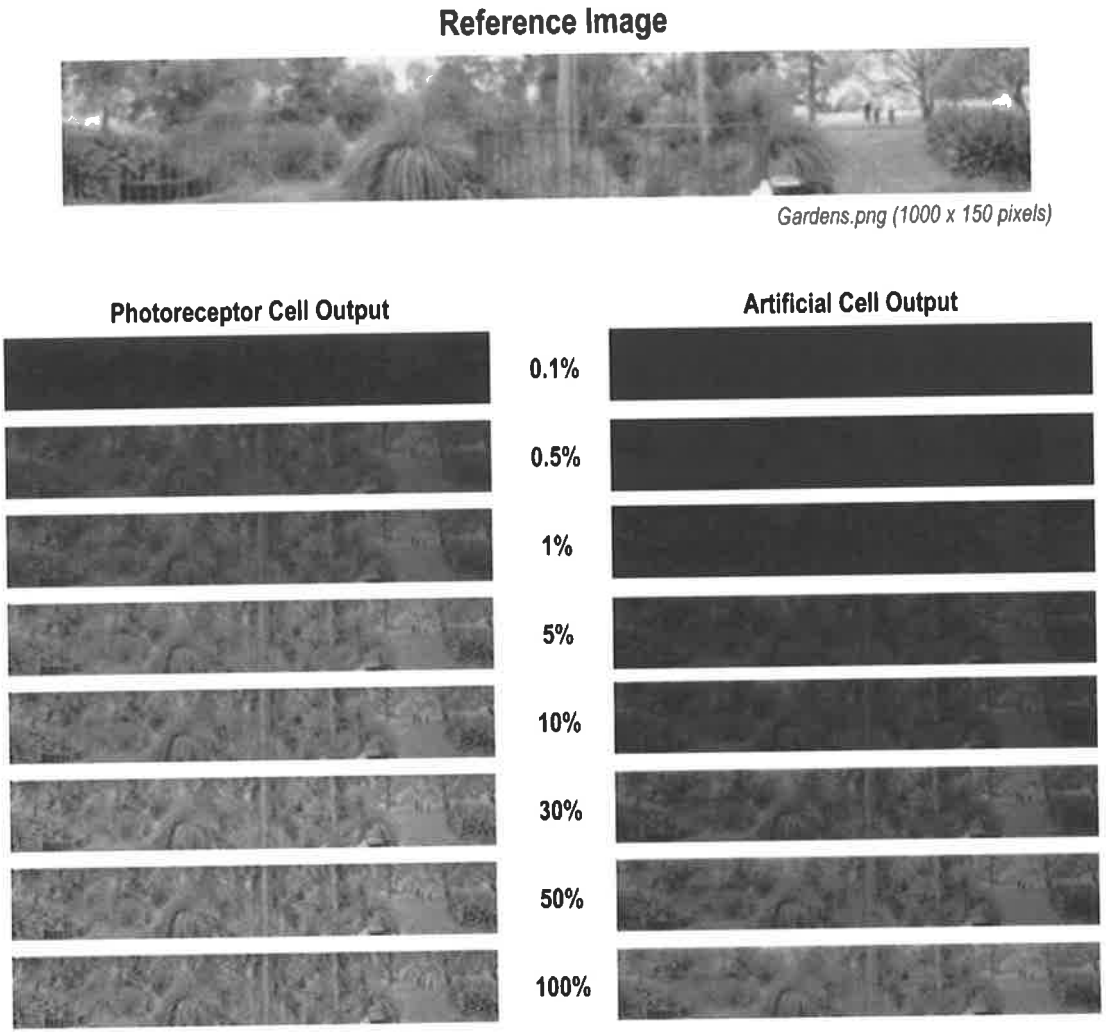

Figure A-1: Reconstructed output images *(Gardens)* from both the actual biological photoreceptors *(average of 4 trials)* and the artificial photoreceptor *(no repeats)* at several maximum brightness playbacks – 0.1%, 0.5%, 1%, 5%, 10%, 30%, 50% and 100%. The image at the top of the figure was used as a reference for all mathematical analyses.

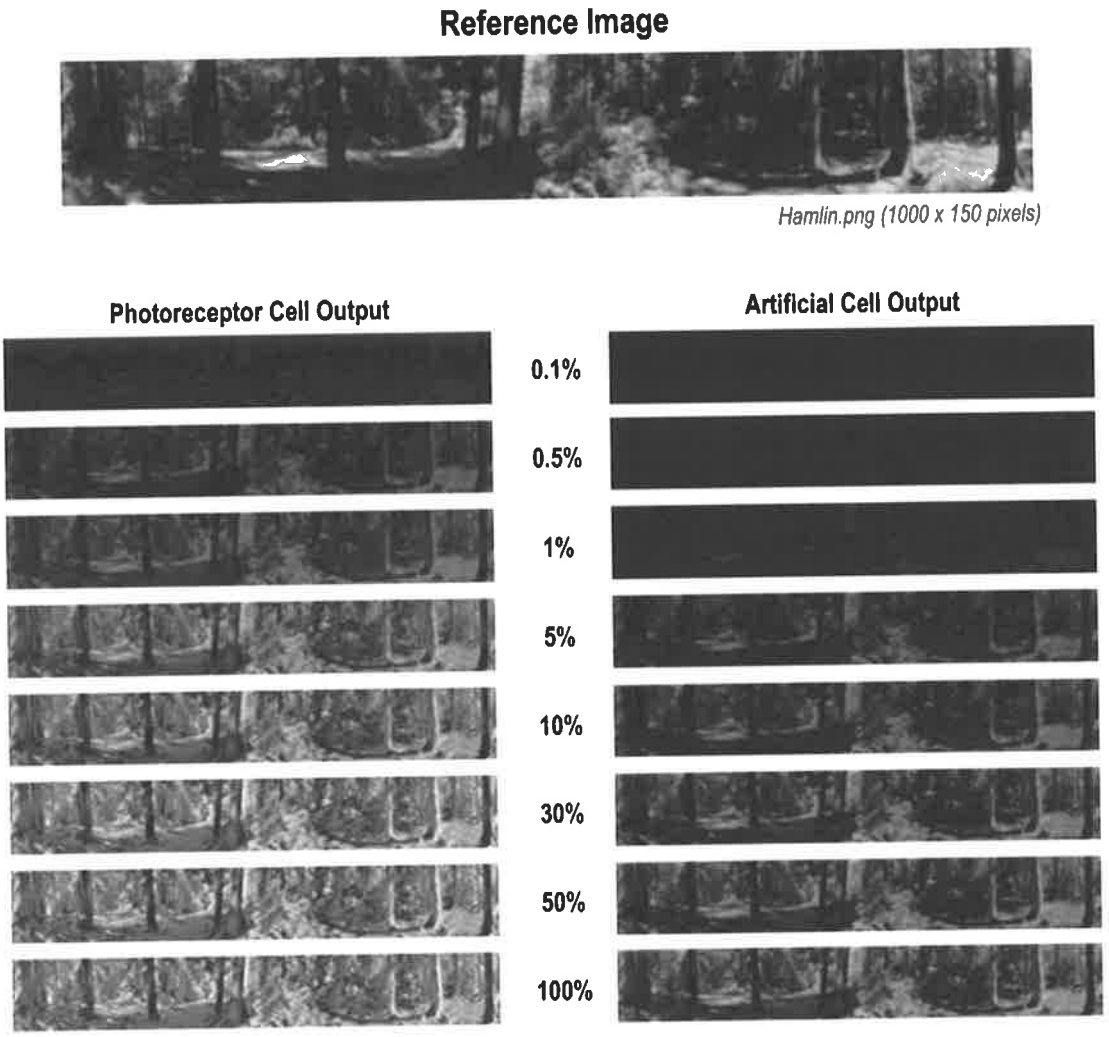

Figure A-2: Reconstructed output images *(Hamlin)* from both the actual biological photoreceptors *(average of 4 trials)* and the artificial photoreceptor *(no repeats)* at several maximum brightness playbacks – 0.1%, 0.5%, 1%, 5%, 10%, 30%, 50% and 100%. The image at the top of the figure was used as a reference for all mathematical analyses.

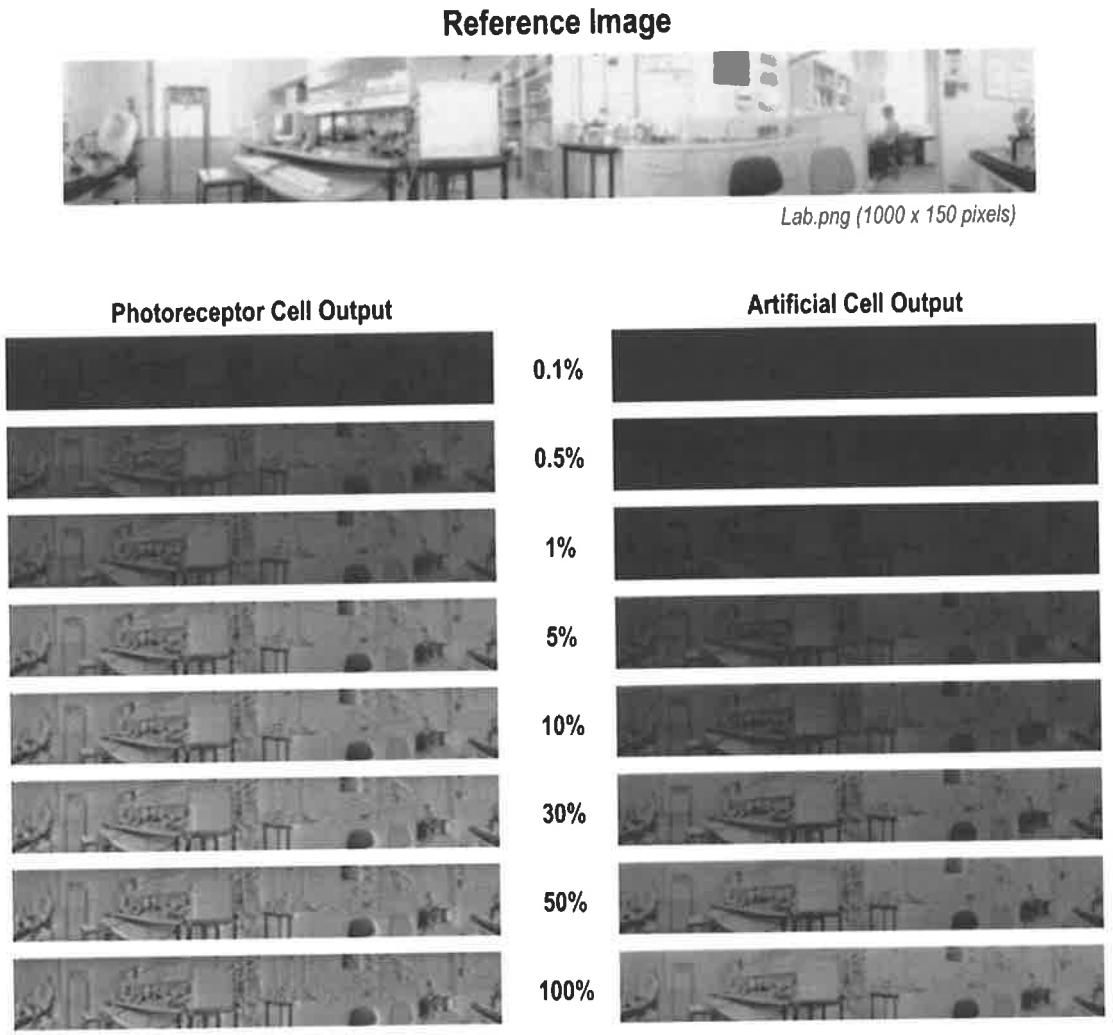

Figure A-3: Reconstructed output images *(Lab)* from both the actual biological photoreceptors *(average of 4 trials)* and the artificial photoreceptor *(no repeats)* at several maximum brightness playbacks – 0.1%, 0.5%, 1%, 5%, 10%, 30%, 50% and 100%. The image at the top of the figure was used as a reference for all mathematical analyses.

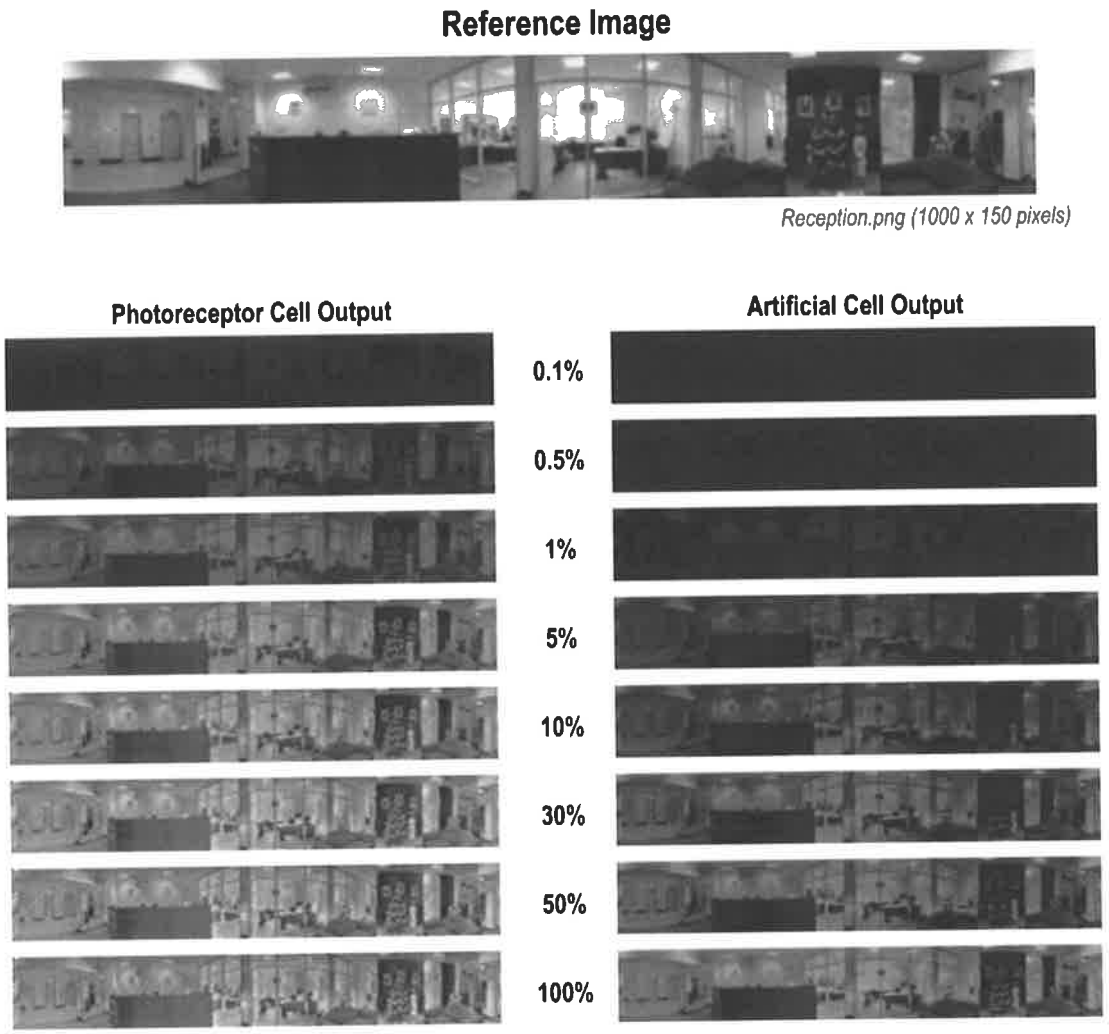

Figure A-4: Reconstructed output images *(Reception)* from both the actual biological photoreceptors *(average of 4 trials)* and the artificial photoreceptor *(no repeats)* at several maximum brightness playbacks – 0.1%, 0.5%, 1%, 5%, 10%, 30%, 50% and 100%. The image at the top of the figure was used as a reference for all mathematical analyses.

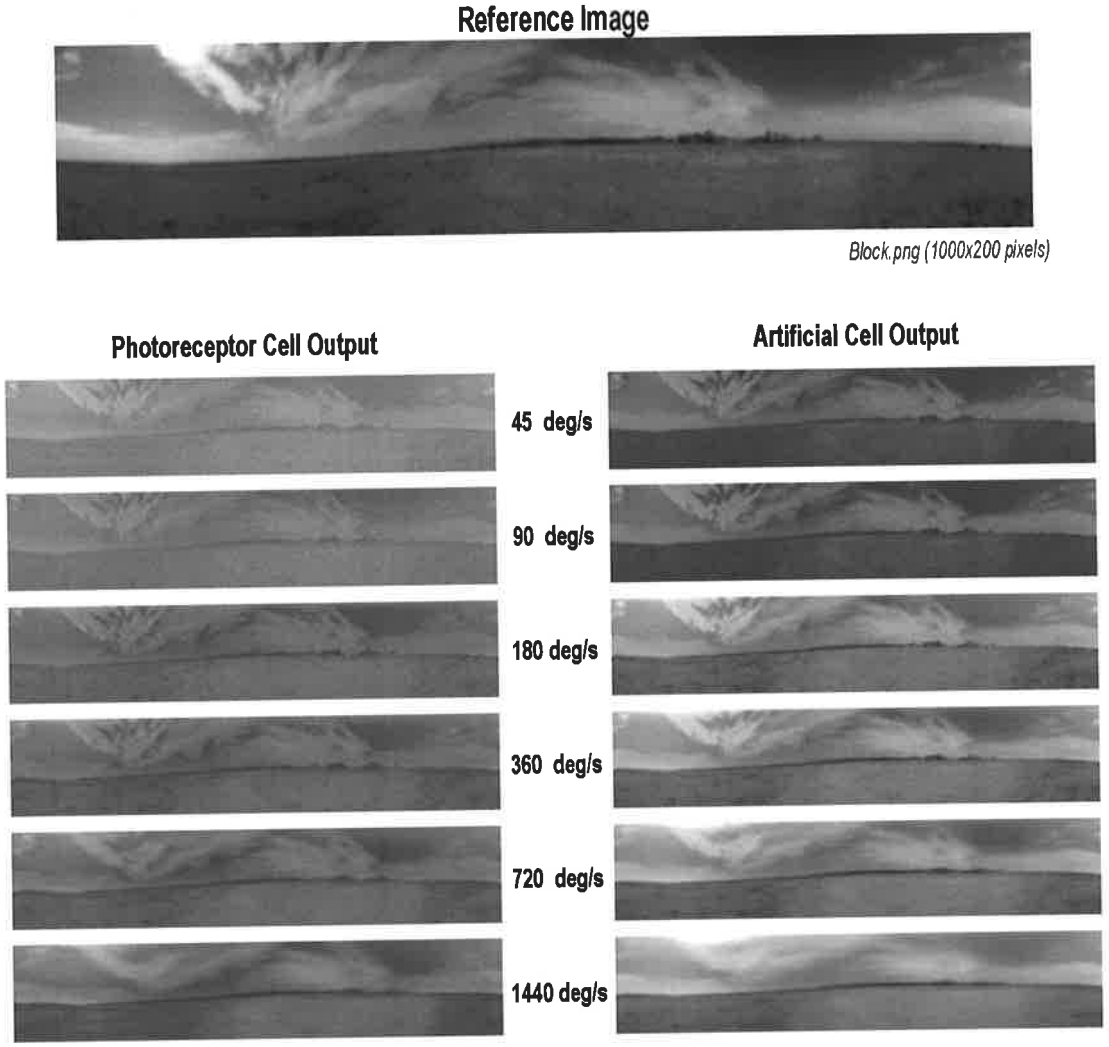

Figure A-5: Reconstructed output images *(Block)* from both the actual biological photoreceptors *(average of 4 trials)* and the prototype circuit *(no repeats)* at several playback speeds – 45°/s, 90°/s, 180°/s, 360°/s, 720°/s and 1440°/s. The image at the top of the figure was used as a reference for all mathematical analyses.

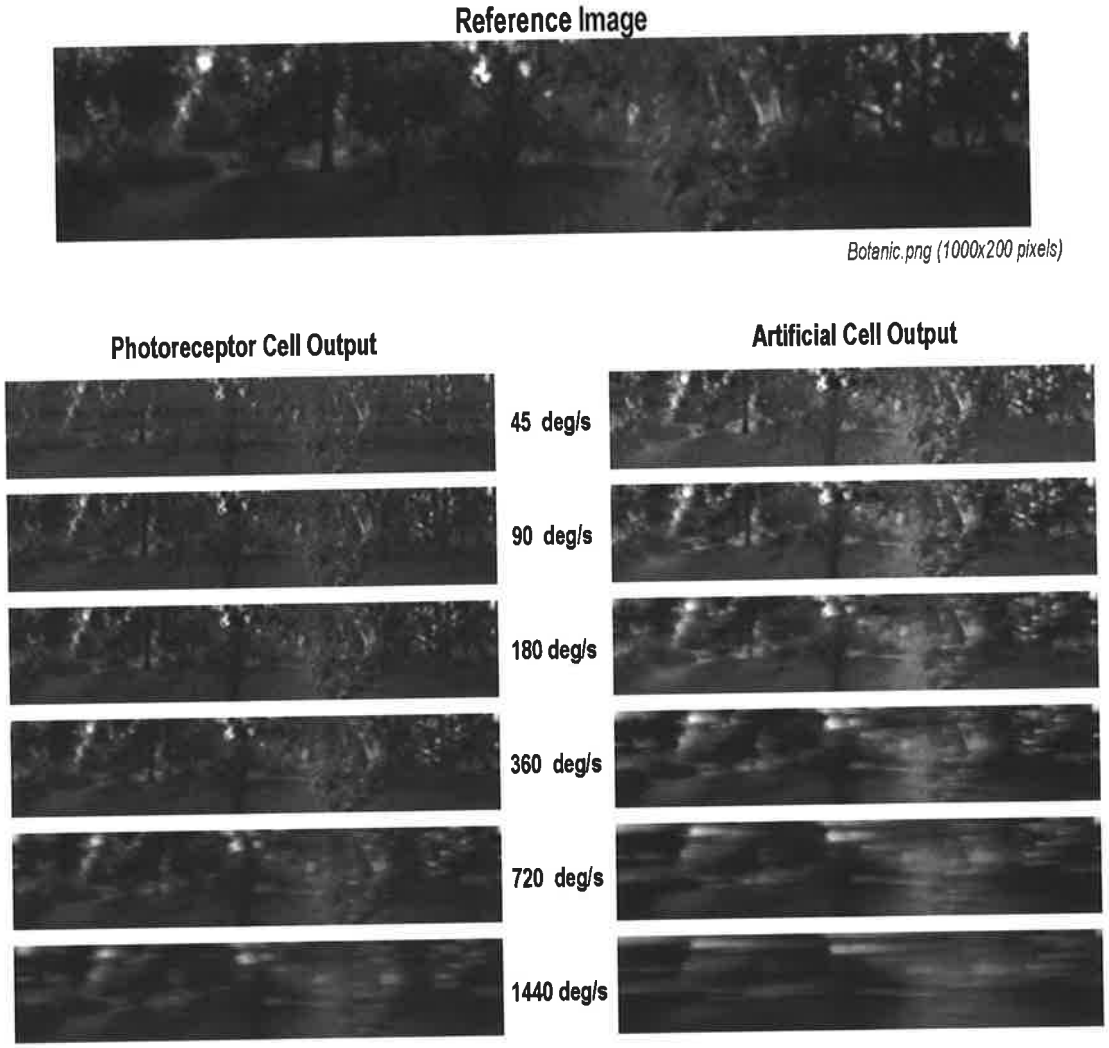

Figure A-6: Reconstructed output images *(Botanic)* from both the actual biological photoreceptors *(average of 4 trials)* and the prototype circuit *(no repeats)* at several playback speeds – 45°/s, 90°/s, 180°/s, 360°/s, 720°/s and 1440°/s. The image at the top of the figure was used as a reference for all mathematical analyses.

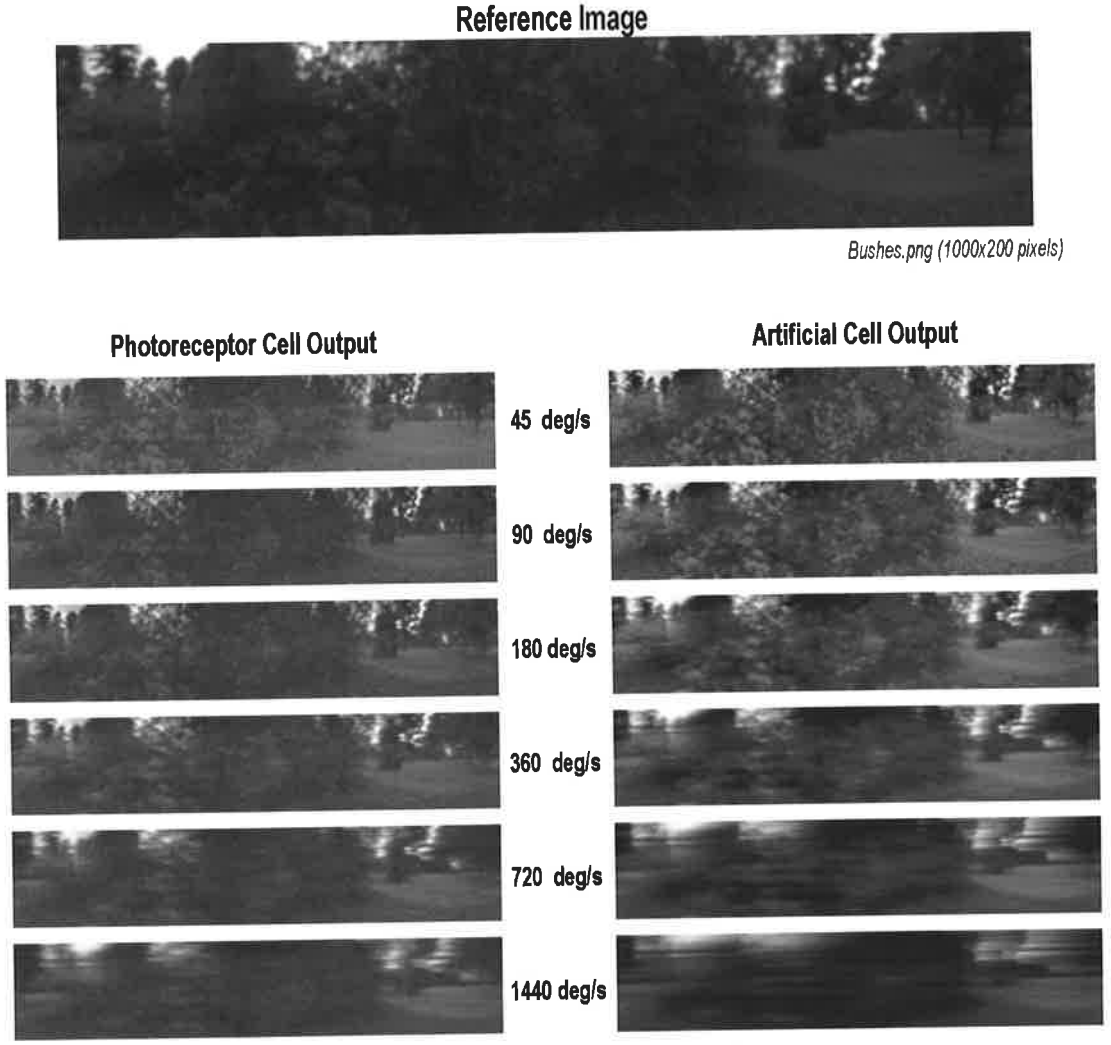

Figure A-7: Reconstructed output images *(Bushes)* from both the actual biological photoreceptors *(average of 4 trials)* and the prototype circuit *(no repeats)* at several playback speeds – 45°/s, 90°/s, 180°/s, 360°/s, 720°/s and 1440°/s. The image at the top of the figure was used as a reference for all mathematical analyses.

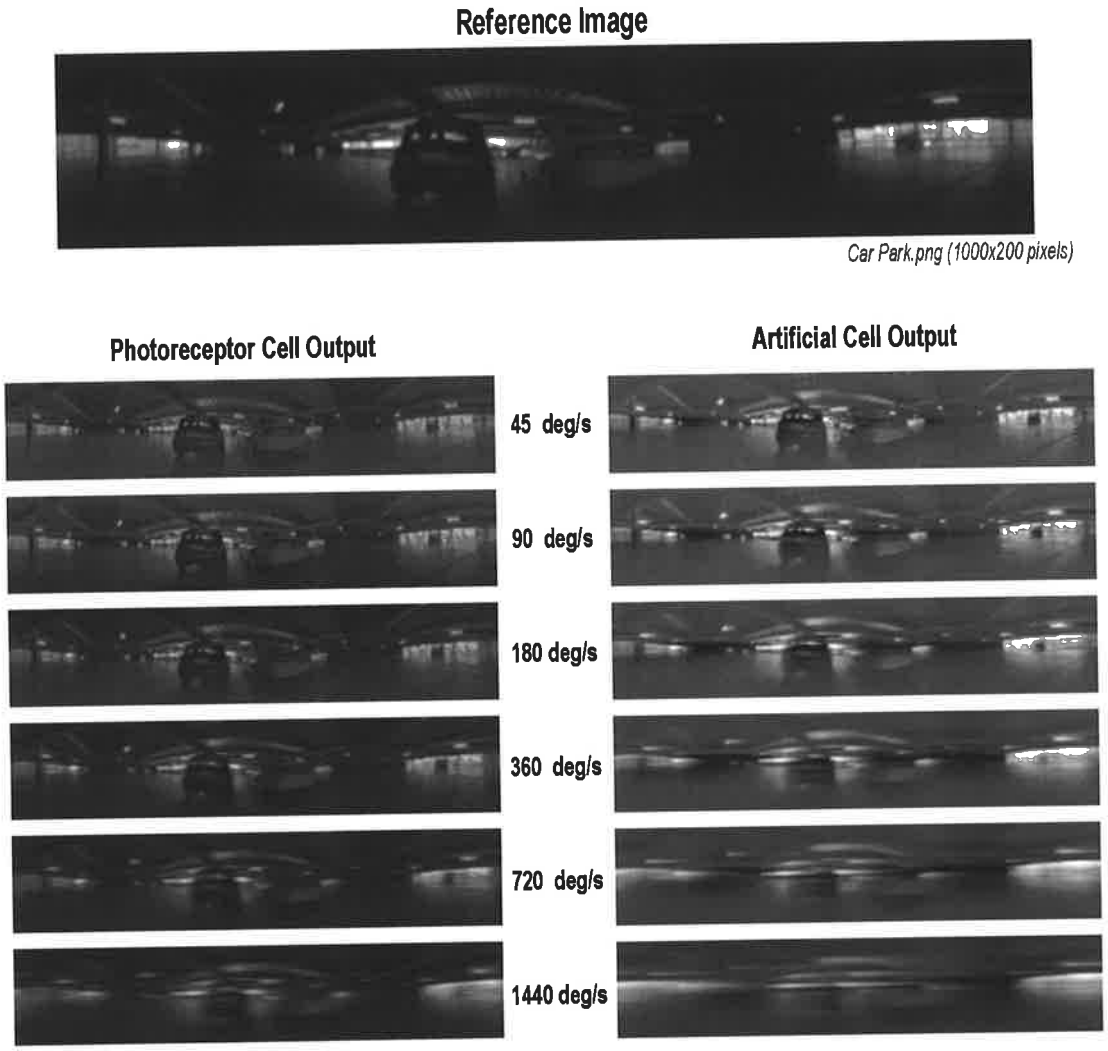

Figure A-8: Reconstructed output images *(Car Park)* from both the actual biological photoreceptors *(average of 4 trials)* and the prototype circuit *(no repeats)* at several playback speeds – 45°/s, 90°/s, 180°/s, 360°/s, 720°/s and 1440°/s. The image at the top of the figure was used as a reference for all mathematical analyses.

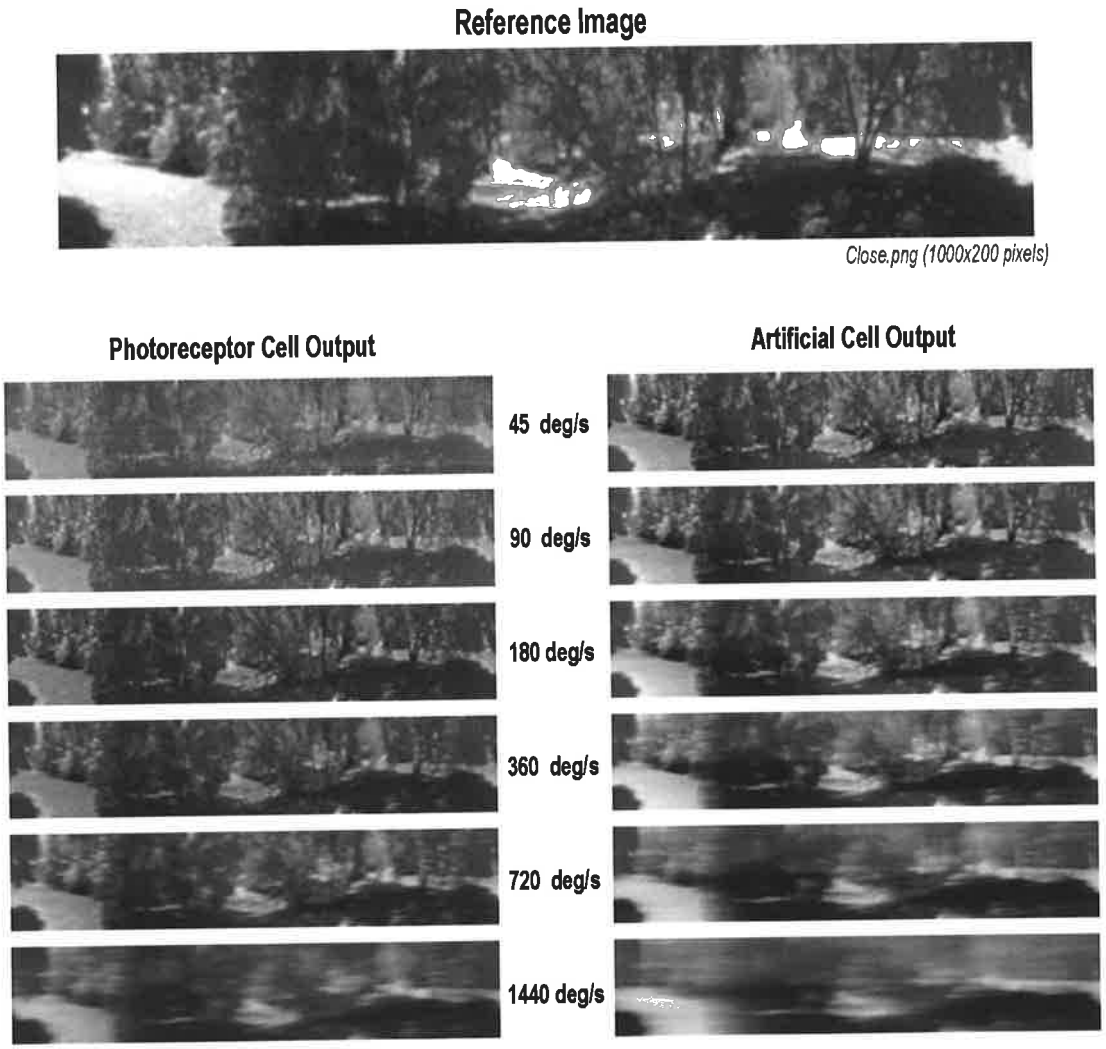

Figure A-9: Reconstructed output images *(Close)* from both the actual biological photoreceptors *(average of 4 trials)* and the prototype circuit *(no repeats)* at several playback speeds – 45°/s, 90°/s, 180°/s, 360°/s, 720°/s and 1440°/s. The image at the top of the figure was used as a reference for all mathematical analyses.

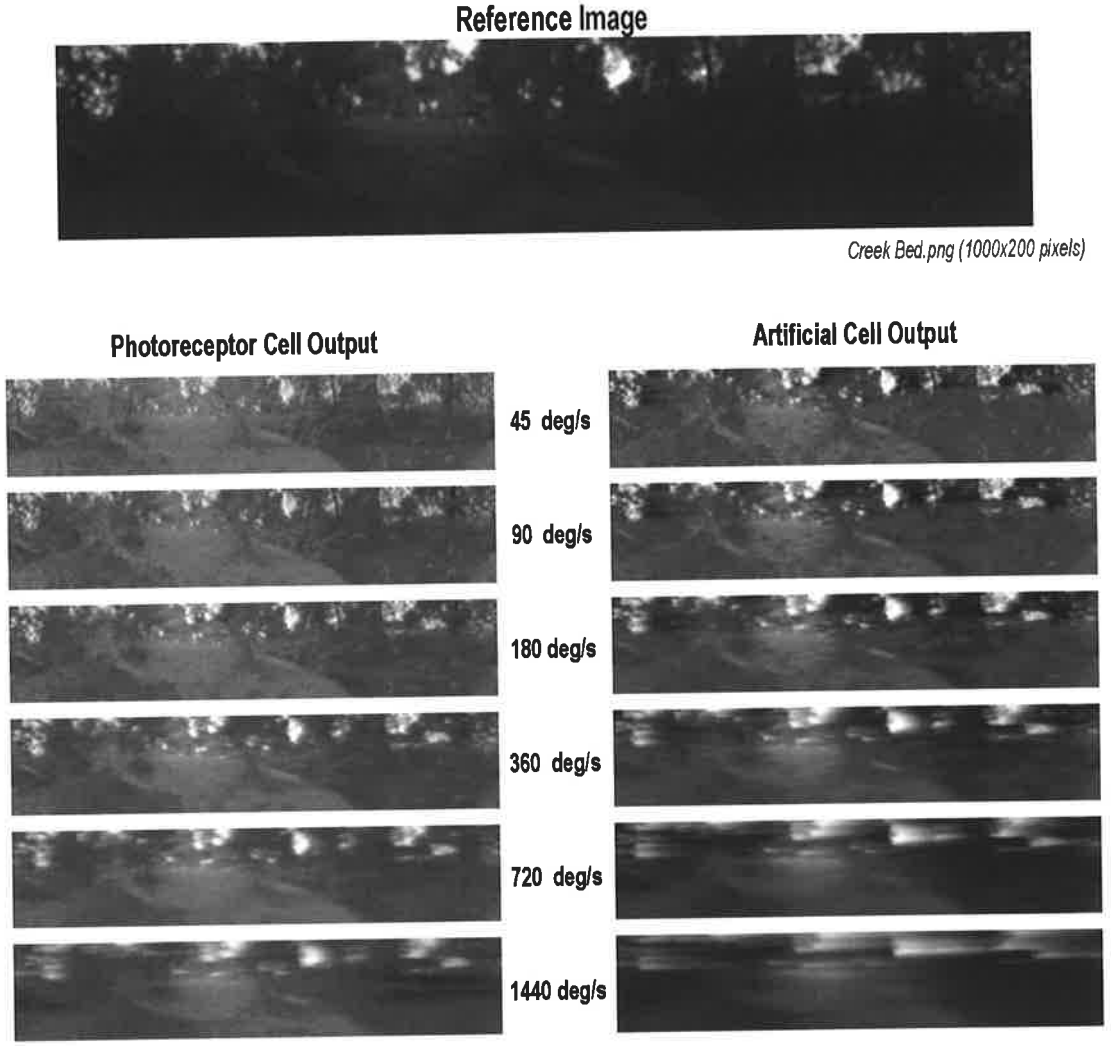

Figure A-10: Reconstructed output images *(Creek Bed)* from both the actual biological photoreceptors *(average of 4 trials)* and the prototype circuit *(no repeats)* at several playback speeds – 45°/s, 90°/s, 180°/s, 360°/s, 720°/s and 1440°/s. The image at the top of the figure was used as a reference for all mathematical analyses.

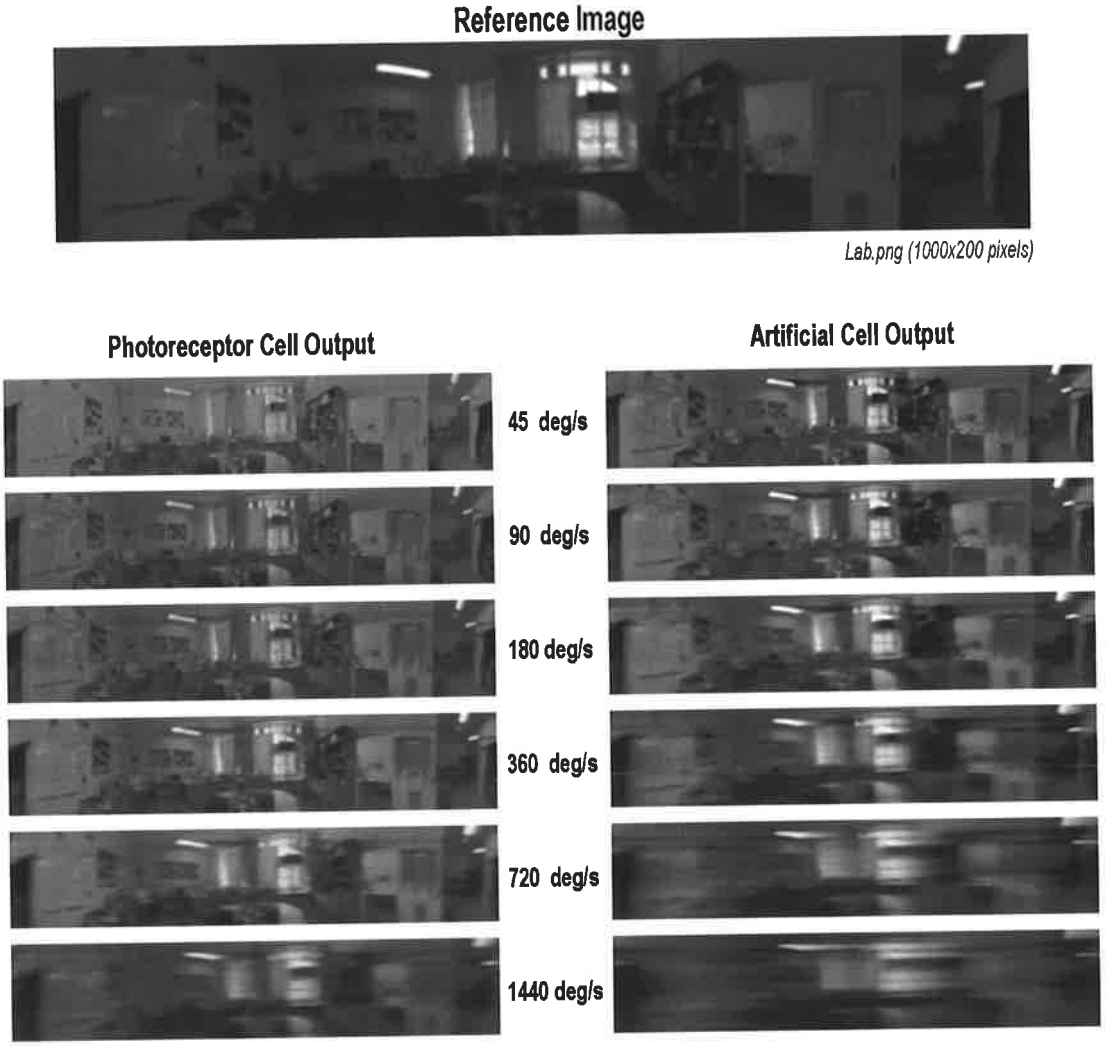

Figure A-11: Reconstructed output images *(Lab)* from both the actual biological photoreceptors *(average of 4 trials)* and the prototype circuit *(no repeats)* at several playback speeds – 45°/s, 90°/s, 180°/s, 360°/s, 720°/s and 1440°/s. The image at the top of the figure was used as a reference for all mathematical analyses.

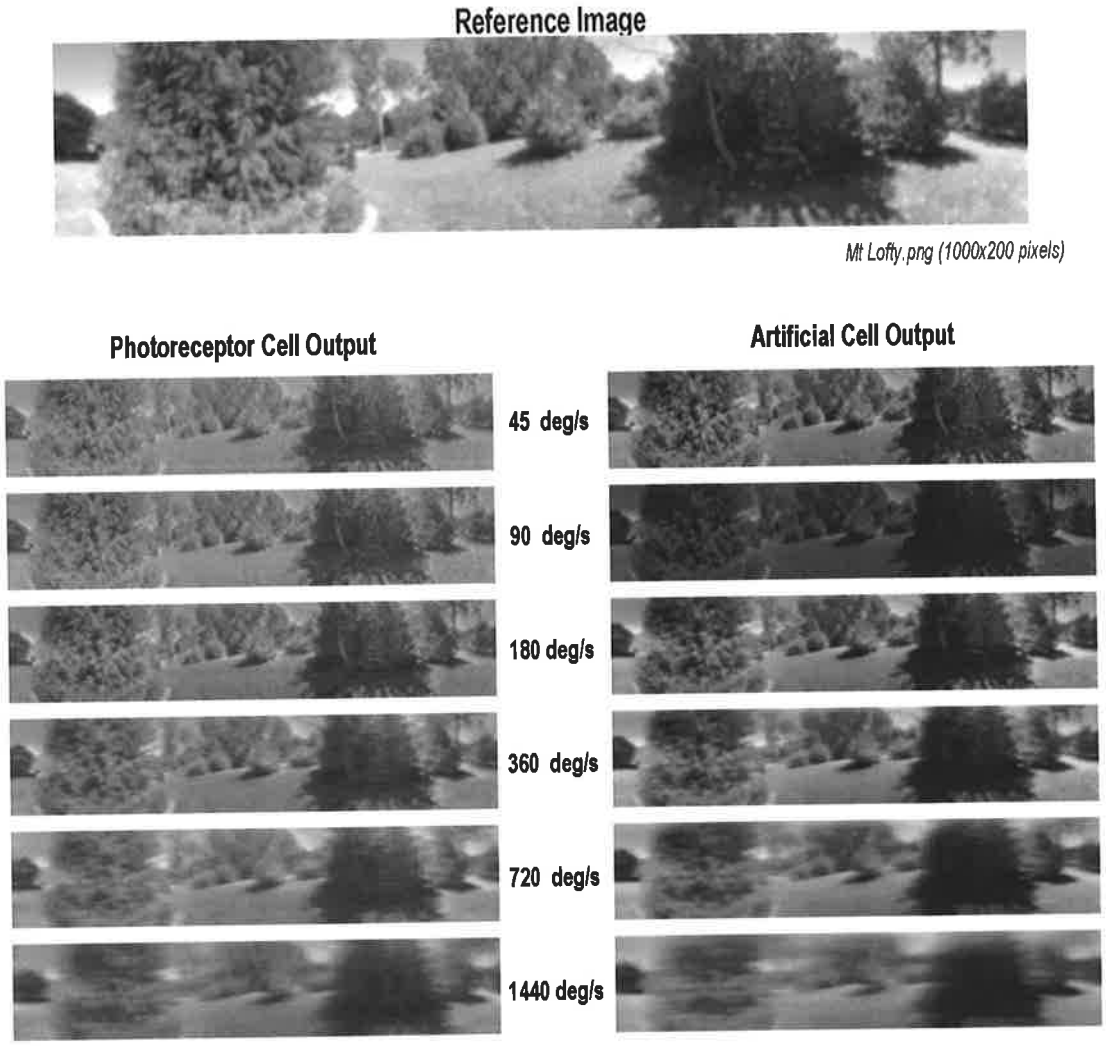

Figure A-12: Reconstructed output images *(Mt Lofty)* from both the actual biological photoreceptors *(average of 4 trials)* and the prototype circuit *(no repeats)* at several playback speeds – 45°/s, 90°/s, 180°/s, 360°/s, 720°/s and 1440°/s. The image at the top of the figure was used as a reference for all mathematical analyses.

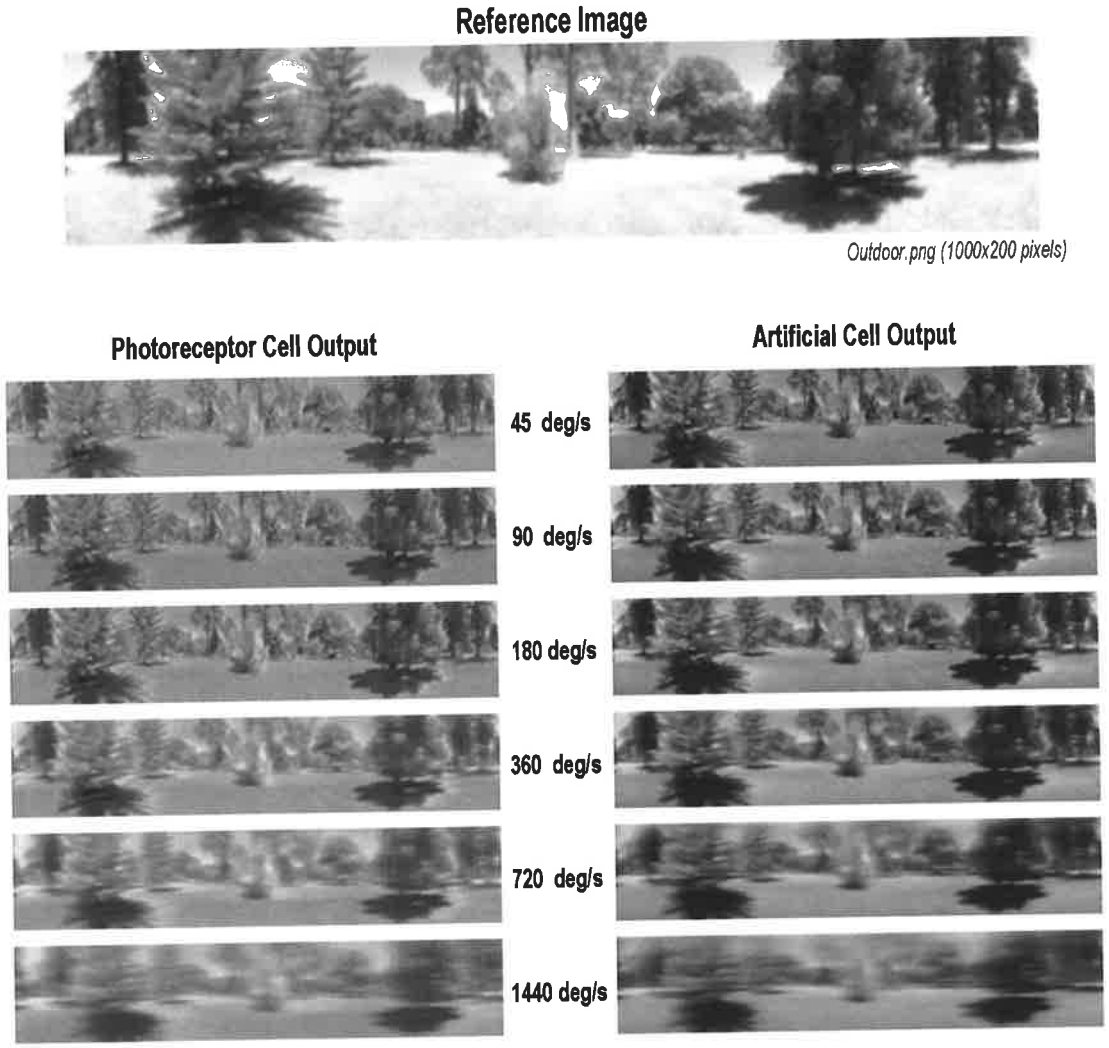

Figure A-13: Reconstructed output images *(Outdoor)* from both the actual biological photoreceptors *(average of 4 trials)* and the prototype circuit *(no repeats)* at several playback speeds – 45°/s, 90°/s, 180°/s, 360°/s, 720°/s and 1440°/s. The image at the top of the figure was used as a reference for all mathematical analyses.

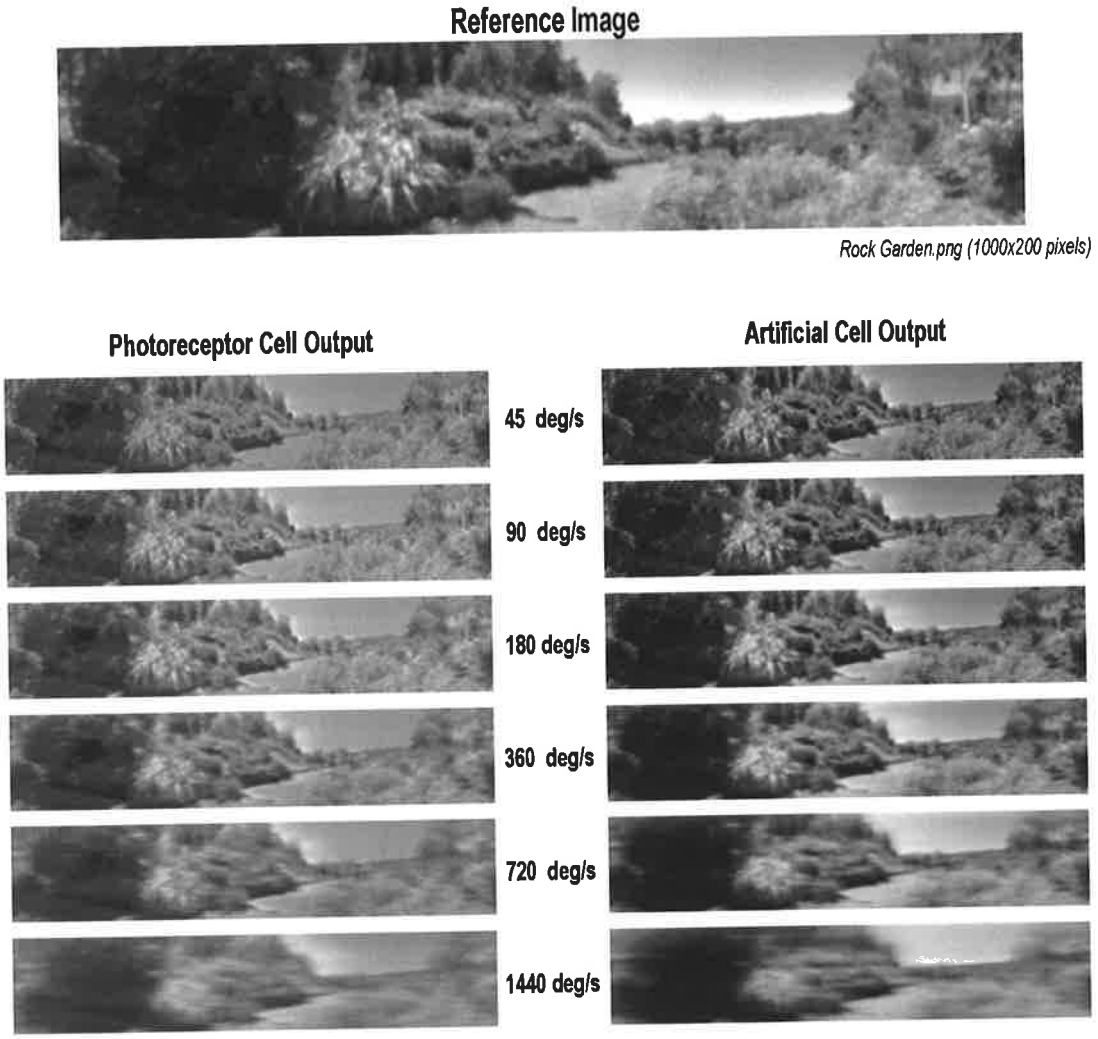

Figure A-14: Reconstructed output images *(Rock Garden)* from both the actual biological photoreceptors *(average of 4 trials)* and the prototype circuit *(no repeats)* at several playback speeds – 45°/s, 90°/s, 180°/s, 360°/s, 720°/s and 1440°/s. The image at the top of the figure was used as a reference for all mathematical analyses.

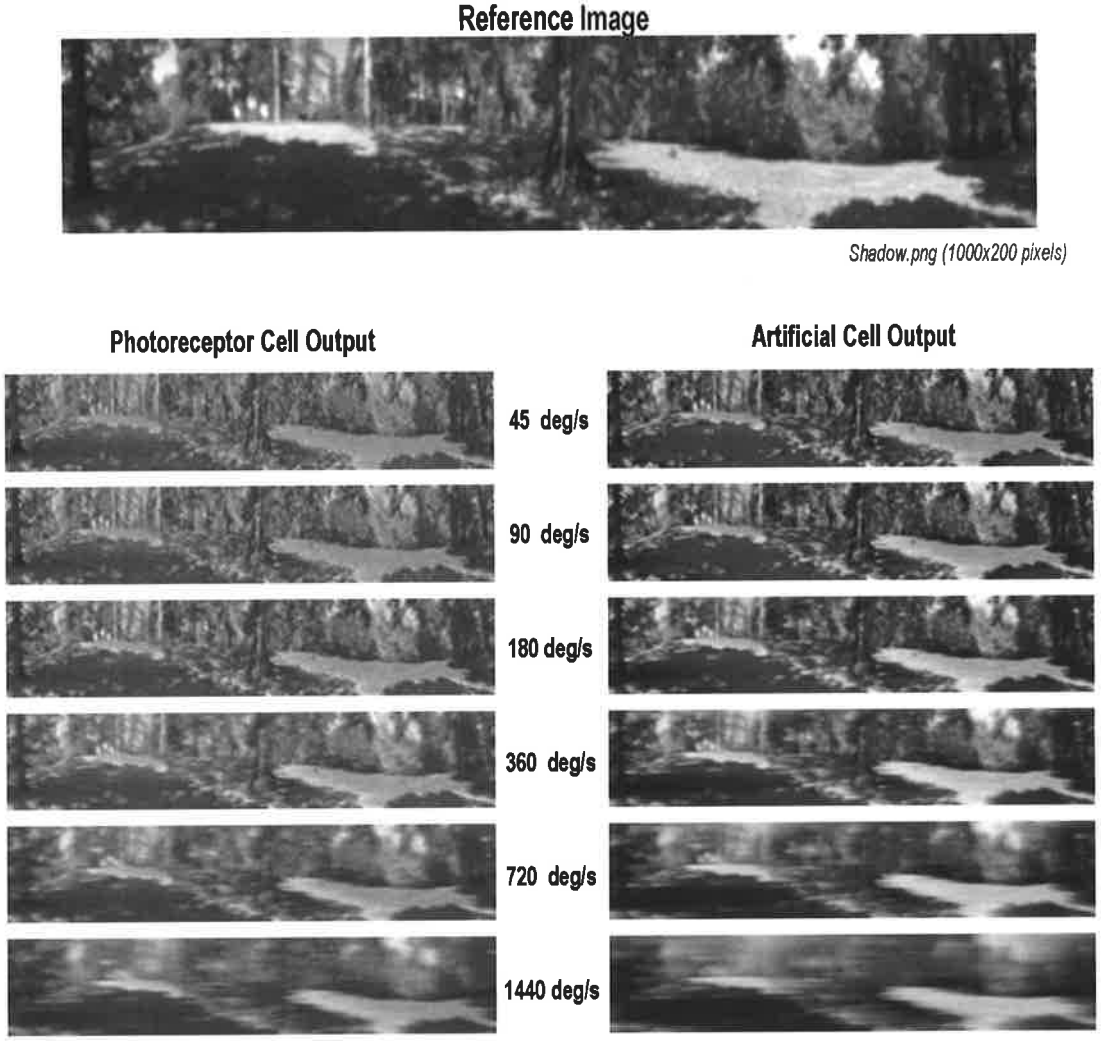

Figure A-15: Reconstructed output images *(Shadow)* from both the actual biological photoreceptors *(average of 4 trials)* and the prototype circuit *(no repeats)* at several playback speeds – 45°/s, 90°/s, 180°/s, 360°/s, 720°/s and 1440°/s. The image at the top of the figure was used as a reference for all mathematical analyses.

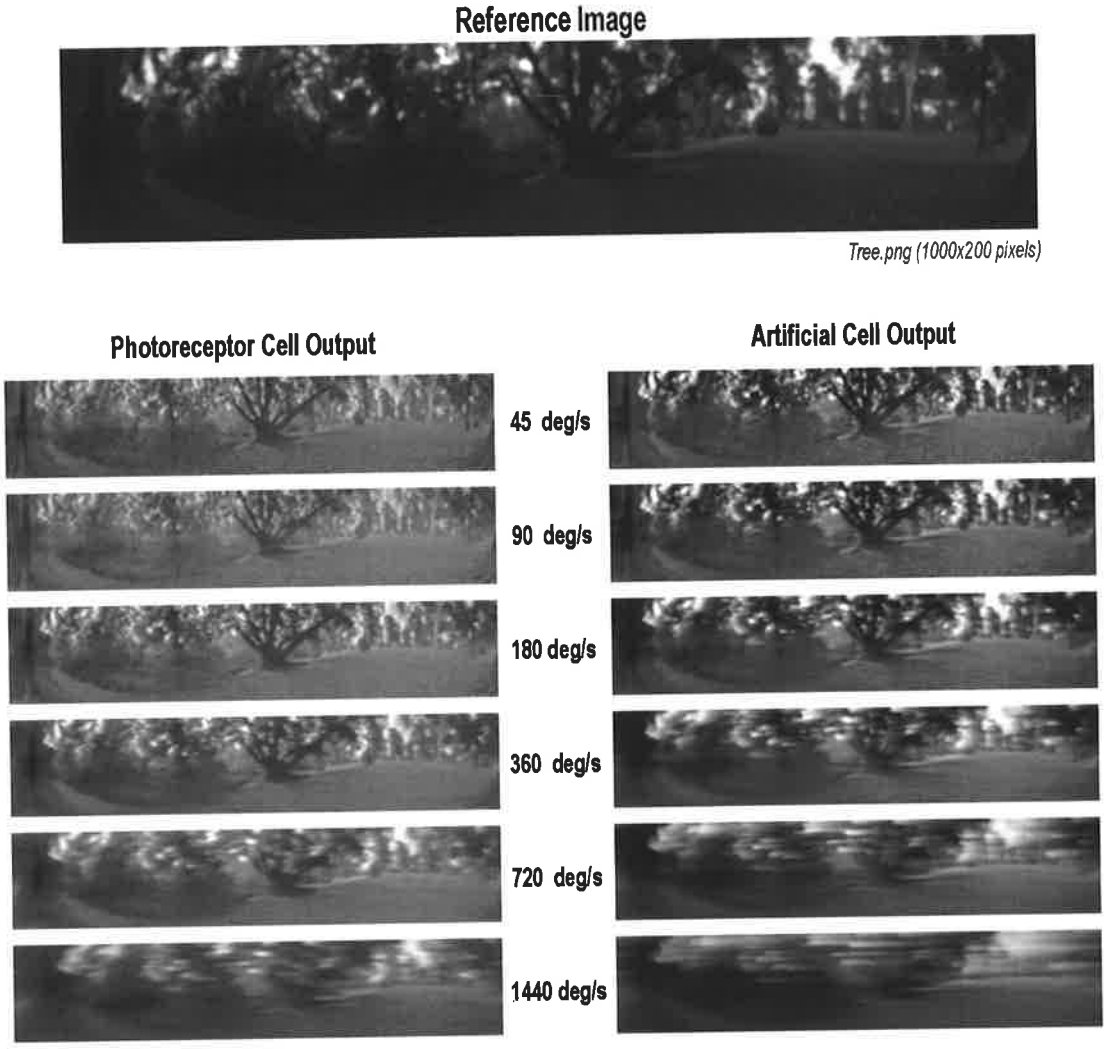

Figure A-16: Reconstructed output images *(Tree)* from both the actual biological photoreceptors *(average of 4 trials)* and the prototype circuit *(no repeats)* at several playback speeds – 45°/s, 90°/s, 180°/s, 360°/s, 720°/s and 1440°/s. The image at the top of the figure was used as a reference for all mathematical analyses.